Effects of glutamine deprivation on oxidative stress and cell survival in breast cancer cell lines

by

Mokgadi Violet Gwangwa

Submitted in fulfilment of the requirements for the degree,

Master of Science (Physiology)

Faculty of Health Sciences,

University of Pretoria

2019

Candidate
Name: M. Gwangwa
Student number: 11080478
Department: Physiology
Faculty of Health Sciences
University of Pretoria

Supervisor
Name: Dr M.H. Visagie
Department: Physiology
Faculty of Health Sciences
University of Pretoria

Co-supervisor
Name: Prof A.M. Joubert
Department: Physiology
Position: Professor
Faculty of Health Sciences
University of Pretoria

Head of Department
Name: Prof A.M. Joubert
Department: Physiology
Faculty of Health Sciences
University of Pretoria

DECLARATION

1. I understand what plagiarism is and am aware of the University's policy in this regard.

2. I declare that this dissertation is my own original work. Where other people's work has been used (either from a printed source, Internet or any other source), this has been properly acknowledged and referenced in accordance with departmental requirements.

3. I have not used work previously produced by another student or any other person to hand in as my own.

4. I have not allowed, and will not allow, anyone to copy my work with the intention of passing it off as his or her own work.

SIGNATURE: .....

SUMMARY

Tumourigenic cells utilize aberrant metabolic process that supports the biosynthetic requirements for hyperproliferation, survival and prolonged maintenance characterised by glucose metabolism to lactate dehydrogenase independent of oxygen availability (Warburg effect). In addition, tumourigenic cells exert increased glycolytic- and glutaminolytic activity in order to provide increased quantities of adenosine triphosphate. The aim of this research project was to investigate the influence of glutamine deprivation on proliferation, morphology, oxidative stress, mitochondrial membrane potential, cell cycle progression, antioxidant defences, deoxyribonucleic acid (DNA) damage, energy status, cell survival signaling and cell death induction in tumourigenic- and non-tumourigenic breast cell lines.

In this study it was found that glutamine deprivation results in differential antiproliferative activity where the MCF-7 cell line was the most affected with decreased cell growth to 61% after 96 h of glutamine deprivation. Aberrant redox activity was most prominently observed in the MCF-7 cell line accompanied with biphasic mitochondrial membrane potential- and reactive oxygen species production. The MCF-7 cell line showed significant mitochondrial membrane depolarisation after 24 h and 96 h deprivation from glutamine (1.5- and 1.37 fold). Cell cycle progression analysis illustrated an increase in the amount of cells present in the S-phase in the MCF-7 cell line after 72 h of glutamine deprivation. The MDA-MB-231 cell line resulted in a significant increase in cells occupying the G_2/M phase after 24 h of glutamine deprivation. Glutamine deprivation in the BT-20 cell line resulted in a significant increase in cells occupying G_1 phase after 72 h of glutamine deprivation. The MCF-7 cell line demonstrated the least amount of viable cells when analysing apoptosis induction, when compared to the MDA-MB-231-, MCF-10A- and BT-20 cell lines after glutamine deprivation suggesting that the MCF-7 cell line is the most affected cell line. Analysis of antioxidant mechanism via superoxide dismutase (SOD) inhibition illustrated increased SOD activity in the MCF-7 cell line (9.1%) after 72 h of glutamine deprivation. Evaluation of catalase protein concentration indicated that the MCF-7 catalase expression increased to 1.28 fold after 24 h of glutamine deprivation when compared to cell propagated in complete growth medium. DNA damage was demonstrated by visualising the presence of fluorescent 8-hydroxydeoxyguanosine and showed that the MCF-7 cell line presented with significant 8-

hydroxydeoxyguanosine staining. Survival signaling was also evaluated through visualising extracellular signal-regulated kinase (ERK) and phosphoinositide 3-kinase (PI3K) signaling which demonstrated increased ERK activation in the non-tumourigenic MCF-10A cell line and decreased PI3K activation.

This study provides evidence that there are differential- and time-dependent responses in breast tumourigenic cells versus non-tumourigenic cells, to glutamine deprivation thus unraveling the crosstalk between glutamine deprivation, oxidative stress and cell death and different cell types will enable us to better understand the basics of tumour cell metabolism and thus develop therapeutics that provide promising pre-sensitization potential for chemotherapeutic agents.

Keywords: Glutamine deprivation, ROS, mitochondrial membrane potential, cell cycle, SOD, catalase

ACKNOWLEDGEMENTS

This project was be supported by grants from the Cancer Association of South Africa and Medical Research Council awarded to Prof Joubert from the Department of Physiology. This project was also funded from grants received from the Struwig Germeshuysen Trust, School of Medicine Research Committee of the University of Pretoria and The South African National Research Foundation (NRF) provided by Prof A.M. Joubert and Dr M.H. Visagie. Furthermore, I thank Prof S. Manda and Miss N. Abdelatif (Biostatistics Unit, South African Medical Research Council, and Pretoria, South Africa) for consulting on the statistical planning of this project. I thank Dr I. van den Bout (Centre for Neuroendocrinology) for the usage of the confocal microscope and added support. I thank the Department of Pharmacology for the use of the flow cytometer. I thank my supervisor Dr M.H. Visagie for the patience and support given to me throughout the project. I would also like to thank Prof A.M. Joubert for providing time to lend her expertise in my project. I would like to thank my family for the support given through the project.

TABLE OF CONTENTS

LIST OF ABBREVIATIONS

αKG	α-Ketoglutarate
ADP	Adenosine Diphosphate
AKT	Protein Kinase B
AMP	Adenosine Monophosphate
AMPK	5' Adenosine Monophosphate-Activated Protein Kinase
AP-1	Activator Protein 1
Apaf-1	Apoptotic Protease Activating Factor 1
ASCT2	Alanine-Serine-Cysteine Transporter Subtype 2
ATCC	American Type Culture Collection
ATG	Autophagy-Related Genes
ATM	Ataxia Telangiectasia Mutated
ATP	Adenosine Triphosphate
Bad	Bcl-2-Associated Death Promoter
Bak	Bcl-2 Homologous Antagonist Killer
Bax	Bcl-2 Associated X Protein
Bcl-2	B-Cell Lymphoma-2
Bcl-xL	B-Cell Lymphoma Extra-Large
BH3	Bcl-2 Homology
Bid	BH3 Interacting-Domain Death Agonist
BRCA1	Breast Cancer 1
BRCA2	Breast Cancer 2
BSA	Bovine Serum Albumin
CAMKK-ß	Calmodulin-Dependent Protein Kinase Kinase Beta
cAMP	Cyclic Adenosine Monophosphate
CDK	Cyclin Dependent Kinases
CEM	Lymphoblastic Leukaemia Cell Line
CoA	Coenzyme A
cMyc	Cellular Myelocytomatosis
DAPI	4′,6-Diamidino-2-phenylindole
DSB	Double Stranded Breaks
DCF	2, 7-Dichlorofluorescein
DCFDA	2, 7-Dichlorofluoresceindiacetate

DHE	Dehydroethidine
DISC	Death-Inducing Signaling Complex
DMEM	Dulbecco's Minimum Essential Medium Eagle
DNA	Deoxyribonucleic Acid
dNTP	Deoxyribonucleotide Triphosphate
EDTA	Ethylenediaminetetraacetic Acid
Elk-1	ETS Transcription Factor
ER	Oestrogen Receptor
ERK	Extracellular Signal-Regulated Kinase
ETS	E-Twenty Six Transformation Specific
FADD	Fas-Associated Death Domain
Fas	Apoptosis Stimulating Fragment
Fas-L	Fas Ligand
FITC	Isothiocyanate
FOXO	Forkhead Box O
GCL	Glutathione Cysteine Lipase
GDH	Glutamate Dehydrogenase
GS	Glutamine Synthetase
GSH	Glutathione
H2A	Histone Family, Member A
H2AX	Histone Family, Member Y
H_2O_2	Hydrogen Peroxide
HER2	Human Epidermal Growth Factor Receptor 2
HIF 1	Hypoxia-Inducible Factor
HL-60	Promyelocytic Leukaemia Cell Line
JNK	c-Jun N-Terminal Kinase
LC3	Microtubule-Associated Protein 1A/1B-Light Chain 3
LMIC	Low and Middle-Income Country
MAPK	Mitogen Activated Protein Kinase
MCF-7	Michigan Cancer Foundation-7
MDA-MB-231	M.D Anderson Metastatic Breast
Mn	Manganese
mTOR	Mammalian Target of Rapamycin
mTORC1	Mammalian Target of Rapamycin Complex 1

mTORC2	Mammalian Target of Rapamycin Complex 2
NADH	Nicotinamide Adenosine Dinucleotide Hydrogen
NADPH	Nicotinamide Adenine Dinucleotide Phosphate Hydrogen
NOX	NADPH Oxidase
O_2^-	Superoxide
$OH^{\cdot}$	Hydroxyl Radical
OXPHOS	Oxidative Phosphorylation
PBS	Phosphate Buffered Saline
PCD	Programmed Cell Death
PDK1	Phosphoinositide-Dependent Protein Kinase-1
PE	Phosphatidylethanolamine
PI	Phosphatidylinositol
PI3K	Phosphoinositide 3-Kinase
PIP	Phosphatidylinositol-5-Bisphoshate
PIP2	Phosphatidylinositol-4, 5-Bisphoshate
PIP3	Phosphatidylinositol-3, 4, 5-Bisphoshate
PKB	Serine/Threonine Protein Kinase B
PMSF	Phenylmethane Sulfonyl Fluoride
PR	Progesterone Receptor
PVDF	Polyvinylidene Fluoride
RAS	Ras
Rb	Retinoblastoma Protein
Rheb	Ras Homolog Enriched In Brain
RIPA	Radioimmunoprecipitation Assay
ROS	Reactive Oxygen Species
SDS-PAGE	Sodium Dodecyl Sulphate Polyacrylamide Gel Electrophoresis
SN2	System N Transporter 2
SOD	Superoxide Dismutase
TSC	Tuberous Sclerosis Complex
U937	Histiocytic Lymphoma Cell line

LIST OF FIGURES

LIST OF TABLES

ABSTRACT

Tumourigenic cells utilize aberrant metabolic process that supports the biosynthetic requirements for hyperproliferation, survival and prolonged maintenance characterised by glucose metabolism to lactate dehydrogenase independent of oxygen availability (Warburg effect). In addition, tumourigenic cells modify glycolytic- and glutaminolytic pathways in order to facilitate increased proliferation and cell survival resulting in subsequent glucose- and glutamine addiction. Literature suggests particular promise in studying glutamine deprivation since tumourigenic cells have an elevated consumption rate when compared to non-tumourigenic cells. The aim of this research project was to investigate the influence of glutamine deprivation on proliferation, morphology, oxidative stress, mitochondrial membrane potential, cell cycle progression, antioxidant defences, deoxyribonucleic acid (DNA) damage, energy status, cell survival signaling and cell death induction in breast tumourigenic cell lines MCF-7-, MDA-MB-231-, BT-20- and a non-tumourigenic breast cell line MCF-10A.

Spectrophotometry data obtained from crystal violet staining demonstrated that glutamine deprivation resulted in decreased cell growth in a time-dependent manner. MCF-7 cell growth was decreased to 86%, 80%, 69% and 61% after 24 h, 48 h, 72 h and 96 h of glutamine deprivation, respectively. MDA-MB-231 cell growth was decreased to 93%, 89%, 88% and 78% cell growth after 24 h, 48 h, 72 h and 96 h of glutamine deprivation, respectively. MCF-10A- and BT-20 cell growth was decreased to 89% and 86% after 96 h of glutamine deprivation, respectively. Thus suggesting differential antiproliferative activity. Furthermore, glutamine deprivation resulted in oxidative stress, assessed via flow cytometry, where superoxide levels were chronically elevated with the MCF-7 cell line reaching 1.23 fold after 96 h of glutamine deprivation when compared to cells propagated in complete growth medium. Hydrogen peroxide production increased to 1.16 fold after 24 h of glutamine deprivation in the MCF-7 cell line accompanied by mitochondrial membrane potential depolarisation of 1.5 when compared to cells propagated in complete growth medium. The effects on reactive oxygen species (ROS) and the mitochondrial membrane potential, assessed via flow cytometry, were more prominently observed in the MCF-7 cell line when compared to the MDA-MB-231-, MCF-10A- and BT-20 cell lines. Analysis of antioxidant mechanism via superoxide dismutase (SOD)

inhibition analysed via spectrophotometry illustrated increased SOD activity in the MCF-7 cell line (9.1%) after 72 h of glutamine deprivation. Evaluation of catalase protein concentration analysed via spectrophotometry indicated that the MCF-7 catalase expression increased to 1.28 fold after 24 h of glutamine deprivation when compared to cell propagated in complete growth medium. Flow cytometry revealed that glutamine deprivation resulted in significant changes within the cell cycle where 34% of cells were present in the S-phase after 72 h of glutamine deprivation. The MDA-MB-231 cell line resulted in a significant increase in cells occupying the G_2/M phase after 24 h of glutamine deprivation. Glutamine deprivation in the BT-20 cell line resulted in a significant increase in cells occupying G_1 phase after 72 h of glutamine deprivation. The MCF-7 cell line demonstrated the least amount of viable cells when analysing apoptosis induction, when compared to the MDA-MB-231-, MCF-10A- and BT-20 cell lines after glutamine deprivation suggesting that the MCF-7 cell line is the most affected cell line. Visualising of fluorescent 8-hydroxydeoxyguanosine via fluorescent microscopy demonstrated that glutamine deprivation resulted in significant DNA damage in all cell lines after 96 h deprivation from glutamine. Survival signaling was also evaluated through western blot by visualising extracellular signal-regulated kinase (ERK) and phosphoinositide 3-kinase (PI3K) signaling which demonstrated ERK increased activation in the non-tumourigenic MCF-10A and non-metastatic BT-20 cell lines and decreased activation in the MCF-7 cell line which correlates with decreased cell growth shown in this study.

This study demonstrates that glutamine deprivation results in decreased cell proliferation, differential ROS generation and aberrant mitochondrial membrane potential indicative of cell death induction and disrupted cell cycle progression. In addition, the oestrogen receptor positive, luminal MCF-7 cell line was more prominently affected by glutamine deprivation when compared to the oestrogen receptor negative, basal MDA-MB-231-, MCF-10A- and BT-20 cell lines. This study contributes to knowledge regarding the metabolic changes and interactions between signaling pathways and glutamine sensitivity in breast cancer cells and non-tumourigenic cells which is crucial for future therapeutics targeting cancer cell metabolism. In addition, glutamine deficiency may affect non-tumourigenic response to antitumour treatment which is beneficial in potentially pre-sensitizing therapy of tumourigenic cells to chemotherapeutic treatments.

Keywords: Glutamine deprivation, reactive oxygen species generation (ROS), mitochondrial membrane potential, cell cycle progression, apoptosis, SOD, catalase

CHAPTER 1

1. INTRODUCTION

Breast cancer is the most commonly diagnosed cancer amongst women with numbers reaching 1.4 million per year worldwide. It has been predicted that the worldwide incidence rate will reach approximately 3.2 million new cases per year by 2050 (1). In South Africa, one in four people are affected by cancer with breast cancer being the most commonly diagnosed type of cancer according to the National Cancer Registry (1). South Africa is ranked 50th on the World Cancer Research Fund's list of countries with the highest cancer prevalence rates. Moreover, the five-year overall survival rate for breast cancer patients does not exceed 60% for any low and middle-income country (LMIC) in Africa (2). Epidemiology studies show that a female diagnosed with stage I breast cancer has an 88% chance of survival; however, upon diagnosis at stage IV, the survival rate decreases to 15% that will survive for more than 5 years (3).

Genetic risk factors include germline mutations in the breast cancer 1 (*BRCA1*) and breast cancer 2 (*BRCA2)* genes which increase a woman's risk of developing breast- and ovarian cancer. In addition, acquired mutations in human epidermal growth factor receptor 2 gene (*HER2)* play a fundamental role in the development and growth of breast cancer (4). Other risk factors include age- and lifestyle parameters including tobacco usage, levels of physical activity and excessive alcohol consumption. Furthermore, 89% of breast cancer occurs from ages of 40 years and above (5).

Predictive immunohistochemistry markers in breast pathology include hormone receptor positive factors such as oestrogen receptors (ER), progesterone receptors (PR) and HER2. Tumourigenic cells may have none, one, or all receptors (6). Types of breast cancer that have receptors are subsequently positive for the specific receptor and inversely, breast cancers that lack all receptors are referred to as triple negative suggesting that the growth of the cancer is not supported by oestrogen and progesterone, nor by the presence of HER2 receptors (7). Therefore, triple negative breast cancer does not respond to hormonal therapy (such as tamoxifen or

aromatase inhibitors) or therapies that target HER2 receptors, such as Herceptin (chemical name: trastuzumab) (8). Breast cancer is classified into four stages. Stage I describes invasive breast cancer where tumourigenic cells invade surrounding non-tumourigenic breast cells. Stage I is further categorised into stages IA and IB. Stage IA describes invasive breast cancer whereby the tumour measures up to 2cm and present as HER2-positive and hormone receptor positive (oestrogen and progesterone); nonetheless, in this stage the cancer has not metastasized beyond the breast (9). Stage IB is characterised by a lack of tumour present in the breast; however, tumourigenic cell colonies larger than 2 mm are found in lymph nodes presenting as HER2-positive and hormone-receptor-positive. Stage II is divided into subcategories known as IIA and IIB where stage IIA is characterised by a tumour measuring 2 cm - 5 cm that has not metastasized to the axillary lymph nodes (8). Stage IIB describes a tumour size of 2 cm - 5 cm with tumourigenic cells that have metastasized to 1 to 3 axillary lymph nodes or to lymph nodes near the breastbone. Stage III is divided into subcategories known as IIIA, IIIB, and IIIC. Stage IIIA is characterised by tumourigenic cells found in 4 to 9 axillary lymph nodes or in the lymph nodes near the breastbone, alternatively, a tumour larger than 5 cm. Stage IIIB describes a tumour that has metastasized to the chest wall and/or skin of the breast causing swelling presenting as ER-positive, PR-positive and is HER2-positive. Stage IIIC describes cancer where metastasis to 10 or more axillary lymph nodes has taken place (9). A triple negative breast cancer can be associated with any of the above stages in regards to size and progression of the tumourigenic cells (10). Since the tumour cells lack the necessary receptors, common treatments like hormone therapy and drugs that target oestrogen, progesterone and HER-2 are ineffective. Furthermore, the progression of tumourigenic cells in breast cancer pathology is dependent on the energy provided to the cells to facilitate proliferation hence the importance of fully comprehending the mechanism at which tumourigenic cells attain their ability to proliferate (11).

Key oncogenic signaling pathways including glycolysis and glutaminolysis adapt to tumour cell metabolism in order to support hyperproliferation and survival (12). Due to the increased metabolic rate, malignancy results in a significant deficiency in glutamine. Most of the interest regarding the interplay between glutamine and cancer is based on the foundation that it is an essential nutrient and represents an important

driver of tumour cell anabolism (13). However, glutamine is also involved in several cell signaling pathways that mitigate the effects of increased tumourigenic bioenergetic processes, altered oxidative activity and macromolecule synthesis resulting in increased survival. These additional roles enhance the appeal of targeting glutamine metabolism in cancer treatment (14). Understanding how cells adapt to glutamine deprivation is essential for future treatments targeting tumourigenic metabolism since more therapeutics are being developed that target cancer cell metabolism. Furthermore, glutamine deficiency may influence non-tumourigenic tissue tolerance to antitumour treatment.

CHAPTER 2

2.1 LITERATURE REVIEW

Energy consumption for metabolic activities in non-tumourigenic cells is dependent on mitochondrial oxidative phosphorylation (OXPHOS) and glycolysis (15). OXPHOS generates 36 molecules of adenosine triphosphate (ATP) by oxidizing nutrients. In addition, glycolysis generates 2 molecules of ATP through a series of enzyme-catalysed reactions and is known to be oxygen-independent (16). Pyruvate, which is the end product of glycolysis, is converted to acetyl coenzyme A (CoA) in the mitochondria thus linking the Krebs cycle to glycolysis (Figure 1). The Krebs cycle is defined as a pathway that is central to aerobic cellular respiration (17). The pathway for energy production in tumourigenic cells was first described by Otto Warburg in the 1920s, and is known as the Warburg effect (17). Tumourigenic cells usually prefer glycolysis due to the increased demand for proliferation and associated increased energy requirement. In addition, glycolysis is associated with the Krebs cycle which has intermediates that facilitate synthesis of macromolecules that include nucleic acids, proteins and lipids which are a necessity in the case of increased proliferation (18). Although it is widely accepted that glucose is the dominant energy fuel for most types of cancer, glutamine also supplies energy to the cell. Thus, glutaminolysis is an alternative energy production pathway in cancer, since upregulated glutamine consumption is frequently observed in cancer (19).

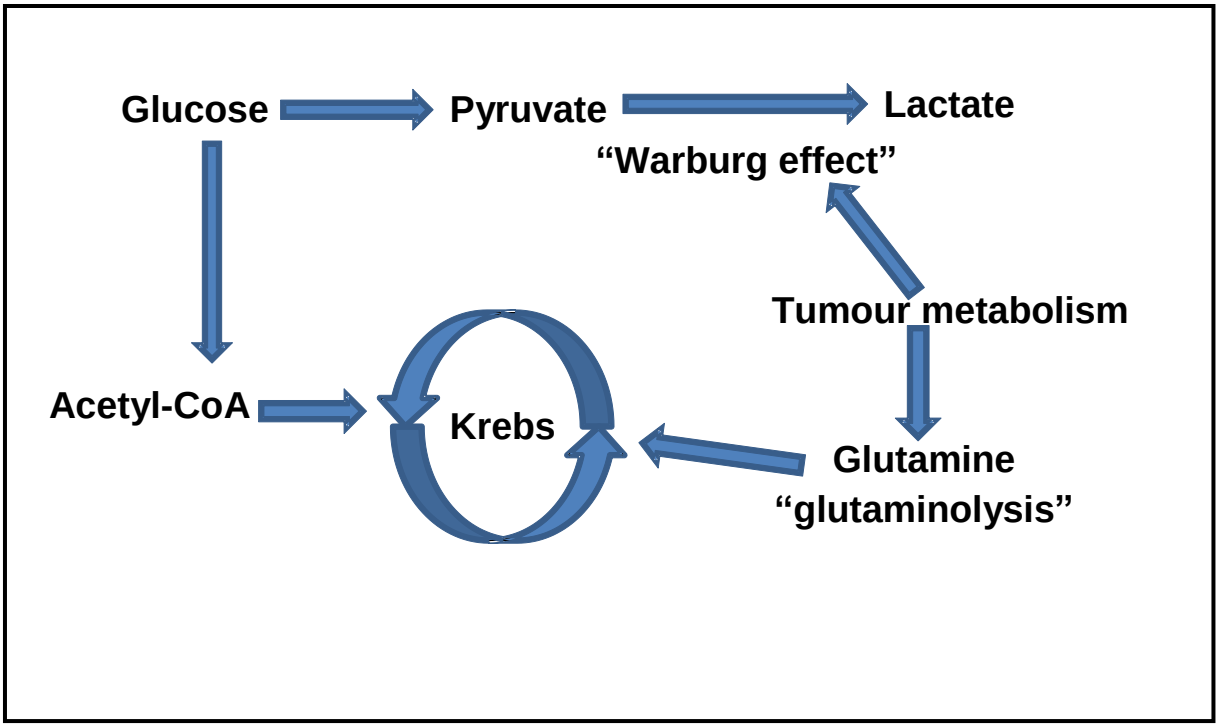

Figure 1: Glucose is converted into pyruvate by a process of glycolysis; however, in a lack of oxygen pyruvate is further converted to lactate. Tumour metabolism, however, converts pyruvate to lactate even in the presence of oxygen which is termed the Warburg effect. Tumourigenic cells have increased metabolic requirements hence the employment of glutaminolysis in order to fuel the Krebs cycle and subsequently produce energy. [Diagram designed in Microsoft (Windows 10) Word by M. Gwangwa].

Glutamine, the most abundant amino acid in the body, is essential for proliferation and acts as a precursor for other amino acids, nucleosides and molecules involved in the maintenance of redox homeostasis (20). Glutamine is transferred into the cells using glutamine importers namely alanine-serine-cysteine transporter subtype 2 (ASCT2) and system N transporter 2 (SN2) (Figure 2). When glutamine enters the cell, it is destined for either nitrogen donation or deamination by glutaminases to form glutamate (21). Glutamate is further catalysed into glutathione (GSH) or glutathione cysteine lipase (GCL) which form part of the cell's innate antioxidant defences. Glutamate dehydrogenase (GDH) reduces glutamate to α-ketoglutarate (αKG), which is catalysed in the mitochondria contributing to energy production. In addition, facilitates the production of acetyl CoA which is essential for the continuation of the Krebs cycle which produces ATP (22). Hence glutamine is known for its fundamental

role as an anapleurotic substrate in tumourigenic cells due to increased carbon donation in order to support the unregulated metabolism and proliferation (Figure 2).

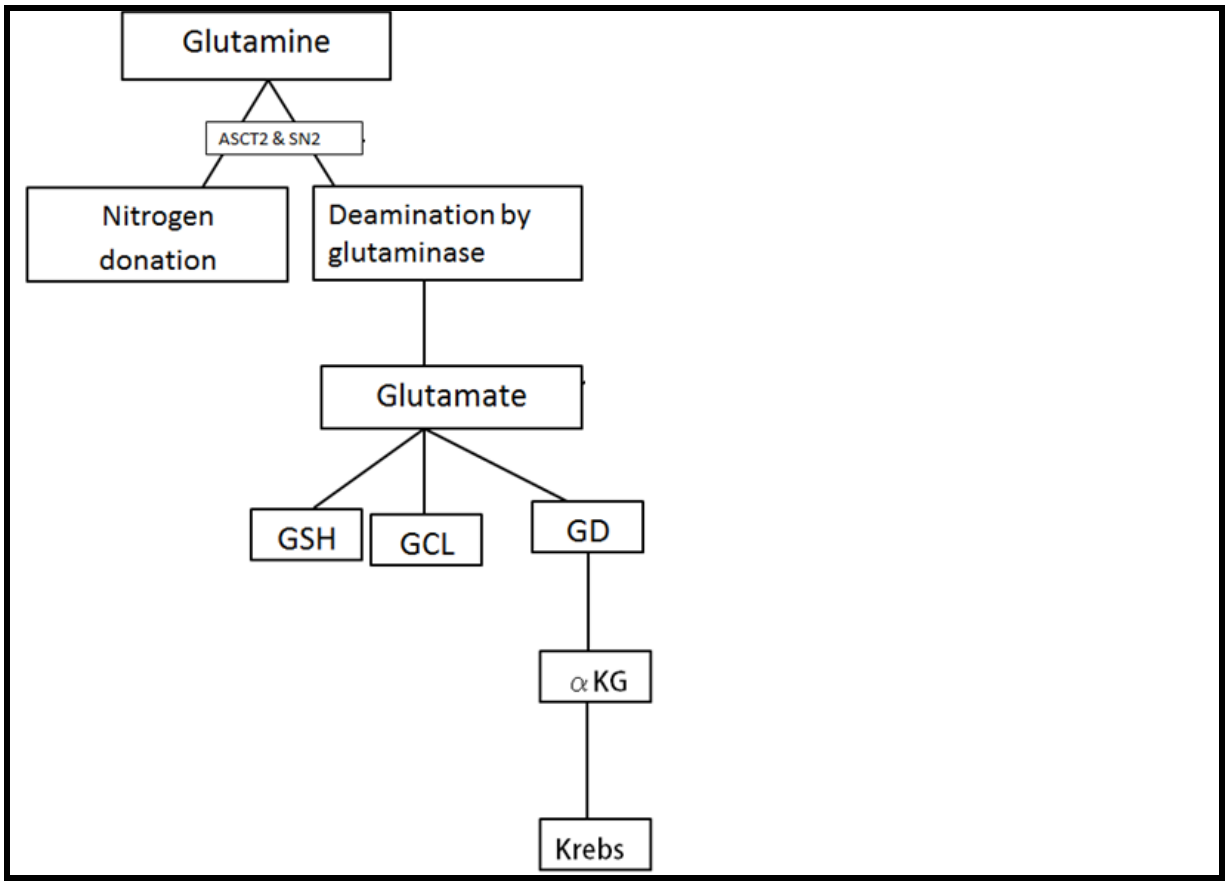

Figure 2: Glutamine is transferred into the cell by ASCT2 & SN2 transporters. Glutamine is subsequently deaminated by glutaminase to form glutamate which is further catalysed by glutamate dehydrogenase to form αKG which further enters the Krebs cycle to produce energy for the cell. [Diagram designed in Microsoft (Windows 10) Word by M. Gwangwa].

Glutamine deprivation resulted in decreased proliferation in the CEM cell line (lymphoblastic leukaemia), HL-60 cell line (promyelocytic leukaemia), Namalwa cell line (Burkitt lymphoma) and U937 cell line (histiocytic lymphoma) suggesting that glutamine is essential to proliferation (23). Furthermore, Harnett, *et al* (2013) reported that glutamine deprivation resulted in oxidative stress via mitochondrial dysfunction, suggesting that glutamine is essential in the redox homeostasis (24). Investigating the crosstalk between the glutamine signal transduction, proliferation, oxidative stress and cell death induction will provide us with the molecular determinants for future improved cancer treatment.

2.2 OXIDATIVE STRESS

Reactive oxygen species (ROS) are a group of molecules produced during oxygen metabolism and are fundamental signaling molecules at low concentrations. Non-tumourigenic cells produce ROS via the electron transport in a process called OXPHOS. ROS includes hydroxyl radical ($OH^{\cdot}$), hydrogen peroxide (H_2O_2) and superoxide (O_2^{-}) (25). Oxygen reduction by one electron produces superoxide, which is known as the precursor of most intracellular ROS. Superoxide is subsequently reduced to hydrogen peroxide. Hydrogen peroxide is reduced to water and oxygen or partially reduced via transition elements to $OH^{\cdot}$ (26).

Aerobic glycolysis and mitochondrial oxidative phosphorylation produces ROS since oxygen is converted into superoxide. This occurs when electrons leak from the electron transport chain and is catalysed by nicotinamide adenine dinucleotide phosphate hydrogen (NADPH) oxidases (27). The leaky electron transport chain complexes include complex I (nicotinamide adenine dinucleotide hydrogen NADH dehydrogenase), complex II (succinate dehydrogenase), complex III (cytochrome *c* reductase), complex IV (cytochrome *c* oxidase) and complex V (mitochondrial F_1F_0 ATP synthase) (25)(26). As the electrons flow through the complexes, there is a release of hydrogen ions which create a gradient in the inner membrane and the hydrogen ions enters complex V in order to produce ATP (25). However, under stress conditions, additional electrons leaks from the respiratory chain prematurely, exacerbating superoxide production, thus causing detrimental effects on the cell such as excessive oxidative stress (27).

Low ROS production is generated by NADPH and NADPH oxidase (NOX) and is required for proliferative signaling events which promote cell proliferation and survival through the post-translational modification of kinases such as tyrosine kinase and the mitogen-activated protein kinase (MAPK) system (28) (29). During cellular stress including anoxia or starvation, high ROS quantities result in damage to macromolecules, including deoxyribonucleic acid (DNA), triggering senescence and permeabilization of the mitochondria, leading to the release of cytochrome *c* which induces apoptosis (30).

ROS resulting in oxidative stress also induce mitochondrial membrane potential abnormalities. The physiological state of the mitochondria is fundamental for cellular homeostasis thus any deviation from homeostasis will trigger an appropriate response from the mitochondria. Upon high levels of physiological stress, various apoptosis-inducing factors are released from the mitochondria through mitochondrial transition pores into the cytoplasm resulting cell death induction (31). The permeability of the mitochondrial pore is dependent on the mitochondrial membrane potential (hyperpolarisation and depolarisation). Mitochondrial membrane potential experiences hyperpolarization in the event of the mitochondrial inner membrane possessing a negative charge (32). The mitochondrial membrane is considered to be depolarised upon the mitochondrial inner membrane experiencing a positive charge. Furthermore, the mitochondrial membrane potential is reliant on the electron transport chain for transferring electrons from NADH to oxygen and ATPase complex. The hydrogen ions fluxed into matrix are used by ATPase to convert adenosine diphosphate (ADP) to ATP during oxidative phosphorylation (33).

2.3 ANTIOXIDANT DEFENCES

The cell possesses several antioxidant defences in order to maintain ROS homeostasis. Antioxidant defences include glutathione, catalase and superoxide dismutase (SOD). SOD reduces superoxide to hydrogen peroxide (Figure 3) (34). Cytochrome *c* mediates the reaction of superoxide to oxygen and is also able to facilitate the transfer of electrons to the final oxidase for energy production (35). Hydrogen peroxide is detoxified by glutathione peroxidase. Catalase is also known to detoxify hydrogen peroxide without cofactors, to water and oxygen (36). These enzymes form an extensive antioxidant network to maintain the steady state and regulation of reactive oxygen species. However, the antioxidant defences can be overwhelmed with increased production of reactive oxygen species and thus fail to regulate redox homeostasis subsequently causing oxidative stress (37).

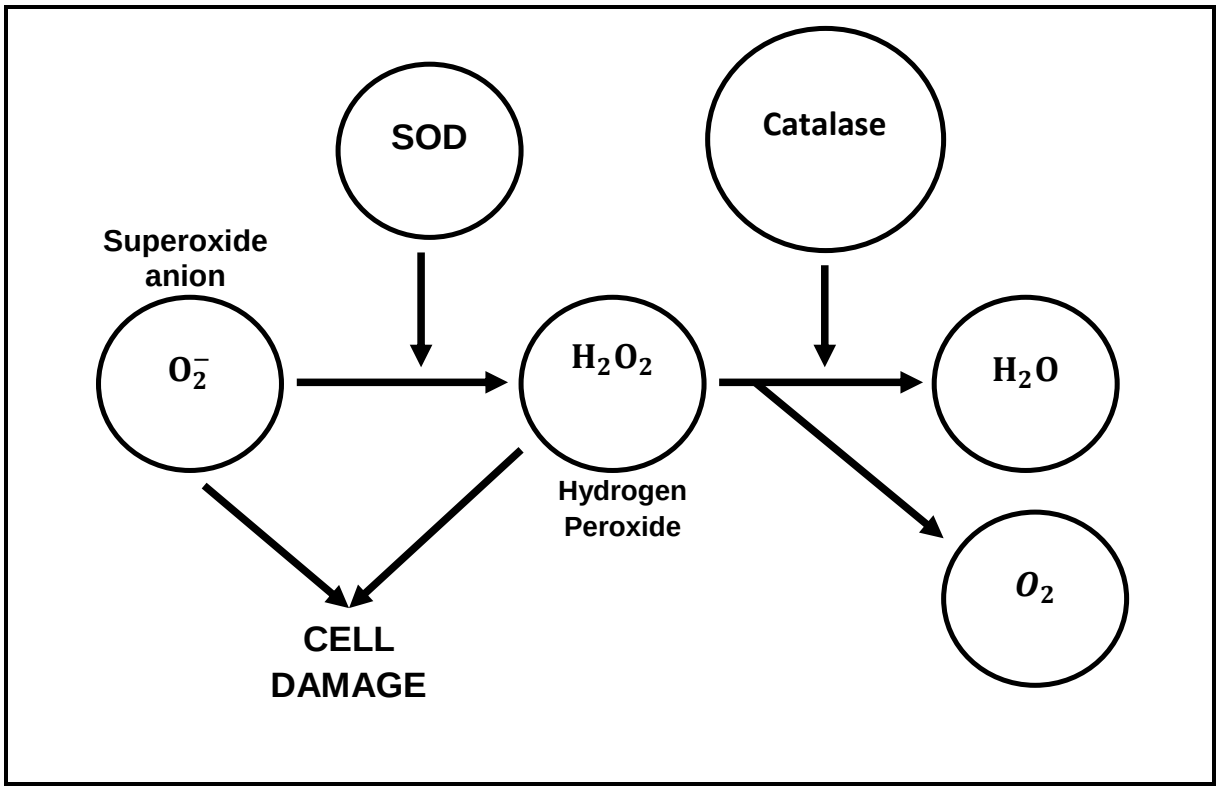

Figure 3: Antioxidant network where superoxide is detoxified by superoxide dismutase to form hydrogen peroxide (H_2O_2) which is further detoxified by catalase to water (H_2O) and oxygen (O_2). Superoxide and hydrogen peroxide constitute as reactive oxygen species which is known to cause cell damage. [Diagram designed in Microsoft (Windows 10) Word by M. Gwangwa].

Oxidative stress is also associated with DNA damage and phosphorylated histone family, member A (H2A). H2A is phosphorylated, activated and recruited to sites of double stranded breaks (DSB) after oxidative damage as part of the DNA repair mechanism. Ataxia telangiectasia mutated (ATM), a serine threonine protein kinase, is recruited and activated by DSB (38). ATM phosphorylates several key proteins that initiate activation of the DNA damage checkpoint, leading to cell cycle arrest, DNA repair or induction of apoptosis. ATM also has several targets that include p53 and histone family, member y (H2AX). Thus detecting the presence of H2AX is confirmation of DNA damage (39). Furthermore, 8-hydroxy-2′-deoxyguanosine is one of the predominant forms of free radical-induced oxidative lesions in mitochondrial- and nuclear- DNA. Hydroxyl radical (•OH) reacts with pyrimidines and purines resulting in base modifications. Therefore, 8-hydroxy-2′-deoxyguanosine is widely used as a biomarker for oxidative stress in tumourigenesis

(40). Thus, 8-hydroxy-2′-deoxyguanosine is an indication of oxidative DNA damage whilst H2AX is indicative of DSB breaks following oxidative stress damage (41).

2.4 CELL SURVIVAL PATHWAYS

Proliferation and cell survival is dependent on the maintenance of several signaling pathways including the MAPK and phosphoinositide 3-kinase (PI3K) pathways (42). MAPK signaling is essential in proliferation, migration, differentiation, apoptosis induction, autophagy induction and sensitivity to chemotherapy (43). Furthermore, MAPK is known to stimulate other signaling pathways including extracellular-signal-regulated kinase (ERK) 1 & 2, which activates proto-oncogene Ras, a common mutation in the several types of cancer including lung- , pancreas- and colon cancer which subsequently leads to increased proliferation (44). ERK is activated by cellular myelocytomatosis (cMyc), which forms a complex with E-twenty six transformation specific (ETS) transcription factor (Elk-1) and subsequently promotes proliferation via glutaminolysis. The proto-oncogene cMyc transcriptionally binds to the promoter regions of high-affinity glutamine importers, including ASCT2 and SN2 resulting in higher glutamine uptake (45). Overexpression of cMyc promotes the expression of mitochondrial GLS through transcriptional repression of miR-23a and miR-23b (46). Furthermore, cMyc also directly targets genes involved in deoxyribonucleotide triphosphate (dNTP) metabolism to enhance glutaminolysis in order to derive amide nitrogens for nucleotide synthesis (47). MAPK, oxidative stress and DNA damage stimulates c-Jun N-terminal kinase (JNK) thus activating activator protein 1 (AP-1) or p53 that induces apoptosis (48).

Tumourigenic cell metabolism stimulated by PI3K/protein kinase B (AKT) pathway regulates proliferation, growth and differentiation. Furthermore, hypoxia, a characteristic of tumourigenic cells, enhances the PI3K pathway, ROS production and proliferation (49). Literature states that PI3K activation, which is hyperactivated by excessive cell growth, leads to increased proliferation, cellular mobility and promotes cell survival. PI3K's phosphorylates the 3'-hydroxyl position of the inositol ring in phosphatidylinositides including phosphatidylinositol (PI) and phosphatidylinositol-4, 5-bisphoshate (PIP2). PIP2 phosphorylation results in the formation of phosphatidylinositol-3,4,5-triphosphate which activates AKT (50).

Phosphatidylinositol-3,4,5-bisphoshate (PIP3) binds to AKT and subsequently AKT moves to the cell membrane where AKT is activated by phosphoinositide-dependent protein kinase-1 (PDK1) and mammalian target of rapamycin complex 2 (mTORC2) phosphorylation by Thr308 and Ser473, respectively (51). AKT inhibits tuberous sclerosis complex (TSC) by phosphorylating TSC2 at Ser939 and binding to 14-3-3 protein. Subsequently, TSC promotes activation of RAS homolog enriched in brain (Rheb) and inhibits mammalian target of rapamycin (mTOR), thus promoting cell survival (52). PI3K can be activated by external stimuli including heat shock that further activate serine/threonine protein kinase B (PKB) (53). PKB phosphorylates forkhead box O (FOXO) transcriptional factors, which positively regulate the expression of glutamine synthetase (GS) which also then supports the tumourigenic cells to generate energy through the alternative pathway, glutaminolysis (54).

2.5 ADENOSINE MONOPHOSPHATE KINASE PATHWAY

AMP-activated protein kinase (AMPK) is an essential sensor of energy status and plays a significant role in cellular responses to metabolic stress (55). AMPK consist of an alpha (catalytic), beta and gamma (both regulatory) subunits and are activated by numerous kinases through phosphorylation and the increment of calcium in the cytosol through the calmodulin-dependent protein kinase kinase beta (CAMKK-ß) (56).

During periods of metabolic stress, AMPK is activated in response to an increased adenosine monophosphate (AMP)/ATP ratio indicating an energy deficit (57). AMPK binds directly to AMP, ATP or ADP resulting in conformational changes of the enzyme and activation, thus promoting phosphorylation and subsequently preventing further dephosphorylation of the adenosine molecules (58). AMPK is responsible for shifting cells to an oxidative metabolic phenotype and inhibiting cell proliferation (59). Furthermore, AMPK opposes the effects of AKT, inhibits mTOR and thus functions as a metabolic checkpoint, regulating the cellular response to energy availability (60). Inhibition of the alpha isoform results in decreased ATP levels which triggers AMPK signaling and subsequently, induces autophagy (61). Tumourigenic cells overcome this checkpoint in order to proliferate in response to activated growth signaling pathways, even in unfavourable microenvironments (62). The Ras pathway

suppresses AMPK and deactivates growth signals thus creating an inhibitory effect and subsequently allows for proliferation in aberrant nutrient conditions (63). Accordingly, tumourigenic cells exhibit a loss of appropriate AMPK signaling; an event that also contributes to their glycolytic phenotype (64). Furthermore, AMPK is required to maintain glutaminolysis by consistently activating the secretion of secondary messengers such as interleukin-4 which forms part of the microenvironment created in tumourigenic cells (65).

2.6 CELL CYCLE PROGRESSION

The cell cycle consists of six stages: apoptosis (sub-G_1), quiescent phase (G_0), the synthesis (S) phase, the mitotic phase (M) and two gap phases (G_1 and G_2) (66). Sub-G_1 is classified as dead cells and G_0 is characterized by non-dividing cells and cells that are exiting the cell cycle (67). The S phase is where DNA replication occurs and the M phase is where one cell divides into two daughter cells in a process called mitosis (68). The gap junction, G_1, is where majority of the organelles and proteins are formed while the other gap junction, G_2, is where preparation for mitosis occurs including the production of microtubules, verification of the duplicated chromosomes and detection of DNA errors and subsequent repair of the detected errors (69). Regulatory mechanisms are employed between the G_1 and S phase as well as between G_2 and mitosis. Regulatory mechanisms include proteins called cyclin dependent kinases (CDK) that are constitutively produced but are only activated upon the binding of cyclins which forms a complex (70) (Figure 4). For example, cyclins D and E are found in the G_1 phase where the cyclins will bind to CDK2 and 4 respectively. Furthermore, retinoblastoma (Rb) is known to inhibit S phase entry; however, Rb is inactive due to phosphorylation by CDK4-cyclin D complex and subsequently cells continue into the S phase (71). The S phase contains cyclin A which binds to CDK2 thus mediating DNA synthesis. In the G_2 phase, cyclin B binds to CDK1 which facilitates the cell transitioning to mitosis (72). Any interruption in any of these phases caused by glutamine deprivation will be indicative of a disruption in the regulation of cell cycle progression thus indicating the importance of glutamine dependency in the particular phase (Figure 4).

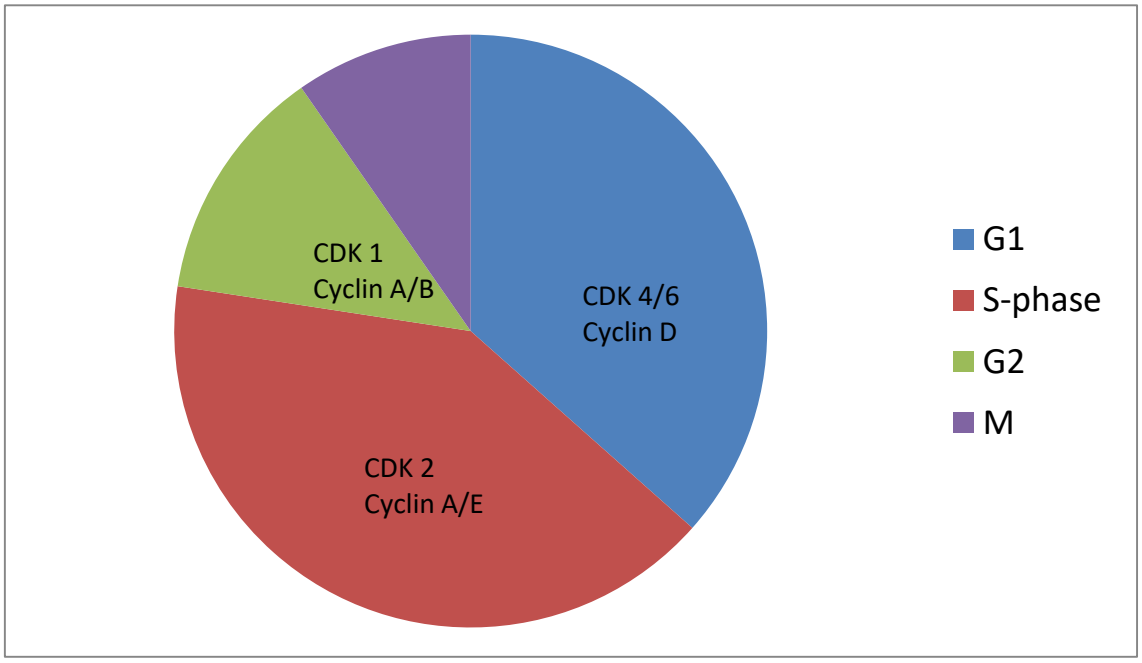

Figure 4: Illustration of the different stages of cell cycle with associated proteins involved in the progression of the chromosomes. The G_1 phase is propelled by CDK4/6-cyclin D followed by the S-phase which is propelled by CDK2-cyclin A/E and the G_2 phase which is propelled by CDK1-cyclin A/B. [Diagram designed in Microsoft (Windows 10) Word by M. Gwangwa].

The G_1/S checkpoint is responsible for the accuracy of chromosomes created in the G_1 and S phases. An accumulation in these phases is indicative of cellular damage thus causing slower DNA replication (73). This is due to the detection of ATM that phosphorylates active protein-checkpoints signaling cascade. Subsequently, DNA replication is possibly slowed down by the checkpoint or inhibition of the replication fork in the synthesis phase (74). As a cell approaches the end of the G_1 phase a vital checkpoint called G_1/S checkpoint is used to determine whether or not to replicate the DNA contained in the cell. At this checkpoint the DNA integrity is evaluated for any damage to ensure that it has all the necessary cellular machinery to allow for successful cell division. Cells with intact DNA continue to S phase; cells with damaged DNA that cannot be repaired are arrested and undergo programmed cell death (75). A second checkpoint occurs at the G_2 phase following the synthesis of DNA in the S phase however, before cell division in M phase. When fully functional,

cell cycle regulatory proteins act as the innate tumour suppressors by controlling cell growth and inducing the death of damaged cells (76). Genetic mutations causing the malfunction or absence of one or more of the regulatory proteins at cell cycle checkpoints can result in the consistent activation permitting uncontrolled multiplication of the cell, leading to tumourigenesis (77).

2.7 CELL DEATH PATHWAYS

2.7.1 Apoptosis

Programmed cell death (PCD) is an evolutionarily conserved and highly regulated pathway resulting in type I cell death also known as apoptosis. The term, apoptosis, was first reported by Kerr, Wyllie, and Currie in 1972 to describe a morphologically distinct form of cell death characterized by membrane blebbing, cell shrinkage, chromatin condensation and endonucleolytic cleavage of DNA (78).

There are several different stimuli that induce apoptosis including irradiation, heat shock, oxidative stress, hypoxia, death domain receptor binding and nutrient deprivation. The pathways of apoptosis include the extrinsic (death receptor pathway), intrinsic pathway (mitochondrial pathway), endoplasmic reticulum pathway and caspase-independent pathway (79).

The extrinsic pathway is triggered by binding of apoptosis stimulating fragment (Fas) and other death receptors to the plasma membrane death receptor with its extracellular ligand, Fas ligand (Fas-L). Fas-L binds to Fas and forms death-inducing signaling complex (DISC) consisting of adaptor protein fas-associated death domain (FADD) and procaspase 8 (80). This complex facilitates the conversion of procaspase 8 to caspase 8 which subsequently triggers effector caspase 3-, 6- and 7 (81).

The intrinsic pathway is induced by ROS and toxic injury, which activates proapoptotic members of the B-cell lymphoma-2 (Bcl-2) family including Bcl-2 associated X protein (Bax) and Bcl-2 homologous antagonist killer (Bak). The mitochondrial membrane potential is subsequently depolarized resulting in the

release of cytochrome *c* and ATP from the inner membrane of the mitochondria (82). Cytochrome *c* binds to apoptotic protease activating factor 1 (Apaf-1) and aided by ATP activates procaspase 9. The apoptosome, a multimeric complex, subsequently forms and consists of cytochrome *c,* ATP, Apaf-1 and caspase 9. This results in the activation of effector procaspase 3-, 6- and 7. The intrinsic- and extrinsic converge at a common point in the apoptotic pathway at activation of effector caspase 3- ,6- and 7 (83). The balance between apoptosis and survival is maintained by the Bcl-2 family members. This family is further divided into three subfamilies: Bcl-2 (including Bcl-2 and B-Cell Lymphoma Extra-Large (Bcl-xL)), Bax (including Bax and Bak), and BH3-only proteins (including Bcl-2-associated death promoter (Bad) and BH3 interacting-domain death agonist (Bid)). The Bcl-2 subfamily promotes cell survival whereas Bax and the BH3-only subfamily members are proapoptotic (84).

2.7.2 Autophagy

Autophagy is a compensatory mechanism that produces energy from damaged and/or redundant organelles and proteins which subsequently prevents the accumulation of waste products thereby maintaining homeostasis (85). In non-tumourigenic cells, autophagy maintains cellular homeostasis by clearing damaged organelles or misfolded proteins (86).

Macroautophagy (here-after referred to as autophagy) commences with an isolation membrane, also known as a phagophore which expands to engulf proteins and organelles, thus forming a double membrane structure, namely autophagosome (87). The elongation of the autophagosome is dependent on the autophagy-related genes (ATG) 12 & 5 aided by ATG 7 & 10. ATG 12 & 5 interacts with ATG 16 forming a complex and is subsequently added onto the phospholipids in the membrane, in a process that is similar to ubiqutination. ATG 4 protease aids the above-mentioned reaction and continues to cleave microtubule-associated protein 1A/1B-light chain 3 (LC3) which is further incorporated into the membrane subsequently closing the double membrane structure (88).

LC3 competes with LC3-I to bind to phosphatidylethanolamine (PE) in order to form LC3II on the surface of the autophagosomes (89). The autophagosomes fuse with lysosomes, promoting the degradation of autophagosomal contents by lysosomal

acid protease. Lysosomal permeases and transporters export amino acids and other by-products of degradation out to the cytoplasm, where they can be salvaged to produce macromolecules (90). However, the role of autophagy in cancer is complex and paradoxical as it is an adaptive process which is responsive to changes in the cellular microenvironment. Beclin 1 is a protein associated with autophagy and is essential for embryonic development and autophagy initiation in non-tumourigenic cells and if present is able to distinguish whether the fate of the cell is pro-death or pro-survival (91). Beclin 1 interacts with Bcl-xL resulting in autophagy inhibition suggesting the existence of a crosstalk between autophagy and apoptosis (92). Fingar, *et al* (2002*)* observed that deletion of mTOR reduces cell size and subsequent restoration of mTOR signaling also restores cell size thus suggesting that mTOR signaling regulates both cell cycle progression and cell growth/cell size (93).

Tumourigenic cells possess increased metabolism required for sustainable hyperproliferation resulting in glutamine deprivation (94). In addition to glutamine's bioenergetic role, glutamine also possesses non-anabolic functions pertaining to oxidative stress and cell survival. These additional responsibilities enhance the appeal of targeting glutamine metabolism in tumourigenic treatment (95). The knowledge pertaining to how tumourigenic- and non-tumourigenic cells adapt to glutamine deprivation is crucial to therapeutics targeting cancer cell metabolism. In addition, glutamine deficiency may affect non-tumourigenic response to antitumour treatment, and potentially could pre-sensitize tumourigenic cells to chemotherapeutic treatments. Thus, the aim of this research project was to investigate the differential signaling events exerted by glutamine deprivation on cell proliferation, morphology, oxidative stress, mitochondrial membrane potential, cell cycle progression, antioxidant defences, DNA damage, energy status, cell survival signaling and cell death via apoptosis and autophagy induction in breast cell lines.

2.8 OBJECTIVES

The *in vitro* influence of glutamine deprivation was investigated in tumourigenic breast cell lines and a non-tumourigenic cell line on:

1. cell proliferation by means of crystal violet staining and spectrophotometry.

2. morphology by means of haematoxylin and eosin staining using light microscopy.
3. superoxide and hydrogen peroxide- production by using 2, 7-dichlorofluoresceindiacetate (DCFDA) and dihydroethidine (DHE), respectively via flow cytometry.
4. the innate antioxidant system by demonstrating effects on catalase- and superoxide dismutase activity by means of spectrophotometry.
5. the energy status of cells by determining the AMP/AMPK ratio by means of spectrometry
6. cell survival by means of ERK phosphorylation and PI3K phosphorylation utilizing western blot.
7. DNA damage by investigating H2A phosphorylation and 8-hydroxyguanosine via confocal microscopy and fluorescent microscopy, respectively.
8. cell cycle progression by using propidium iodide and flow cytometry.
9. mitochondrial functioning by using Mitocapture ^{TM} and flow cytometry.
10. cell death induction via apoptosis induction by using flow cytometry and Annexin V-fluorescein isothiocyanate (FITC).
11. cell death induction via autophagy induction by using LC3II fluorescence

2.9 HYPOTHESIS

In this study, it was hypothesized that glutamine deprivation differentially affects proliferation, morphology, oxidative stress, cell survival, innate antioxidant systems, energy status, DNA damage, mitochondrial functioning, cell cycle progression, cell survival signaling and cell death induction in tumourigenic breast cell lines when compared to a non-tumourigenic breast cell line.

CHAPTER 3

3 MATERIALS

3.1 Cell lines

MCF-7 is an adherent tumourigenic luminal subtype A human breast cell line that is ER positive, PR positive and HER2 negative and is derived from a metastatic site (90). It is commercially available from American Type Culture Collection (ATCC) (Manassas, Virginia, United States of America). Cells were cultured in 75cm^2 tissue

culture flasks at 37°C and 5% CO_2 humidified atmospheric conditions in Dulbecco's Minimum Essential Medium Eagle (DMEM) supplemented with heat-inactivated dialysed fetal calf serum (56°C, 30 min), 100 U/ml penicillin G, 100 µg/ml streptomycin and fungizone (250 µg/l) (Sigma Chemical Co (St. Louis, Missouri, United States of America)) (96).

MDA-MB-231 is an adherent tumourigenic basal subtype human breast cell line that is ER negative, PR negative and HER2 negative and is derived from a metastatic site. It is commercially available from ATCC (Manassas, Virginia, United States of America). Cells were cultured 75cm^2 tissue culture flasks at 37°C and 5% CO_2 humidified atmospheric conditions in DMEM supplemented with heat-inactivated dialysed fetal calf serum (56°C, 30min), 100 U/ml penicillin G, 100 µg/ml streptomycin and fungizone (250 µg/l) (Sigma Chemical Co) (St. Louis, Missouri, United States of America)) (96).

BT-20 is an adherent tumourigenic basal subtype non-metastatic human breast cell that is ER negative, PR negative and HER2 negative. The BT-20 cell line was supplied by ATCC (Manassas, Virginia, United States of America). Cells were cultured in 75cm^2 tissue culture flasks at 37°C and 5% CO_2 humidified atmospheric conditions. BT-20 cells were cultured in growth medium consisting of a 1:1 mixture of DMEM and Ham's-F12 medium, 10% heat-inactivated dialysed fetal calf serum (56°C, 30 min), 100 U/ml penicillin G, 100 µg/ml streptomycin and fungizone (250 µg/l) (Sigma Chemical Co (St. Louis, Missouri, United States of America)) (97).

MCF-10A is an adherent non-tumourigenic basal subtype human breast cell line that is ER negative, PR negative and HER2 negative. It is commercially available from the ATCC (Manassas, Virginia, United States of America). Cells were cultured 75cm^2 tissue culture flasks at 37°C and 5% CO_2 humidified atmospheric conditions. MCF-10A cells were cultured in growth medium consisting of a 1:1 mixture of DMEM and Ham's-F12 medium, 20 ng/ml epidermal growth factor (EGF), 100 ng/ml cholera toxin, 10 µg/ml insulin and 500 ng/ml hydrocortisone, supplemented with 10% heat-inactivated dialysed fetal calf serum (56°C, 30 min), 100 U/ml penicillin G, 100 µg/ml streptomycin and fungizone (250 µg/l) (Sigma Chemical Co) (St. Louis, Missouri, United States of America) (98).

3.2 Reagents

All reagents were obtained from (Sigma Chemical Co) (St. Louis, Missouri, United States of America) unless otherwise specified. The Annexin V-FITC antibody and Mitocapture^{TM} were obtained from Biolegend (San Diego, California, United States of America) and Biovision (Milpitas, California, United States of America), respectively. Haematoxylin, eosin, propidium iodide, anti-ERK antibodies, monoclonal anti-ERK1 (pT202/pY204) antibody, anti-LC3II antibodies, anti-H2AX antibodies, dehydroethidium (DHE) and dichlorofluoresceindiacetate (DCFDA) were purchased from Sigma Chemical Co (St. Louis, Missouri, United States of America). Crystal violet dye was provided by Merck (Pty) Ltd (Johannesburg, Gauteng, South Africa). The SOD activity assay kit, human catalase activity kit simplestep and anti-8 hydroxyguanosine antibody were obtained from Abcam plc. (Cambridge, England, United Kingdom). The Phospho-AMPKa1 (Ser487) ELISA kit was purchased from RayBiotech, Inc. (Norcross, Georgia, United States of America).

3.3 Cell culture

Cells were grown and maintained in 75 cm^2 tissue culture flasks in a humidified atmosphere at 37°C, 5 % CO_2 in a Forma Scientific water-jacketed incubator (Ohio, United States of America). Cells were cultured in complete growth medium with glucose, glutamine, and sodium pyruvate supplemented with 10% heat-inactivated dialysed fetal calf serum (56 °C, 30 min), 100 U/ml penicillin G, 100 µg/ml streptomycin and fungizone (250 µg/l). Cells were grown in flasks to 80% confluence and then trypsinized and seeded according to each method specifications. The positive control for morphological studies comprised of cells propagated in complete growth medium containing actinomycin D (0.1µg/ml) for 48 h, all other experiments used 2-ethyl-3-O-sulphamoyl-estra1,3,5(10),15-tetraen-17-ol (ESE-15-ol) for 48 h as a positive control. Negative controls for exposure conditions comprised of cells propagated in complete growth medium. Exposure condition referred to cells propagated in DMEM not containing glutamine, but supplemented with heat-inactivated dialysed fetal calf serum, penicillin G, streptomycin and fungizone as mentioned above. For all experiments cells exposed to growth medium not containing glutamine were compared to cells propagated in complete growth medium containing glutamine for the same time period.

3.4 METHODS

3.4.1 CELL PROLIFERATION

3.4.1.1 Crystal violet staining (spectrophotometry)

Crystal violet was used to demonstrate the influence of glutamine deprivation on proliferation where the nuclei were stained with crystal violet, a triphenylmethane cation dye. Crystal violet thus allows for the quantification of cell number by intercalating with the DNA resulting in a purple colour that correlates with cell number in monolayer. Crystal violet staining is measured with spectrophotometry at a wavelength of 570 nm (99).

MCF-7-, MDA-MB-231-, BT-20- and MCF-10A cells were seeded in a 96 well plate at a density of 4000 cells per well. The plate was incubated overnight at 37°C to allow for cell attachment. Cells were washed with phosphate buffer saline (PBS) thrice and DMEM was replaced with DMEM not containing glutamine. Samples were incubated for 24 h, 48 h, 72 h and 96 h at 37°C and 5% CO_2 humidified atmospheric conditions since literature has shown that glutamine deprivation for these time intervals include optimal antiproliferative activity (100). Cells were fixed using 1% gluteraldehyde (100 µl) for 15 min at room temperature. Gluteraldehyde was discarded and cells were stained using 0.1% crystal violet (100 µl). The plate was incubated at room temperature for 30 min. Excess crystal violet was discarded and the plate was submersed under running water and the plate was left to dry. Crystal violet was solubilized by adding 0.2% Triton X-100 (200 µl) to the wells and the plate was incubated at room temperature for 1 h. Solubilized crystal violet solution (100 µl) was transferred to a new microtitre plate. The absorbance was determined at 570 nm using an EPOCH Microplate Reader (Biotek Instruments, Inc. (Winooski, Vermont, United States of America)) (99)

3.4.2 MORPHOLOGY

3.4.2.1 Haematoxylin and eosin staining (light microscopy)

Haematoxylin and eosin staining was used to determine the effects of glutamine starvation on cell morphology and mitotic indices were also determined. Haematoxylin stains the nucleus blue, whilst eosin stains the cytoplasm pink (101).

Haematoxylin and eosin staining also allows for the identification of different mitotic phases which include interphase (dispersed chromosome), prophase (condensed chromosomes), anaphase (chromosomes at spindle poles), metaphase (chromosomes aligned at metaplate), telophase (uncoiling of chromosomes, formation of new nuclei) and also allows for the identification of apoptotic bodies and shrunken- and elongated cells (101). Quantitative data for mitotic indices was obtained by counting 1000 cells on each slide of the biological replicates (repeated three times) and expressing data as a percentage of cells in each phase of interphase, mitosis (anaphase, metaphase, telophase and prophase) and cells demonstrating abnormal characteristics including cell elongation, blebbing, apoptotic bodies.

MCF-7-, MDA-MB-231-, BT-20- and MCF-10A cells were seeded on heat-sterilized coverslips in a six well plate with a cell density of 200 000 cells per well and left overnight to attach. Cells were washed with PBS three times and DMEM was replaced with DMEM not containing glutamine. Samples were incubated for 24 h, 48 h, 72 h and 96 h at 37°C and 5% CO_2 humidified atmospheric conditions. Coverslips were moved to staining dishes and samples were exposed to Bouin's fixative for 30 min. The fixative was discarded and subsequently 70% ethanol was added to the coverslips and left for 20 min at room temperature. Coverslips were washed with distilled water and haematoxylin was added. Samples were incubated at room temperature for 20 min and the haematoxylin was subsequently discarded. Coverslips were washed with distilled water followed by the addition of 70% ethanol for 5 min. Ethanol was discarded and 1% of eosin was added and left for 5 min. The eosin was discarded and the coverslips were rinsed twice with 70% ethanol, 96% ethanol, 100% ethanol and xylol for 5 min each. Coverslips were mounted on microscope slides using Entelan. Photos were taken with a Zeiss Axiovert MRc microscope (Zeiss, Oberkochen, Germany) (101).

3.4.3 OXIDATIVE STRESS

3.4.3.1 Superoxide generation using dehydroethidium (flow cytometry)

Flow cytometry and dehydroethidium (DHE) were used to determine how glutamine deprivation influences superoxide production as an indicator of oxidative stress. A unique red fluorescent product, 2-hydroethidine cation, is produced by oxidation of DHE. DHE is oxidized by superoxide and not by hydroxyl radicals, singlet O_2 or nitrogen radicals (102).

MCF-7-, MDA-MB-231-, BT-20- and MCF-10A cells were seeded at 500 000 cells per T25 cm^2 flask and left overnight to attach. Cells were washed with PBS thrice and DMEM was replaced with DMEM not containing glutamine. Samples were incubated for 24 h, 48 h, 72 h and 96 h at 37°C and 5% CO_2 atmospheric conditions. Cells were trypsinized and collected in 15 ml conical tubes. After centrifugation, DHE (0.5 µl:0.5 ml PBS) was added to the samples and incubated 15 min at 25°C. The fluorescent product was measured with a FC500 System flow cytometer (Beckman Coulter South Africa (Pty) Ltd) (Pretoria, Gauteng, South Africa)) using CXP software (Beckman Coulter South Africa (Pty) Ltd) (Pretoria, Gauteng, South Africa)). Data generated from at least 10 000 cells was analyzed by means of Cyflogic version 1.2.1 software from Perttu Terho & Cyflo Ltd (Pertu Therho, Turko, Finland) (103).

3.4.3.2 Hydrogen peroxide generation using 2, 7-dichlorofluoresceindiacetate (flow cytometry)

The influence of glutamine on hydrogen peroxide was quantified as an indicator of oxidative stress. Hydrogen peroxide production was measured using 2, 7-dichlorofluoresceindiacetate (DCFDA). DCFDA, a non-fluorescence probe, is oxidized by ROS and peroxides to DCF, a fluorescent derivative that can be detected by maximum excitation and emission spectra of 495 nm and 529 nm. DCF compounds trapped in cells by deacetylation pass through the cytoplasm to ensure specific binding hydrogen peroxide (103).

MCF-7-, MDA-MB-231- , BT-20- and MCF-10A cells were seeded at 500 000 cells per T25 cm^2 flask and left overnight to allow for attachment. Cells were washed with

PBS thrice and DMEM was replaced with DMEM not containing glutamine. Samples were incubated for 24 h, 48 h, 72 h and 96 h at 37°C and 5% CO_2 atmospheric conditions. Cells were trypsinized and collected in 15 ml conical tubes. After centrifugation (500 g), DCFDA (0.5 µl: 0.5 ml PBS) was pipetted to all samples and samples were incubated for 25 min at 37°C, 5% CO_2 atmospheric conditions. The DCF fluorescent product was measured with a FC500 System flow cytometer (Beckman Coulter South Africa (Pty) Ltd) (Pretoria, Gauteng, South Africa)) using CXP software (Beckman Coulter South Africa (Pty) Ltd) (Pretoria, Gauteng, South Africa)). Data generated from at least 10 000 cells was analyzed by means of Cyflogic version 1.2.1 software from Perttu Terho & Cyflo Ltd (Pertu Therho, Turko, Finland) (103).

3.4.4 ANTIOXIDANT ACTIVITY

3.4.4.1 Superoxide dismutase activity (spectrophotometry)

The influence of glutamine deprivation on the cells' innate antioxidant systems was investigated by quantifying superoxide dismutase (SOD). SOD is an antioxidant enzyme involved in the defence system against ROS. SOD catalyses the reaction of superoxide radical anion to hydrogen peroxide (104). Quantification of SOD was used as an indication of the cells' innate antioxidant defence systems present when the cells are deprived of glutamine thus also confirming the possibility of oxidative stress.

MCF-7-, MDA-MB-231-, BT-20- and MCF-10A cells were seeded at 500 000 cells per T75 cm^2 flasks and left overnight to allow for attachment. Cells were washed with PBS thrice and DMEM were replaced with DMEM not containing glutamine. Samples were incubated for 24 h, 48 h, 72 h and 96 h at 37°C and 5% CO_2 atmospheric conditions. Cells were trypsinized and samples were lysed in ice cold 0.1M Tris/HCl, (pH 7.4) containing 0.5% triton X-100, 5mM β-ME and 0.1 mg/ml PMSF. Samples were centrifuged at 14,000 x *g* for 5 minutes at 4°C. The supernatant was transferred to clean tubes and samples were kept on ice. WST working solution (200 µL) (provided by supplier) was added to each well. Dilution buffer (20 µL) (provided by supplier) was added to Blank 2 and Blank 3. Enzyme working solution (20 µL) (provided by supplier) was added to each sample well and Blank 1. The samples

were mixed well and incubated for 1 hour on the plate shaker at 400 rpm (covered in foil). After the incubation period, the plate was read at 450 nm using an EPOCH Microplate Reader (Biotek Instruments, Inc. (Winooski, Vermont, United States of America)). The SOD inhibition rate was calculated using the following equation:

SOD Activity (inhibition rate %) = $\frac{(Ablank1-Ablank3)-(Asample-Ablank2)}{(Ablank1-Ablank3)}$ x 100 %.

(105).

3.4.4.2 Catalase activity (spectrophotometry)

The influence of glutamine deprivation on the cells' innate antioxidant systems were investigated by quantifying catalase. Hydrogen peroxide is catalysed to water and oxygen by catalase and thus protects the cell from oxidative stress (106).

MCF-7-, MDA-MB-231-, BT-20- and MCF-10A cells were seeded at 2 000 000 cells per T75 cm^2 flasks and left overnight to allow for attachment. Cells were washed with PBS thrice and DMEM were replaced with DMEM not containing glutamine. Samples were incubated for 24 h, 48 h, 72 h and 96 h at 37°C and 5% CO_2 atmospheric conditions. Cells were scraped and samples were placed in ice-cold 0.1 M Tris/HCl, (pH 7.4) containing 0.5% triton X-100, 5 mM β-mercaptoethanol and 0.1 mg/ml PMSF. Cells were centrifuge at 14 000 x *g* for 5 min at 4°C. Supernatant were discarded and samples were transferred to new eppendorfs and kept on ice. WST (200 µl) working solution (provided by supplier), dilution buffer (20 µl) (provided by supplier) and enzyme working solution (200 µl) (provided by supplier) were added to each well. Samples were mixed and incubated at 37°C for 20 min. The absorbance was measured at 450 nm using an EPOCH Microplate Reader (Biotek Instruments, Inc. (Winooski, Vermont, United States of America)) (107). A standard curve created by using catalase standards (provided by supplier) was used to extrapolate the protein concentration of each sample.

3.4.5 ENERGY STATUS

3.4.5.1 5' Adenosine monophosphate protein kinase activation (spectrometry)

The influence of glutamine deprivation on the energy state of the cell was determined by quantifying the AMP-activated protein kinase activity. AMPK plays a fundamental

role in the regulation of energy homeostasis by controlling phosphorylation and dephosphorylating of adenosine molecules and subsequent change in energy production (108). AMPK is activated by an elevation of AMP/ATP ratio signifying an energy deficit due to cellular stress including nutrient deprivation, metabolic stress and oxidative stress (109).

MCF-7-, MDA-MB-231-, BT-20- and MCF-10A cells were seeded at 2 000 000 cells per T75 cm^2 flasks and left overnight to allow for attachment. Cells were washed with PBS thrice and DMEM were replaced with DMEM not containing glutamine. Samples were incubated for 24 h, 48 h, 72 h and 96 h at 37°C and 5% CO_2 atmospheric conditions. Medium was removed and cells were washed once in PBS. Cell lysate buffer (provided by supplier) was added to the cells; cells were resuspended and incubated thereafter for 30 min on ice. Cells were centrifuge at 14 000 x *g* for 5 min at 4°C. Supernatant were discarded and samples were transferred to new eppendorfs and kept on ice. Samples (100 µl) were added to each well. The primary anti-Phospho antibody (100 µl) was added to each well and samples were incubated for 1 h at room temperature. Thereafter, prepared 1X horseradish peroxidase-conjugated secondary antibody (100 µl) was added to each well and incubated for 1 h at room temperature. TMB one-step substrate reagent (100 µl) was added to each well. Samples were then incubated for 30 min at room temperature. Stop solution (100 µl) was subsequently added to each well. The absorbance was measured at 450 nm using an EPOCH Microplate Reader (Biotek Instruments, Inc. (Winooski, Vermont, United States of America)) (110).

3.4.5 SURVIVAL SIGNALING

3.4.5.1 Extracellular-signal-regulated kinase (ERK) phosphorylation (western blot)

The influence of glutamine deprivation on ERK phosphorylation was investigated as an indicator of cell survival signaling. ERK is a pro-survival pathway which is also associated with proliferation and motility by means of upregulating cell cycle factors including cyclins (111).

MCF-7-, MDA-MB-231-, BT-20- and MCF-10A cells were seeded at 200 000 cells per well in a 6 well plate and left overnight to attach. Cells were washed with PBS thrice and DMEM was replaced with DMEM not containing glutamine. Samples were incubated for 24 h, 48 h, 72 h and 96 h at 37°C and 5% CO_2 humidified atmospheric conditions. Subsequently, the medium was removed and cells were washed with PBS. Protease inhibitor (1:100), sodium orthovandate $NaVO_4$ (1:100) and radioimmunoprecipitation assay (RIPA) buffer containing 1mM Tris-Cl (pH 8.0), 1 mM ethylenediaminetetraacetic acid (EDTA), 1% Triton X-100, 0.1% sodium deoxycholate, 0.1% SDS, 140 mM NaCl and 1 mM phenylmethane sulfonyl flouride (PMSF) were made as lysis buffer and were added to each well (150 µl). Cells were scraped together and passed through a syringe in order to lyse cells. Cell lysates were heated to 80°C for 10 min and then centrifuged at 8117 x *g* for 15 min. Supernatants were loaded onto 4-12% sodium dodecyl sulphate polyacrylamide gel electrophoresis (SDS-PAGE) gels. After resolving proteins on the gel, samples were transferred onto a 0.2 µm polyvinylidene fluoride (PVDF) membrane overnight at 60 V. Membranes were blocked in 2% bovine serum albumin (BSA) before being incubated with a 1:1000 dilution of monoclonal anti-ERK1 (pT202/pY204) antibody and 1:10000 dilution of the monoclonal actin antibody for 1 h and secondary goat anti-mouse horseradish peroxidase antibody for 1 h with washes in between using PBS-tween. Proteins were visualized using enhanced chemiluminescence substrate and the Biorad Chemidoc MP system (Bio-Rad Laboratories, Inc. (California, United States of America). Bands were quantified and ratios of ERK to actin were calculated using Image Lab™ software version 5.2.1 developed by Bio-Rad Laboratories Inc. (Hercules, California, United States of America) (112).

3.4.5.2 Phosphoinositide 3-kinase phosphorylation (western blot)

The influence of glutamine deprivation on phosphoinositide 3-kinase phosphorylation (PI3K) phosphorylation was also investigated as an indicator of cell survival signaling. PI3K phosphorylates PI, phosphatidylinositol-4, 5-bisphoshate (PIP), PIP2 and PIP3. Growth factors and hormones activate PI3K to coordinate various cellular events including cell growth, cell cycle entry, cell migration and cell survival (113).

MCF-7-, MDA-MB-231-, BT-20- and MCF-10A cells were seeded at 200 000 cells per well in a 6 well plate and left overnight to attach. Cells were washed with PBS thrice and DMEM was replaced with DMEM not containing glutamine. Samples were incubated for 24 h, 48 h, 72 h and 96 h at 37°C and 5% CO_2 humidified atmospheric conditions. The medium was removed and cells were carefully washed with PBS. Protease inhibitor (1:100), sodium orthovandate $NaVO_4$ (1:100) and RIPA buffer (1mM Tris-Cl (pH 8.0), 1 mM EDTA, 1% Triton X-100, 0.1% sodium deoxycholate,0.1% SDS, 140 mM NaCl and 1 mM PMSF) were made as lysis buffer and were added to each well (150 µl). Cells were scraped together and passed through a syringe in order to lyse cells. Cell lysates were heated to 80°C for 10 min and then centrifuged at 8117 x *g* for 15 min. Supernatants were loaded onto 4-12% SDS-PAGE gels. After resolving proteins on the gel, samples were transferred onto a 0.2 µm PVDF membrane overnight at 60 V. Membranes were blocked in 2% BSA before being incubated with 1:1000 dilution of monoclonal anti-Pi3K kinase p85 antibody and 1:10000 dilution of the monoclonal actin antibody for 1 h and secondary goat anti-mouse horseradish peroxidase antibody for 1 h with washes in between with PBS-tween. Proteins were visualized using enhanced chemiluminescence substrate and the Biorad Chemidoc MP system (Bio-Rad Laboratories, Inc. (California, United States of America). Bands were quantified of ratios of PI3K to actin were calculated using Image Lab™ software version 5.2.1 developed by Bio-Rad Laboratories Inc. (Hercules, California, United States of America) (112).

3.4.6 DEOXYRIBONUCLEIC ACID DAMAGE

3.4.6.1 Anti-8 hydroxyguanosine visualisation (fluorescent microscopy)

The effects of glutamine deprivation on DNA damage was investigated by visualising 8-hydroxyguanosine formation. 8-Hydroxyguanosine is a modified base that occurs in DNA due to damage by hydroxyl radicals formed during aerobic metabolism and oxidative stress (114).

MCF-7-, MDA-MB-231-, BT-20- and MCF-10A cells were seeded at 50 000 cells per well in a 24 well plate and left overnight to allow for attachment. Cells were washed with PBS thrice and DMEM was replaced with DMEM not containing glutamine. Samples were incubated for 24 h, 48 h, 72 h and 96 h at 37°C and 5% CO_2

atmospheric conditions. The medium was removed and cells were washed with PBS. Cells were fixed in 2% paraformaldehyde for 20 min. Samples were washed with distilled water three times and permeabilized with 0.2% triton X-100 for 5 min. Samples were blocked with 2% BSA in PBS for 1 h. Samples were subsequently incubated with anti-8 hydroxyguanosine for 1 h at room temperature (1:50 dilution). Cells were washed with PBS and incubated with anti-mouse alexa 488 donkey antibodies and 4′,6-diamidino-2-phenylindole (DAPI) for 1 h at room temperature. After washing with PBS, coverslips were mounted using mounting fluid. Photos were taken with the appropriate filters in a dark room to prevent quenching. Zeiss Axiovert CFL40 microscope and the Zeiss Axiovert MRm monochrome camera (Zeiss, Oberkochen, Germany) were employed with a Zeiss filter 2 for DAPI stained blue-cells and a Zeiss filter 9 for the 8 hydroxyguanosine-stained (green) cells. At least 1000 cells were measured per condition in each experiment and the graymean value was calculated to achieve a ratio (115).

3.4.6.2 H2A phosphorylation visualisation (confocal microscopy)

The effects of glutamine deprivation on DNA damage was investigated by visualising H2A phosphorylation. Oxidative stress frequently results in DNA damage associated with phosphorylated H2A. H2A is phosphorylated, activated and recruited to sites of double stranded breaks (DSB) after oxidative damage as part of the DNA repair mechanism (116).

MCF-7-, MDA-MB-231-, BT-20- and MCF-10A cells were seeded on heat-sterilized coverslips at 50 000 cells per well in a 24 well plate and left overnight to allow for attachment. Cells were washed with PBS thrice and DMEM was replaced with DMEM not containing glutamine. Samples were incubated for 24 h, 48 h, 72 h and 96 h at 37°C and 5% CO_2 atmospheric conditions. The medium was removed and cells were washed once with PBS. Cells were fixed in 2% paraformaldehyde for 15 min. Slides were washed with PBS and permeabilized with 0.2% triton X-100. Samples were subsequently blocked with 2% BSA in PBS for 1 h. Thereafter, samples were incubated with primary antibody against phosphorylated H2A for 1 h at room temperature. Cells were washed with PBS and incubated with fluorescein isothiocyanate (FITC)-conjugated anti-mouse secondary antibodies and DAPI, dihydrochloride for 1 h at room temperature. After washing with PBS, coverslips were

mounted using mounting fluid. Slides were examined using a Zeiss LSM510 Meta confocal (Centre of Neurosciences, Pretoria, South Africa) microscope furnished with a 63x magnification oil objective. Images were analyzed using Image J software developed by the National Institutes of Health (Bethesda, Maryland, United States of America) (117).

3.4.7 CELL CYCLE PROGRESSION

3.4.7.1 Propidium iodide staining (flow cytometry)

The effects of glutamine deprivation on cell cycle progression and cell death induction was investigated by means of ethanol fixation, propidium iodide and flow cytometry. Propidium iodide stains the DNA and thus enables the quantification of DNA correlating with stages of the cell cycle during cell division (118).

MCF-7-, MDA-MB-231-, BT-20- and MCF-10A cells were seeded at 500 000 cells per T25 cm^2 flask and left overnight to allow for attachment. Cells were washed with PBS thrice and DMEM was replaced with DMEM not containing glutamine. Samples were incubated for 24 h, 48 h, 72 h and 96 h at 37°C and 5% CO_2 atmospheric conditions. Subsequently, cells were trypsinized and resuspended in 1 ml PBS. Cells were centrifuged for 5 min at 300 x *g*. The supernatant was discarded and cells were resuspended in ice-cold PBS (200 µl) containing 0.1% FCS. Ice-cold 70% ethanol (4 ml) was added in a drop-wise manner and samples were stored at 4°C for 24 h. Cells were centrifuged at 300 x *g* for 5 min and the supernatant was removed. Cells were resuspended in 1 ml PBS containing propidium iodide (40 µg/ml), RNAse A (100 µg/ml) and triton X-100 (0.1%) and incubated at 37°C for 45 min. Propidium iodide fluorescence was measured using a FC500 System flow cytometer (Beckman Coulter South Africa (Pty) Ltd) (Pretoria, Gauteng, South Africa)) using CXP software (Beckman Coulter South Africa (Pty) Ltd) (Pretoria, Gauteng, South Africa)). Data from cell debris particles) and clumps of 2 or more cells were removed from further analysis. Cell cycle distributions were calculated with Cyflogic version 1.2.1 software from Perttu Terho & Cyflo Ltd (Pertu Therho, Turko, Finland) by assigning relative DNA content per cell to sub-G_1, G_1, S and G_2/M fractions (103).

3.4.8 MITOCHONDRIAL MEMBRANE POTENTIAL

3.4.8.1 Mitocapture™ (flow cytometry)

The effect of glutamine deprivation on the mitochondrial membrane potential was investigated using Mitocapture™. The cationic dye, 5,5',6,6'-tetrachloro-1,1',3,3'-tetraethylbenzimidazolylcarbocyanine iodide is provided in the Mitocapture™ Kit and fluoresces a bright red colour when bound to cells possessing a polarised or hyperpolarised mitochondrial membrane potential whereas cells possessing depolarised mitochondrial membrane potential fluoresce green (119).

MCF-7-, MDA-MB-231-, BT-20- and MCF-10A cells were seeded at 500 000 cells per T25 cm^2 flask and left overnight to allow for attachment. Cells were washed with PBS thrice and DMEM was replaced with DMEM not containing glutamine. Samples were incubated for 24 h, 48 h, 72 h and 96 h at 37°C and 5% CO_2 atmospheric conditions. Cells were trypsinized and centrifuged at 13 000 x *g.* Cells were resuspended in diluted Mitocapture solution (1 µl mitocapture: 1 ml pre-warmed incubation buffer) and incubated for 20 min at room temperature. Cells were centrifuged at 500 x *g*, the supernatant was discarded and cells were resuspended in 1 ml pre-warmed incubation buffer (37°C). Cells were analyzed with a FC500 System flow cytometer (Beckman Coulter South Africa (Pty) Ltd) (Pretoria, Gauteng, South Africa)) using CXP software (Beckman Coulter South Africa (Pty) Ltd) (Pretoria, Gauteng, South Africa)). Data generated from at least 10 000 cells was analyzed by means of Cyflogic version 1.2.1 software from Perttu Terho & Cyflo Ltd (Pertu Therho, Turko, Finland) (120).

3.4.9 CELL DEATH

3.4.9.1 Apoptosis induction using Annexin V- fluorescein isothiocyanate (flow cytometry)

The influence of glutamine deprivation on apoptosis and necrosis was evaluated and quantified using flow cytometry in combination with Annexin V-FITC and propidium iodide. Cells possess several phospholipids between inner and outer portions of the plasma membrane. The latter is regulated by phospholipid translocases that are lipid specific and require ATP for translocation. Phosphatidylserine is mainly located in the

inner membrane facing the cytosol (121). In apoptosis, the calcium-dependent phospholipids scramblase activity is activated which results in the scrambling of the aminophospholipids over the inner- and outer membrane and subsequent loss of the plasma membrane organisation. This process is aided by an enzyme named flippase and results in the externalization of the phosphatidylserine layer of the cell membrane thus providing Annexin V a binding site (122). Propidium iodide is membrane impermeable and thus only enters the cell when the membrane is compromised due to apoptosis or necrosis (123).

MCF-7-, MDA-MB-231-, BT-20- and MCF-10A cells were seeded at 500 000 cells per T25 cm^2 flask and left overnight to allow for attachment. Cells were washed with PBS thrice and DMEM was replaced with DMEM not containing glutamine. Samples were incubated for 24 h, 48 h, 72 h and 96 h at 37°C and 5% CO_2 atmospheric conditions. Cells were trypsinized and resuspended in 1x binding buffer (1 ml) and centrifuged at 300 x *g* for 10 min. The supernatant was removed and cells were resuspended in 1x binding buffer (100 µl). Annexin V-FITC (2.5 µl) was added and samples were incubated for 15 min in the dark at room temperature. Cells were washed by adding 1x binding buffer (1 ml) and thereafter cells were centrifuged at 300 x *g* for 10 min. The supernatant was pipetted off and cells were resuspended in of 1x binding buffer (500 µl). Immediately prior to analysis, 12.5 µl propidium iodide (40 µg/ml) was added and gently mixed. Propidium iodide fluorescence and Annexin V FITC fluorescence were analyzed with a FC500 System flow cytometer (Beckman Coulter South Africa (Pty) Ltd) (Pretoria, Gauteng, South Africa)) using CXP software (Beckman Coulter South Africa (Pty) Ltd) (Pretoria, Gauteng, South Africa)). Data generated from at least 10 000 cells were analyzed by means of Cyflogic version 1.2.1 software from Perttu Terho & Cyflo Ltd (Pertu Therho, Turko, Finland) (118).

3.4.9.2 Autophagy induction using LC3 Microtubule-Associated Protein 1A/1B-Light Chain 3 visualisation

The influence of glutamine deprivation on autophagy induction was demonstrated by means of light chain 3 (LC3II) visualisation. Autophagy is induced by a variety of insults including stress, starvation and oxidative stress. The autophagy protein light LC3 is a mammalian protein is associated with the autophagosome membranes and used to identify autophagy induction. LC3-I is cytosolic whilst LC3-II is found in the

membrane and predominates the autophagic vacuole. LC3-I conversion to LC3-II serves as a standard marker for autophagy induction (124).

MCF-7-, MDA-MB-231-; BT-20- and MCF-10A cells were seeded at 200 000 cells per well in a 6 well plate and left overnight to allow for attachment. Cells were washed with PBS thrice and DMEM were replaced with DMEM not containing glutamine. Samples were incubated for 24 h, 48 h, 72 h and 96 h at 37°C and 5% CO_2 atmospheric conditions. Medium were removed and cells were washed twice with PBS. The cells were permeabilized with 4% paraformaldehyde for 20 min. The samples were further blocked in 2% milk for an hour. Wash with PBS three times. The anti-LC3B antibody was added to the samples at a dilution of 1:100 000 and incubated for 90 min. The samples are then washed twice with PBS and the secondary antibody was added at 1:10 000 dilution together with DAPI. Samples were then incubated at room temperature for an hour. Samples were then visualised with a Zeiss Axiovert MRc microscope (Zeiss, Oberkochen, Germany) employing a Zeiss filter 2 for blue stained cells detection and a Zeiss filter 9 for green stained cells (125).

3.5 Logistics

All the required equipment were available and all relevant techniques and protocols were standardized in the Department of Physiology (University of Pretoria). The cell culture laboratory of the Department of Physiology at the University of Pretoria was used to conduct the research project. Flow cytometry was done at the Department of Pharmacology (University of Pretoria). Confocal Microscopy was conducted at the Centre for Neuroendocrinology. Dr MH Visagie (University of Pretoria) was consulted on all the required techniques.

3.6 Statistical analysis

All experiments were repeated three times in which the mean and standard deviation were calculated. Means were illustrated by bar charts and standard deviations were shown with errors bars. A *P*-value< 0.05 were used for statistically significance calculated by means of the Student t-test in excel statistically significant and were indicated by an asterisk (*). Qualitative data was obtained from confocal, light and fluorescent microscopy. Quantitative data was supplied by means of cell number

determination, western blot, flow cytometry and calamatric assays. Data for mitotic indices was obtained by counting 1000 cells on each slide of the biological replicates (repeated three times) and expressing data as a percentage of cells in each phase of mitosis, interphase and abnormal cells. Three independent experiments (cell number determination conducted with six replicates) was conducted where the mean ±SD was calculated. Flow cytometry analysis involved at least 10 000 events and was repeated three times. Flow cytometry data was analyzed using Cyflogic version 1.2.1 software (Pertu Therho, Turko, Finland).

Ethical Approval

This research protocol was approved by the Research Ethics Committee (328/2017).

CHAPTER 4

4. RESULTS

4.1 Cell proliferation

The effects of glutamine deprivation on cell growth were assessed using crystal violet staining and spectrometry. Crystal violet is a cationic dye that binds to the DNA of the cell where the staining intensity of the cells is directly proportional to the cell number quantity (99, 126). Thus, crystal violet staining provides us with an effective manner to evaluate cell growth.

Spectrophotometry results of crystal violet staining indicated a time-dependent decrease in proliferation after glutamine deprivation in both tumourigenic both MCF-7 and MDA-MB-231 cell lines (Figure 5). MCF-7 cells showed 87%, 80%, 69%, 62% cell growth after 24 h, 48 h, 72 h and 96 h deprivation from glutamine, respectively. MDA-MB-231 cells showed 93%, 90%, 88% and 78% cell growth after 24 h, 48 h, 72 h and 96 h deprivation from glutamine, respectively. MCF-10A cells showed 108%, 94%, 98% and 89% cell growth after 24 h, 48 h, 72 h and 96 h deprivation from glutamine, respectively. BT-20 cell growth decreased to 86% after 24 h of glutamine deprivation and remained unchanged thereafter. These results suggest tumourigenic cell lines are more prominently affected by glutamine starvation when compared to the non-tumourigenic cell line. Furthermore, the tumourigenic breast oestrogen receptor positive luminal cell line (MCF-7) was most affected by glutamine deprivation when compared to the tumourigenic breast oestrogen receptor negative basal metastatic cell line (MDA-MB-231).

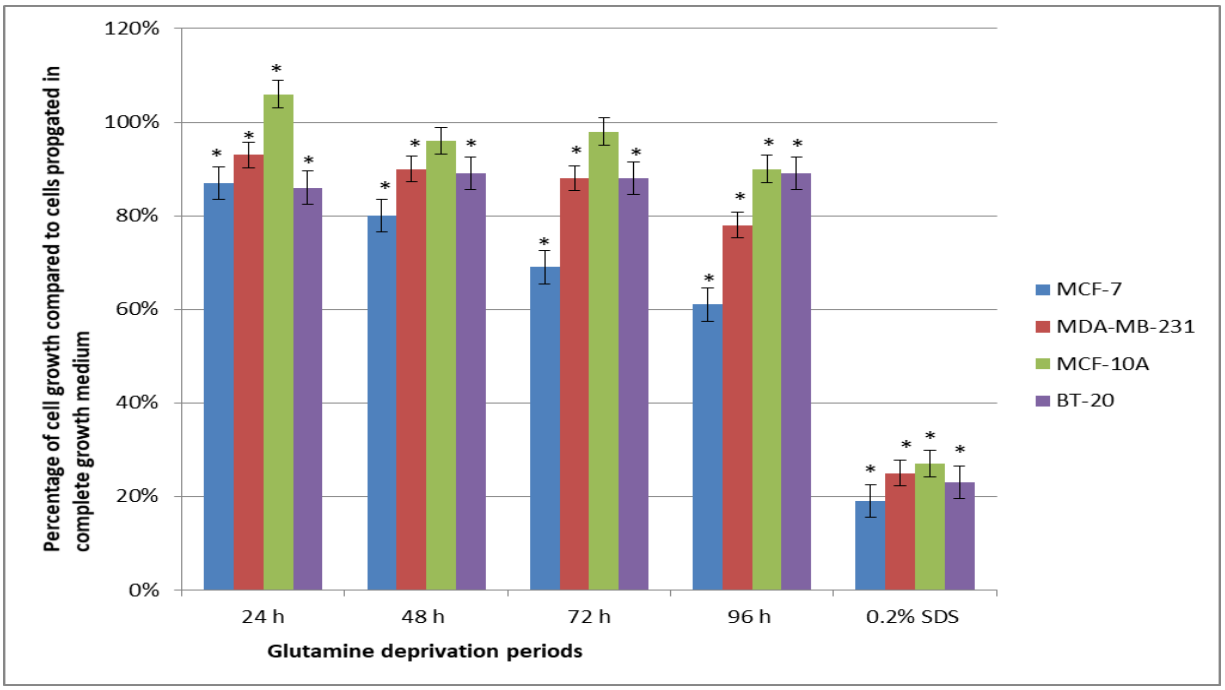

Figure 5: Graph illustrating cell growth after 24 h, 48 h, 72 h and 96 h of glutamine deprivation in MCF-7-, MDA-MB-231-, MCF-10A- and BT-20 cell lines when compared to cells propagated in complete growth medium. The MCF-7 cell line showed to be most prominently affected by glutamine deprivation after 96 h where cell growth was observed to be 62%. An asterisk (*) indicates significance with *p*-value < 0.05 when calculated by means of the student's t-test when compared to cells propagated in complete medium. Cells were treated with 0.2 % of sodium dodecyl sulphate (SDS) as a positive control for anti- proliferative activity detection.

4.2 Morphology

Light microscopy was used to visualize effects of glutamine deprivation on morphology by means of haematoxylin and eosin stained samples (Figure 6-10). Haematoxylin, a basic dye, binds to basophilic, acidic and negatively charged substances such as DNA. Eosin, an acidic dye, binds to proteins located in the cytoplasm (127). Glutamine deprivation resulted in compromised cell density in the MCF-7- and MDA-MB-231 cell lines when compared to cells propagated in complete growth medium. In addition, glutamine deprivation resulted in a non-significant increase in elongated cells ($p>0.05$) and shrunken cells ($p>0.05$) in MCF-7- and MDA-MB-231 cell lines. Mitotic indices were quantified however, a non-significant difference between cells propagated in complete growth medium and cells deprived of glutamine was observed, and thus no significant effect was caused by glutamine deprivation on the mitotic phases and morphology (Table 1-4).

MCF-7 cells propagated in complete growth medium 24 h	MCF-7 cells deprived of glutamine for 24 h
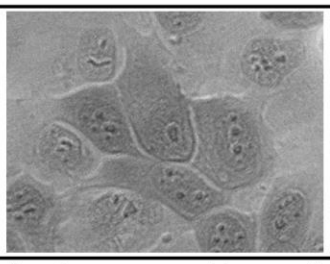	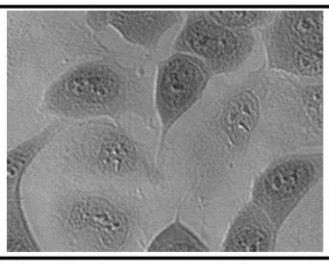
MCF-7 cells propagated in complete growth medium 48 h	MCF-7 cells deprived of glutamine for 48 h
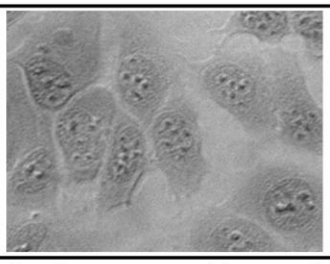	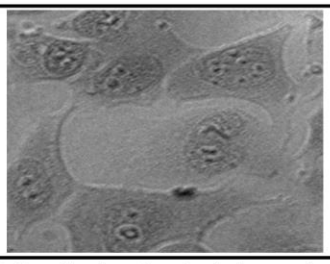
MCF-7 cells propagated in complete growth medium 72 h	MCF-7 cells deprived of glutamine for 72 h
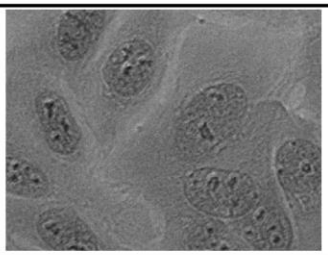	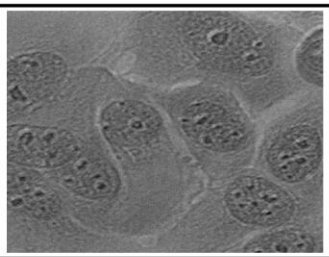
MCF-7 cells propagated in complete growth medium 96 h	MCF-7 cells deprived of glutamine for 96 h
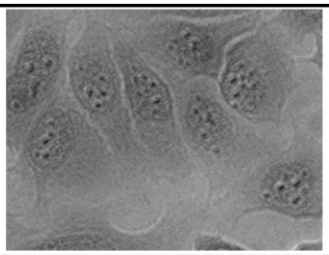	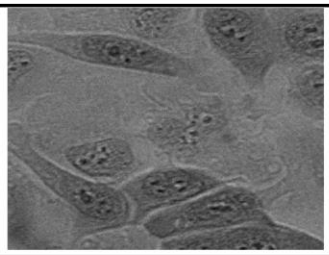

Figure 6: Morphology of the MCF-7 cell line after 24 h, 48 h, 72 h and 96 h of glutamine deprivation compared to MCF-7 cells propagated in complete growth medium 24 h, 48 h, 72 h and 96 h. Starvation of glutamine for (48 h, 72 h and 96 h) resulted in minor decreased cell density and the appearance of elongated cells when compared to cells propagated in growth medium (20X magnification).

MDA-MB-231 cells propagated in complete growth medium 24 h	MDA-MB-231 cells deprived of glutamine for 24 h
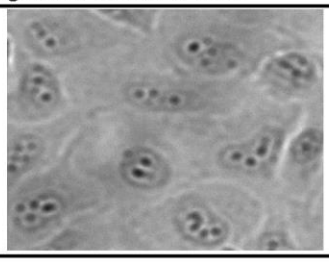	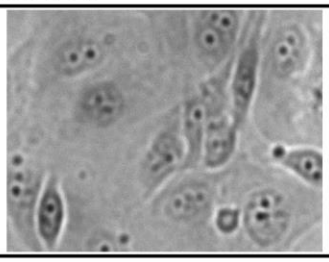
MDA-MB-231 cells propagated in complete growth medium 48 h	MDA-MB-231 cells deprived of glutamine for 48 h
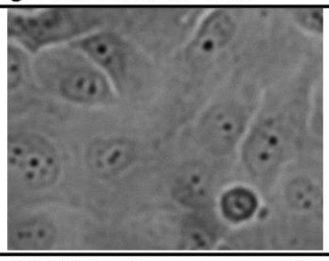	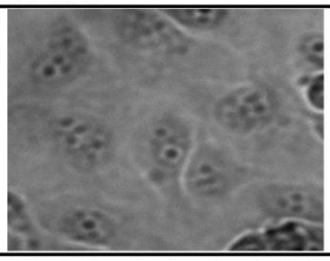
MDA-MB-231 cells propagated in complete growth medium 72 h	MDA-MB-231 cells deprived of glutamine for 72 h
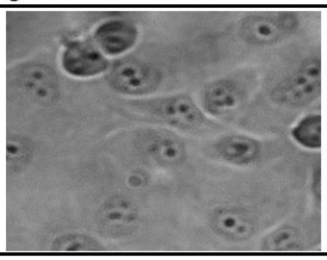	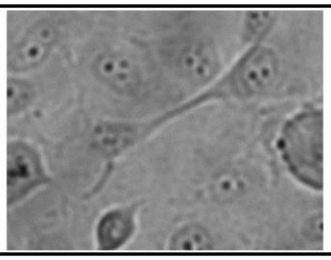
MDA-MB-231 cells propagated in complete growth medium 96 h	MDA-MB-231 cells deprived of glutamine for 96 h
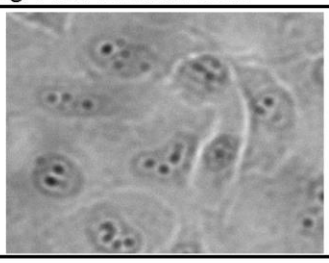	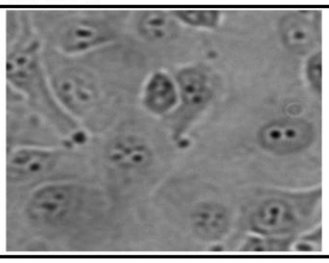

Figure 7: Morphology of the MDA-MB-231 cell line after 24 h, 48 h, 72 h and 96 h of glutamine deprivation compared to MDA-MB-231 cells propagated in complete growth medium 24 h, 48 h, 72 h and 96 h. Glutamine deprivation for 96 h decreased cell density slightly when compared to cells propagated in complete growth medium. No other significant changes in morphology were observed after glutamine deprivation when compared to cells propagated in complete growth medium (20X magnification).

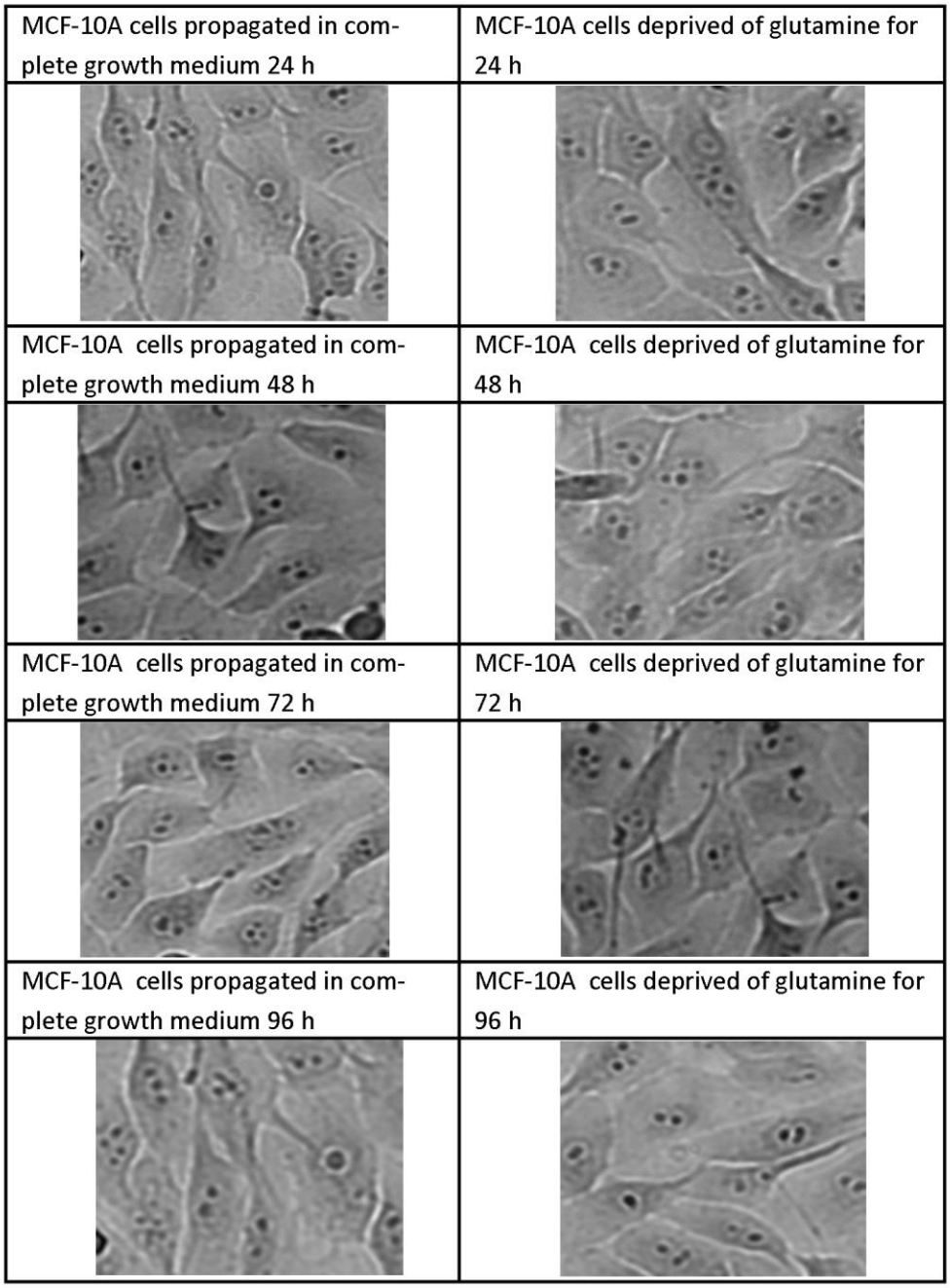

Figure 8: Morphology of the MCF-10A cell line after 24 h, 48 h, 72 h and 96 h of glutamine deprivation compared to MCF-10A cells propagated in complete growth medium 24 h, 48 h, 72 h and 96 h. Glutamine deprivation for 72 h and 96 h decreased cell density slightly when compared to cells propagated in complete growth medium. Furthermore, MCF-10A cells appeared rounded following glutamine deprivation when compared to cells propagated in complete growth medium (20X magnification).

BT-20 cells propagated in complete growth medium 24 h	BT-20 cells deprived of glutamine for 24 h
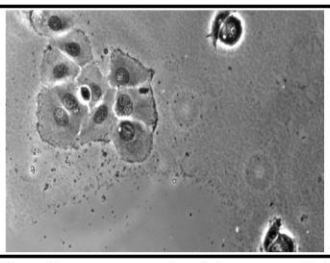	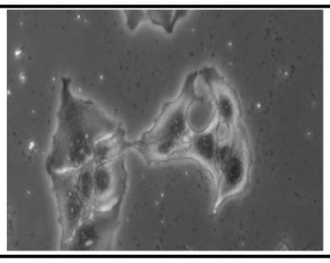
BT-20 cells propagated in complete growth medium 48 h	BT-20 cells deprived of glutamine for 48 h
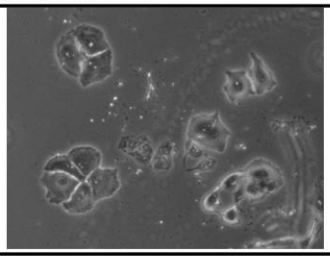	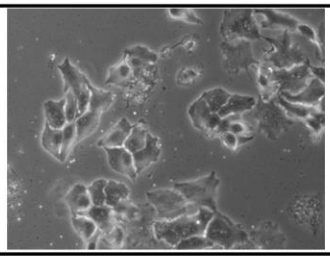
BT-20 cells propagated in complete growth medium 72 h	BT-20 cells deprived of glutamine for 72 h
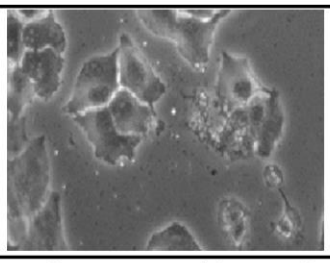	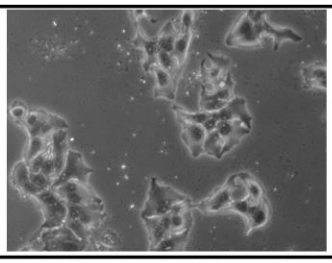
BT-20 cells propagated in complete growth medium 96 h	BT-20 cells deprived of glutamine for 96 h
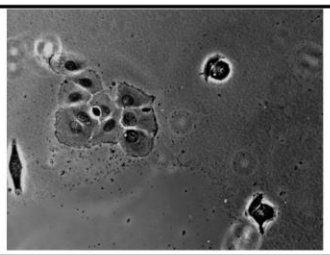	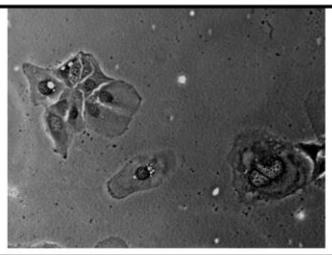

Figure 9: Morphology of the BT-20 cell line after 24 h, 48 h, 72 h and 96 h of glutamine deprivation compared to BT-20 cells propagated in complete growth medium 24 h, 48 h, 72 h and 96 h. Glutamine deprivation for decreased cell density slightly when compared to cells propagated in complete growth medium. The BT-20 cell line displayed minimal effects on morphology due to glutamine deprivation (20X magnification).

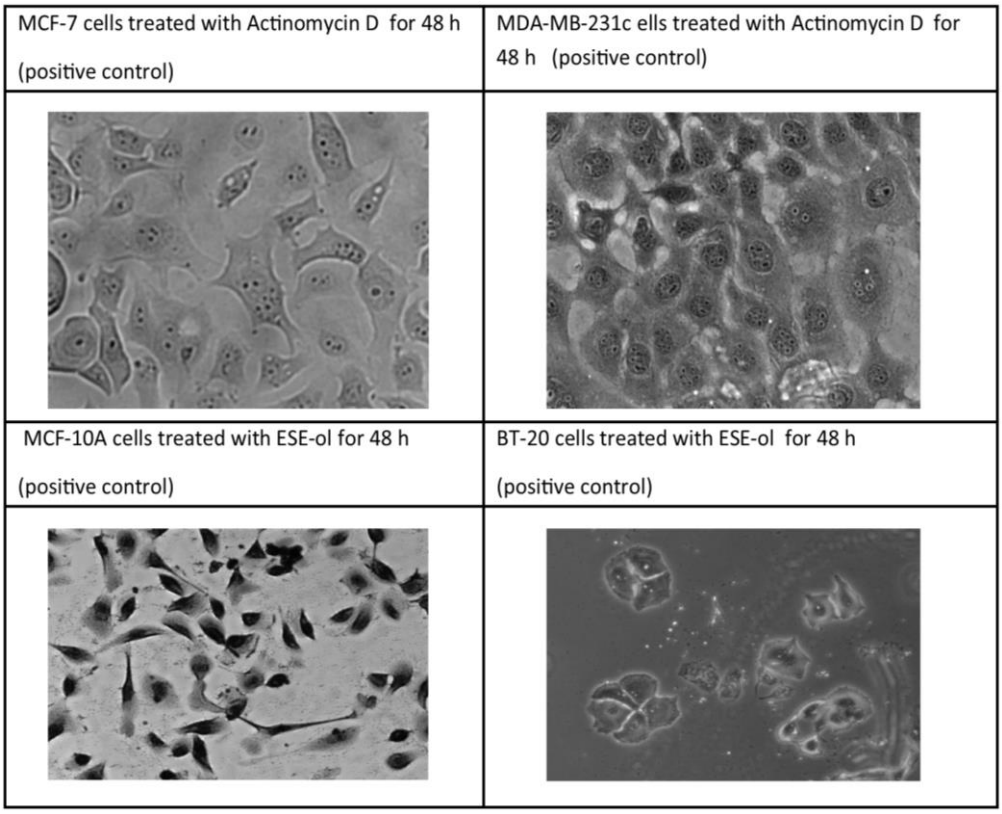

Figure 10: Morphology of the MCF-7-, MDA-MB-231-, MCF10-A and BT-20 cell lines after treated with Actinomycin D (MCF-7 & MDA-MB-231) and ESE-ol (MCF10 & BT-20) for 48 h to serve as a positive control for morphology studies. (20X magnification).

Table 1: Illustration of MCF-7-, MDA-MB-231-, MCF-10A- and BT-20 cell lines after 24 h of glutamine deprivation demonstrating mitotic index and the average percentage present in each phase ± standard deviations.

Condition	**MCF-7**	**MDA-MB-231**	**MCF-10A**	**BT-20**
24 h Medium only	**Average ± SD (%)**	**Average ± SD (%)**	**Average ± SD (%)**	**Average ± SD (%)**
Interphase	96.62 ± 0.91	97.41 ± 1.35	95.92 ± 2.3	97.3± 2.78
Prophase	1.45 ± 0.21	1.38 ± 1.1	2.87 ± 0.36	1.24± 3.6
Metaphase	0.677 ± 0.34	0.85 ± 0.34	0.76 ± 0.27	0.69± 1.87
Telophase	0.23 ± 0.19	0.2 ± 0.15	0.09 ± 0.13	0.26± 1.01
Anaphase	0.49 ± 0.25	0.17 ± 0.6	0.14 ± 0.25	0.18± 2.69
Apoptosis	0.09 ± 0.13	0.00	0.11 ± 0.12	0.007± 0.74
Abnormal	0.44 ± 0.38	0.00	0.11± 4.39	0.014± 0.36
24 h without Glutamine	**Average ± SD (%)**	**Average ± SD (%)**	**Average ± SD (%)**	**Average ± SD (%)**
Interphase	94.97 ± 2.65	95.85 ± 1.67	97.36 ± 0.43	98.36 ± 0.37
Prophase	1.39 ± 0.43	0.75 ± 0.37	1.05 ± 1.96	0.72 ± 0.65
Metaphase	0.68 ± 0.29	1.06 ± 0.19	1.07 ± 2.36	0.63 ± 0.15
Telophase	0.22 ± 0.17	0.55 ± 0.23	0.19 ± 0.37	0.2 ± 0.58
Anaphase	0.45 ± 0.29	0.48 ± 0.13	0.26 ± 2.94	0.012 ± 0.18
Apoptosis	0.76 ± 0.6	0.00	0.09 ± 0.42	0.03 ± 0.47
Abnormal	1.53 ± 1.08	1.32 ± 1.86	0.025 ± 0.78	0.006 ± 0.63

Table 2: Illustration of MCF-7-, MDA-MB-231-, MCF-10A- and BT-20 cell lines after 48 h of glutamine deprivation demonstrating mitotic index and the average percentage present in each phase ± standard deviations.

Condition	**MCF-7**	**MDA-MB-231**	**MCF-10A**	**BT-20**
48 h Medium only	**Average ± SD (%)**	**Average ± SD (%)**	**Average ± SD (%)**	**Average ± SD (%)**
Interphase	96.48 ± 1.08	95.63 ± 0.09	97.38 ± 1.26	95.63 ± 1.36
Prophase	1.89 ± 0.97	2.03 ± 2.36	1.09 ± 0.39	2.63 ± 1.43
Metaphase	0.97 ± 2.3	0.85 ± 0.08	0.75 ± 2.98	0.68 ± 1.68
Telophase	0.21 ± 0.02	0.36 ± 1.83	0.016 ± 1.47	0.28 ± 1.23
Anaphase	0.42 ± 2.36	0.6 ± 1.67	0.34 ± 1.74	0.08 ± 1.37
Apoptosis	0.0134 ± 4.3	0.02 ± 0.41	0.05 ± 1.8	0.135 ± 1.63
Abnormal	0.007 ± 1.36	0.51 ± 1.07	0.374 ± 0.88	0.565 ± 1.18
48 h without Glutamine	**Average ± SD (%)**	**Average ± SD (%)**	**Average ± SD (%)**	**Average ± SD (%)**
Interphase	97.8 ± 0.52	97.08± 0.71	95.85 ± 1.67	96.36± 0.29
Prophase	0.91 ± 0.37	1.23 ± 0.07	1.23 ± 0.07	1.61± 0.87
Metaphase	0.27 ± 0.13	0.92 ± 0.09	0.39 ± 0.89	0.29± 0.5
Telophase	0.24 ± 0.2	0.21 ± 0.02	0.27 ± 2.43	0.87± 1.15
Anaphase	0.23 ± 0.13	0.21 ± 0.08	0.36± 1.91	0.8± 1.67
Apoptosis	0.41 ± 0.45	0.2 ± 0.14	1.8± 0.57	0.07± 0.46
Abnormal	0.86 ± 0.66	0.11 ± 0.09	0.1± 2.12	0.1± 1.89
ESE-ol treated 48h	**Average ± SD (%)**	**Average ± SD (%)**	**Average ± SD (%)**	**Average ± SD (%)**
Interphase	80.19 ± 1.46	92.81 ± 1.63	94.36± 1.84	95.47± 0.56
Prophase	0.51 ± 0.13	0.45 ± 0.33	0.56± 1.04	0.49± 0.26
Metaphase	0.44 ± 0.04	0.18 ± 0.13	0.47± 2.89	0.37± 1.35
Telophase	0.14 ± 0.16	0.00	0.014± 0.96	0.00
Anaphase	0.59 ± 0.43	0.09 ± 0.06	0.36± 0.41	0.53± 3.62
Apoptosis	9.35 ±0.72	2.57 ± 0.65	2.97± 1.3	2.98± 2.69
Abnormal	8.9 ± 0.52	4.12 ± 2.45	1.6± 3.62	0.16± 4.23

Table 3: Illustration of MCF-7-, MDA-MB-231-, MCF-10A- and BT-20 cell lines after 72 h of glutamine deprivation demonstrating mitotic index and the average percentage present in each phase ± standard deviations.

Condition	**MCF-7**	**MDA-MB-231**	**MCF-10A**	**BT-20**
72 h Medium only	**Average ± SD (%)**	**Average ± SD (%)**	**Average ± SD (%)**	**Average ± SD (%)**
Interphase	97.63± 0.78	96.97± 0.43	97.25± 0.69	96.86± 0.23
Prophase	1.24± 0.12	1.39± 0.50	0.87± 0.74	0.89± 0.29
Metaphase	0.18± 0.66	0.25± 1.97	0.21± 1.87	0.34± 0.263
Telophase	0.29± 2.39	0.32± 2.78	0.17± 5.3	0.21± 0.78
Anaphase	0.12± 1.37	0.19± 1.74	0.01± 1.75	0.016± 0.82
Apoptosis	0.15±1.69	0.2± 3.37	0.53± 4.12	0.58± 0.26
Abnormal	0.39± 0.87	0.68± 0.47	0.96± 1.68	1.1± 0.78
72 h without Glutamine	**Average ± SD (%)**	**Average ± SD (%)**	**Average ± SD (%)**	**Average ± SD (%)**
Interphase	97.6± 0.1	96.74± 0.63	95.3± 0.73	96.36± 0.27
Prophase	1.09± 1.23	1.348± 0.24	1.28± 0.53	1.36± 0.43
Metaphase	0.11± 3.9	0.26± 0.29	0.27± 0.13	0.11± 0.63
Telophase	0.01± 0.78	0.29± 0.07	0.31± 1.67	0.213± 0.42
Anaphase	0.00	0.2± 0.05	0.02± 3.98	0.26± 0.68
Apoptosis	0.19± 0.09	0.137± 0.42	0.36± 2.31	0.39± 0.73
Abnormal	1.03± 0.88	1.03± 0.23	1.23± 3.77	1.3± 1.7

Table 4: Illustration of MCF-7-, MDA-MB-231-, MCF-10A- and BT-20 cell lines after 96 h of glutamine deprivation demonstrating mitotic index and the average percentage present in each phase ± standard deviations.

Condition	**MCF-7**	**MDA-MB-231**	**MCF-10A**	**BT-20**
96 h Medium only	**Average ± SD (%)**	**Average ± SD (%)**	**Average ± SD (%)**	**Average ± SD (%)**
Interphase	97.31± 0.56	96.41± 0.65	95.8± 0.63	94.96± 0.15
Prophase	1.22± 1.92	1.3± 0.72	1.28± 0.27	1.36± 0.97
Metaphase	1.01± 0.49	0.98± 0.73	0.64± 0.87	0.29± 0.56
Telophase	0.03± 1.6	0.15± 0.85	0.067± 1.69	0.14± 0.14
Anaphase	0.15± 4.36	0.036± 0.38	0.23± 2.37	0.27± 0.73
Apoptosis	0.12± 2.36	0.12± 0.974	0.97± 5.01	0.19± 1.17
Abnormal	0.16± 1.66	1.04± 0.15	1.01± 1.69	2.79± 1.98
96 h without Glutamine	**Average ± SD (%)**	**Average ± SD (%)**	**Average ± SD (%)**	**Average ± SD (%)**
Interphase	96.3± 1.67	97.96± 1.29	96.34± 0.85	95.6± 0.39
Prophase	1.36± 2.39	1.48± 2.97	1.02± 0.57	1.43± 0.45
Metaphase	0.23± 1.97	0.93± 2.35	0.89± 1.96	0.52± 0.89
Telophase	0.17± 0.56	0.236± 4.85	0.01± 2.39	0.019± 0.78
Anaphase	0.187± 0.42	0.013± 1.48	0.23± 3.97	0.028± 1.02
Apoptosis	0.75± 0.63	0.016± 3.55	0.41± 1.89	0.013± 3.09
Abnormal	1.26± 0.41	0.014± 1.99	1.1± 1.29	2.39± 1.023

4.3 Oxidative stress

4.3.1 Superoxide generation

Superoxide quantification was made possible by using flow cytometry and a freely permeable fluorescent compound, DHE. A unique red fluorescent product, 2-hydroethidine cation, is produced by oxidation of DHE by superoxide (102, 128).

Data demonstrated a significant increase in superoxide production to 1.23 fold in the MCF-7 cell line after 96 h of glutamine deprivation when compared to cells

propagated in complete growth medium (Figure 11). The MDA-MB-231 cell line demonstrated a statically significant increase to 1.19 and 1.63 fold after 72 h and 96 h of glutamine deprivation, respectively, when compared to cells propagated in complete medium. Data demonstrated that the MCF-10A cell line experienced an increase to 1.1 fold after 24 h and 96 h of glutamine deprivation when compared to cells propagated in complete medium. Superoxide production in the BT-20 illustrated a biphasic time-dependent production of superoxide, where the BT-20 cell line experienced a significant fold increase to 1.20 after 72 h of glutamine deprivation (Figure 11).

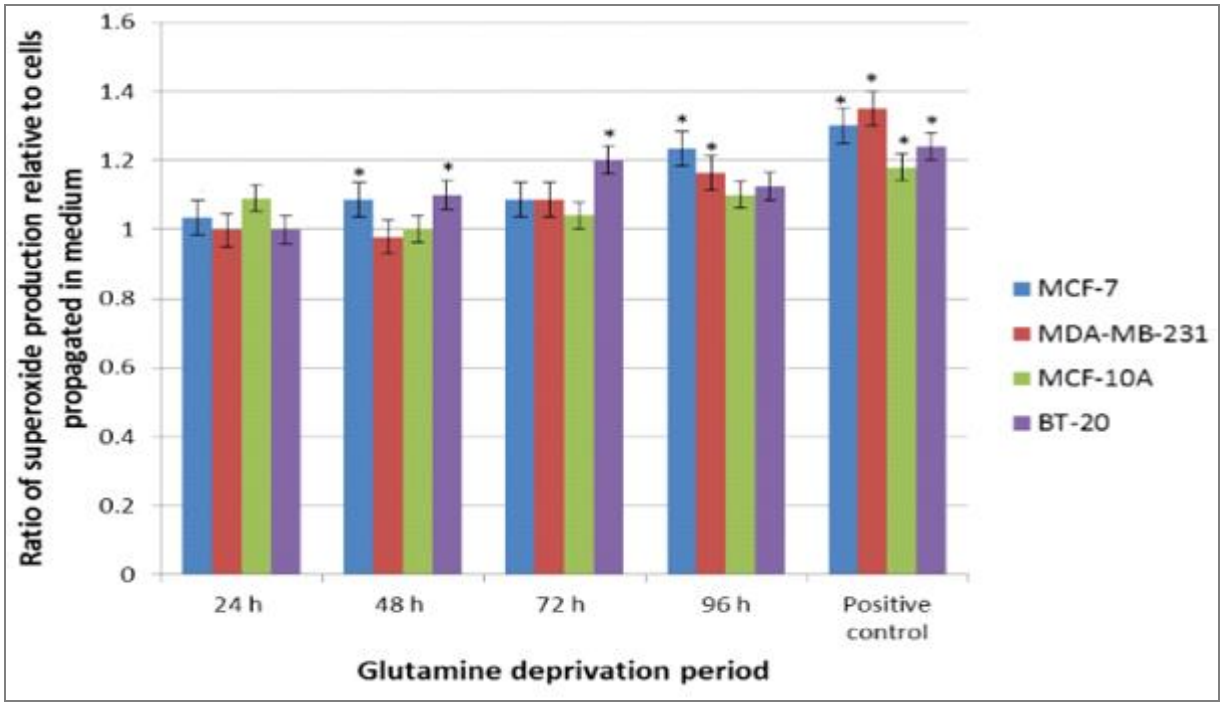

Figure 11: Graph illustrating superoxide production after 24 h, 48 h and 72 h and 96 h of glutamine deprivation in MCF-7-, MDA-MB-231-, MCF-10A- and BT-20 cell line. MCF-7-, MDA-MB-231 and BT-20 cell line illustrated elevated levels of superoxide production. MCF-10A illustrated a biphasic production of superoxide. An asterisk (*) indicates significance with *p*-value < 0.05 when calculated by means of the student's t-test when compared to cells propagated in complete medium. Positive control refers to cells treated with ESE-ol for 48 h.

4.3.2 Hydrogen peroxide

Hydrogen peroxide was quantified using 2, 7-dichlorofluorescein diacetate (DCFDA), a non-fluorescent probe that enters through the cell by means of passive diffusion upon oxidation by ROS and thus is catalysed to the highly fluorescent derivative,

DCF (124). DCFDA was utilized to investigate effects of glutamine deprivation on hydrogen peroxide production.

Data demonstrated that glutamine deprivation in the MCF-7 cell line resulted in a significant increase in hydrogen peroxide production to 1.16 fold after 24 h of glutamine deprivation when compared to cells propagated in complete growth medium (Figure 12). However, after 72 h and 96 h of glutamine deprivation, hydrogen peroxide production decreased to 0.82- and 0.72 folds, respectively, relative to cells propagated in complete growth medium. Glutamine deprivation in the MDA-MB-231 cell line after 24 h deprivation of glutamine demonstrated a significant increase in hydrogen peroxide production to 1.53 fold when compared to cells propagated in complete growth medium. However, after 96 h of glutamine deprivation there was a statically significant decrease in hydrogen peroxide production to 0.89 fold relative to cells propagated in complete growth medium. MCF-10A cell line data resulted in a time-dependent fold decrease to 0.91 and 1.10 in hydrogen production after 24 h and 48 h of glutamine deprivation, respectively, relative to cells propagated in complete growth medium. Furthermore, after 96 h of glutamine deprivation, a statistically significant fold increase to 1.29 was observed relative to cells propagated in complete growth medium. Hydrogen peroxide generation in the BT-20 cell line resulted in a statically significant fold increase to 1.21, 1.31 and 1.29 after 48 h, 72 h and 96 h of glutamine deprivation, respectively, relative to cells propagated in cells propagated in complete growth medium (Figure 12).

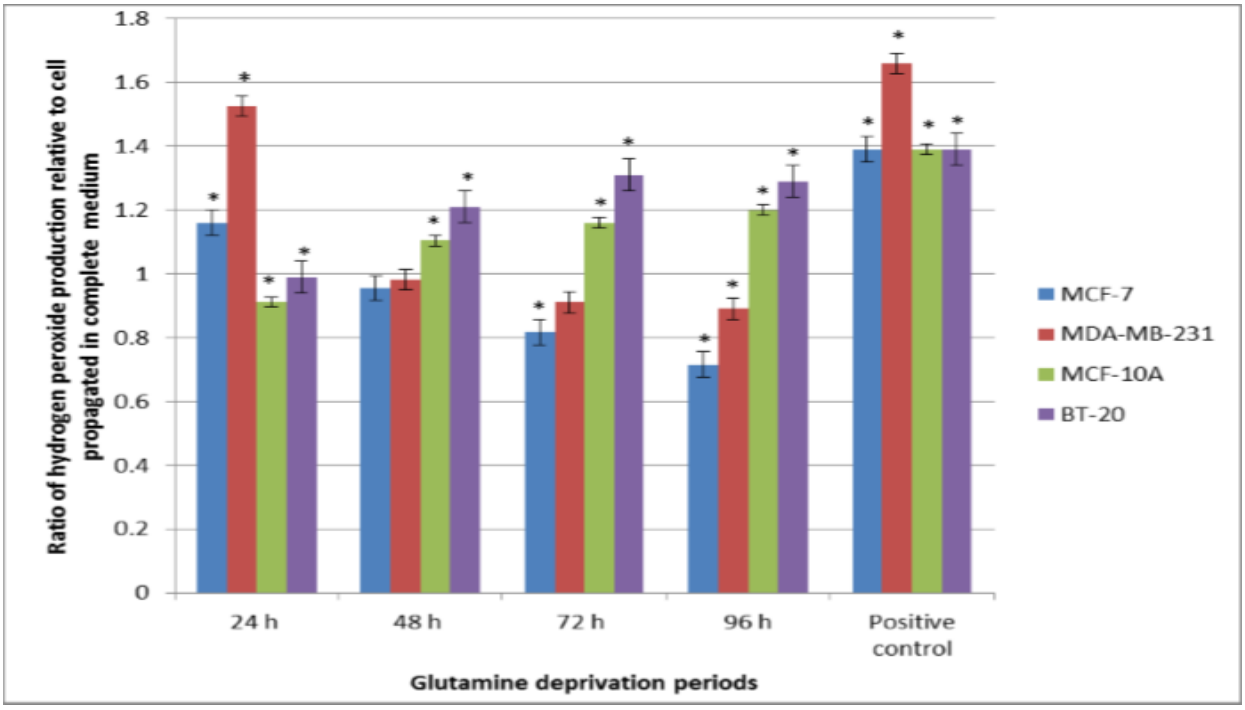

Figure 12: Graph illustrating hydrogen peroxide production after 24 h, 48 h, 72 h and 96 h of glutamine deprivation in MCF-7-, MDA-MB-231-, MCF-10A- and BT-20 cell lines. The MCF-7- and MCF-10A cell lines demonstrated a time-dependent production of hydrogen peroxide whilst the MDA-MB-231 illustrated decreased levels of hydrogen peroxide. The BT-20 cell line illustrated elevated levels of hydrogen peroxide levels. An asterisk (*) indicates significance with *p*-value < 0.05 when calculated by means of the student's t-test when compared to cells propagated in complete medium.

4.4 Antioxidant defences

4.4.1 Superoxide dismutase activity

SOD catalyzes the conversion of the superoxide anion (O_2^-) into hydrogen peroxide (H_2O_2) and is one of the most important antioxidant enzymes. Oxidative stress through ROS plays an important role in the etiology and progression in certain diseases such as cancer (129).

Data showed that in the MCF-7 cell line after 24 h and 48 h of glutamine deprivation, superoxide dismutase inhibition percentage was 5.78% and 5.38%, respectively (Figure 13). However, after 72 h of glutamine deprivation, a significant increase in the SOD inhibition percentage to 9.1% was observed. In addition, the MCF-7 cell line indicated a statically significant increase in the SOD inhibition percentage, where

after 96 h of glutamine deprivation the SOD inhibition percentage increased to 10.34%. The MDA-MB-231 cell line demonstrated 7.85% and 8.44% SOD inhibition percentage after 24 h and 48 h, respectively. However, after 72 h and 96 h of glutamine deprivation, the MDA-MB-231 cell line demonstrated a statistically significant decrease in SOD inhibition percentage to 6.34% and 7.36%, respectively. The MCF-10A cell line showed a statically significant increase in SOD inhibition percentage after 24 h of glutamine deprivation, where the SOD inhibition rate increased to 11.3% after which the SOD inhibition percentage decreased to 8.63% after 48 h of glutamine deprivation. A further decrease was experienced in SOD inhibition percentage to 7.66% after 72 h of glutamine deprivation. An increase was observed in the SOD inhibition percentage after 96 h of glutamine deprivation to 12.33%. The BT-20 cell line indicated a 9.63 % SOD inhibition percentage after 24 h of glutamine deprivation and after 48 h of glutamine deprivation the BT-20 cell line remained constant at 9.44% of SOD inhibition percentage. However, after 72 h of glutamine deprivation, the SOD inhibition percentage increased to 11.36% and experienced a statistically significant decline after 96 h of glutamine deprivation to 4.63% of SOD inhibition.

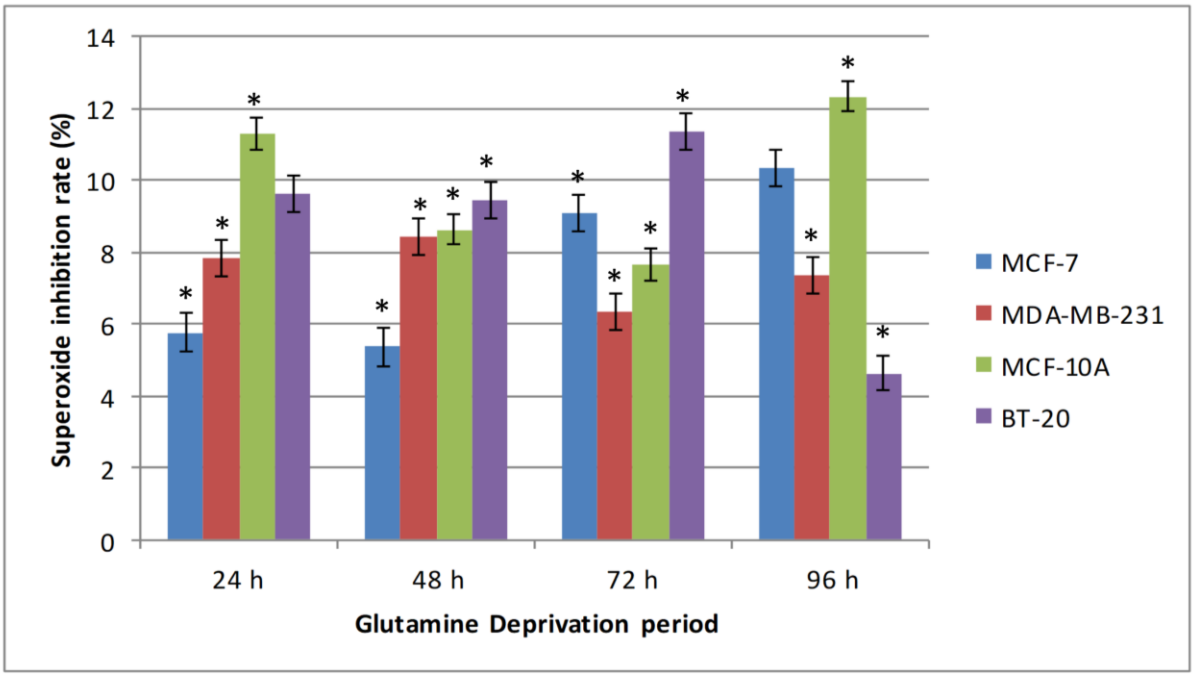

Figure 13: Graph illustrating the superoxide dismutase inhibition percentage, where the MCF-7 cell line indicated the most activity in the levels of SOD enzyme in the first 48 h of glutamine deprivation, however decreased the activity of the SOD enzyme after 72 h and 96 h of glutamine deprivation. The MDA-MB-231 cell line indicated

substantial activity of the SOD enzyme at the different time points. The MCF-10A cell line experienced a temporal increase in the activity SOD after 48 h and 72 h of glutamine deprivation. The SOD inhibition rate equation incorporates cells propagated in completed growth medium. An asterisk (*) indicates significance with *p*-value < 0.05 when calculated by means of the student's t-test when compared to cells propagated in complete growth medium.

4.4.2 Catalase activity

Catalase is an antioxidant enzyme that catalyses hydrogen peroxide to water and oxygen. Catalase is a tetramer of four polypeptide chains, and contains four porphyrin heme groups that allow the enzyme to react with hydrogen peroxide (130). A standard curve was utilized in order to extrapolate the concentration of the catalase from cells deprived of glutamine. The MCF-7 cell line demonstrated a 1.28 fold increase in catalase concentration after 24 h of glutamine deprivation when compared to cell propagated in complete growth medium, followed by a statically significant 0.66 fold decrease in the presence of the catalase concentration after 48 h of glutamine deprivation when compared to cells in complete growth medium (Figure 14). Furthermore, after 72 h of glutamine deprivation, the MCF-7 cell line experienced an increase to 1.23 fold which was subsequently followed by statically significant fold decrease to 0.76 after 96 h of glutamine deprivation when compared to cells propagated in complete growth medium. The MDA-MB-231 cell line demonstrated a 1.1 fold increase when compared to cell propagated in complete growth medium after 24 h of glutamine deprivation, followed by a 0.89 fold decrease in catalase concentration after 48 h of glutamine deprivation. After 72 h of glutamine deprivation a 0.95 fold decrease in catalase concentration when compared to cell propagated in complete growth medium followed by a 0.75 fold decrease in catalase concentration when compared to cells propagated in complete growth medium. The MCF-10A cell line demonstrated a significant fold increase of 1.1 after 48 h of glutamine deprivation when compared to cells propagated in complete growth medium. The BT-20 cell line demonstrated significant fold increases of 1.25 and 1.1 folds after 24 h and 72 h of glutamine deprivation when compared to cells propagated in complete growth medium.

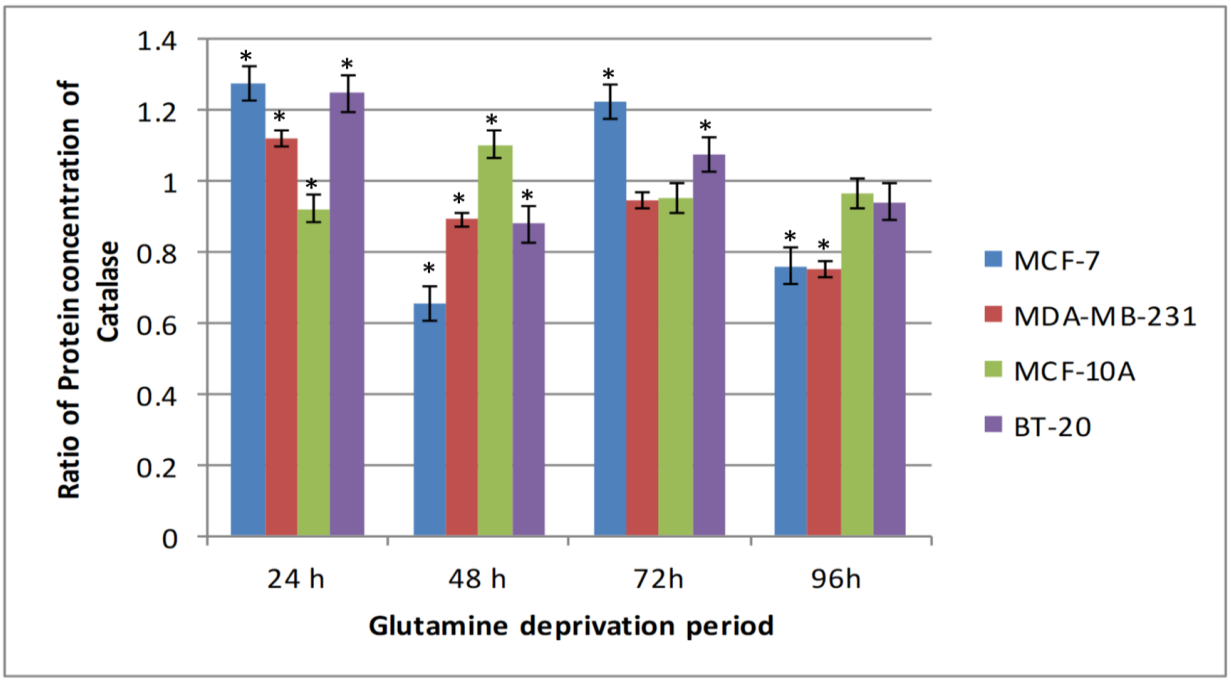

Figure 14: Graph illustrating the ratio of protein concentration of catalase compared to cells propagated in growth medium, where the MCF-7 cell line indicated the most catalase enzyme activity after 24 h of glutamine deprivation, The MDA-MB-231 cell line indicated increased activity of catalase after 24 h and 72 h of glutamine deprivation. The MCF-10A cell line experienced a temporal increase in catalase activity after 48 h and 96 h of glutamine deprivation. An asterisk (*) indicates significance with *p*-value < 0.05 when calculated by means of the student's t-test when compared to cells propagated in complete growth medium.

4.5 Energy status

The influence of glutamine deprivation on the energy state of the cell was determined by quantifying AMP-activated protein kinase (AMPK) compared to cells propagated in complete growth medium (131). AMPK activity is determined by change of AMP/ATP ratio signifying an energy deficit due to cellular stress including nutrient deprivation, metabolic stress and oxidative stress (132).

The MCF-7 cell line indicated significant decrease in the percentage of AMPK present where activity was 80.72% and 70.16% after 24 h and 48 h of glutamine deprivation (Figure 15). Furthermore, after 72 h of glutamine deprivation the AMPK activity decreases to 75.12% and, decreases further to 49.33% after 96 h of glutamine deprivation which is indicative of energy deficit. The MDA-MB-231 cell line

indicated 84.05% AMPK activity after 24 h of glutamine deprivation. However, after 48 h, 72 h and 96 h of glutamine deprivation the AMPK activity decreased to 67.62%, 63.12% and 56%, respectively. The MCF-10A cell line indicated activity of AMPK of 89.48%, 83%, 85.17% and 76.09% after 24 h, 48 h, 72 h and 96 h of glutamine deprivation respectively. The BT-20 cell line indicated the AMPK activity of 92.35%, 84.90%, 88.71% and 83.06% after 24 h, 48 h, 72 h and 96 h of glutamine deprivation (Figure 15).

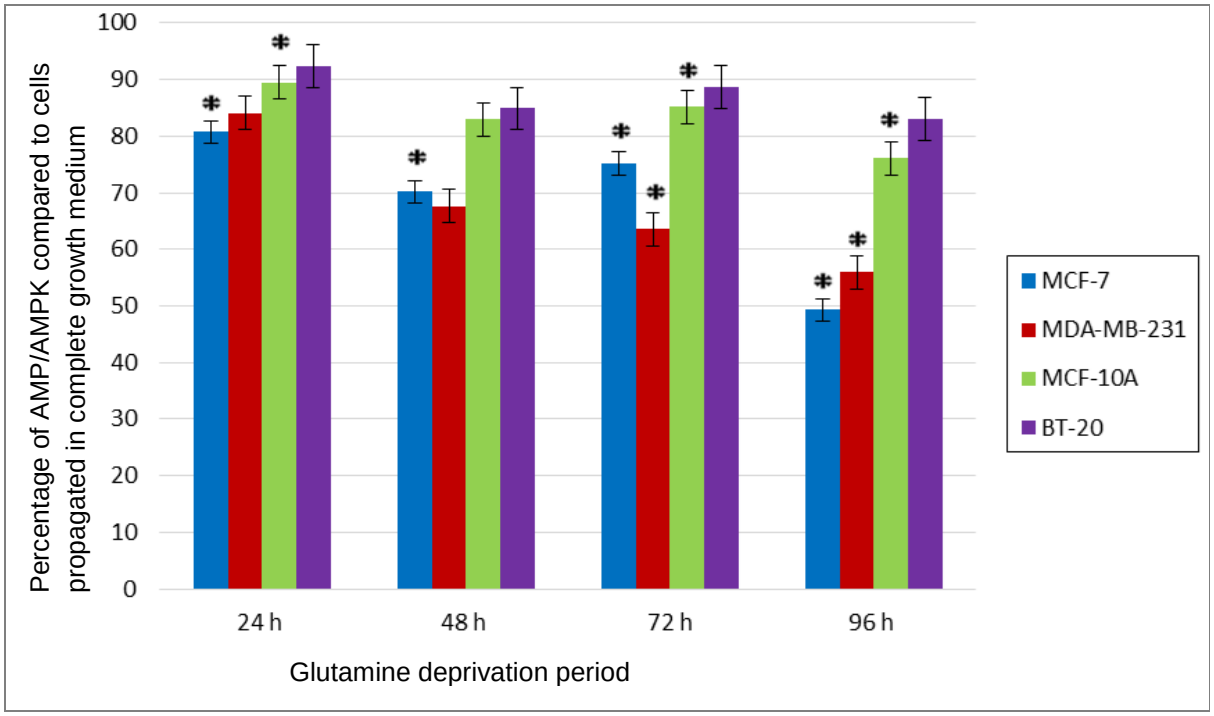

Figure 15: Graph illustrating the AMPK activity percentage over periods of glutamine deprivation. The MCF-7 cell line indicated the least activity after 96 h of glutamine deprivation indicating energy deficit is experienced most prominently after 96 h of glutamine deprivation period. The MDA-MB-231 cell line demonstrated a decrease in the AMPK activity in a time-dependent manner with 96 h of glutamine deprivation period illustrating the least amount of activity. The MCF-10A cell line was the least affected when compared to the MCF-7 and MDA-MB-231 cell lines. The BT-20 cell line indicated a steady activity of the AMPK suggesting there was minimal energy disruption in this cell line. An asterisk (*) indicates significance with p-value < 0.05 when calculated by means of the student's t-test when compared to cells propagated in complete growth medium.

4.6 Cell survival signalling

The influence of glutamine deprivation on phosphoinositide 3-kinase phosphorylation (PI3K) was investigated as an indicator of cell survival signaling. PI3K phosphorylates phosphatidylinositol, PI-4-phosphate and PI-4, 5-bisphosphate to catalyse the production of PI-3, 4, 5-triphosphate (133). PI3K regulates cell growth cell cycle entry, proliferation and cell survival (134). PI3K production was assessed in cells deprived of glutamine and in cells propagated in complete growth medium for all time periods.

The MCF-7 cell line demonstrated decreased PI3K phosphorylation to 0.97-, 0.96-, 0.88- and 0.9 fold after 24 h-, 48 h-, 72 h- and 96 h of glutamine deprivation (Figures 16-17). PI3K phosphorylation of the MDA-MB-231 cell line was affected by glutamine deprivation after 48 and 72 h of glutamine deprivation when compared to cells propagated in complete growth medium The MCF-10A cell line demonstrated decreased PI3K phosphorylation to 0.9-, 0.87-, 0.85- and 0.81 fold after 24 h, 48 h, 72 h and 96 h after glutamine deprivation when compared to cells propagated in complete growth medium. The BT-20 cell line showed decreased PI3K phosphorylation to 0.92-, 0.82-, 0.84- and 0.89- fold after 24 h, 48 h, 72 h and 96 h of glutamine deprivation when compared to cells propagated in complete growth medium (Figures 16-17).

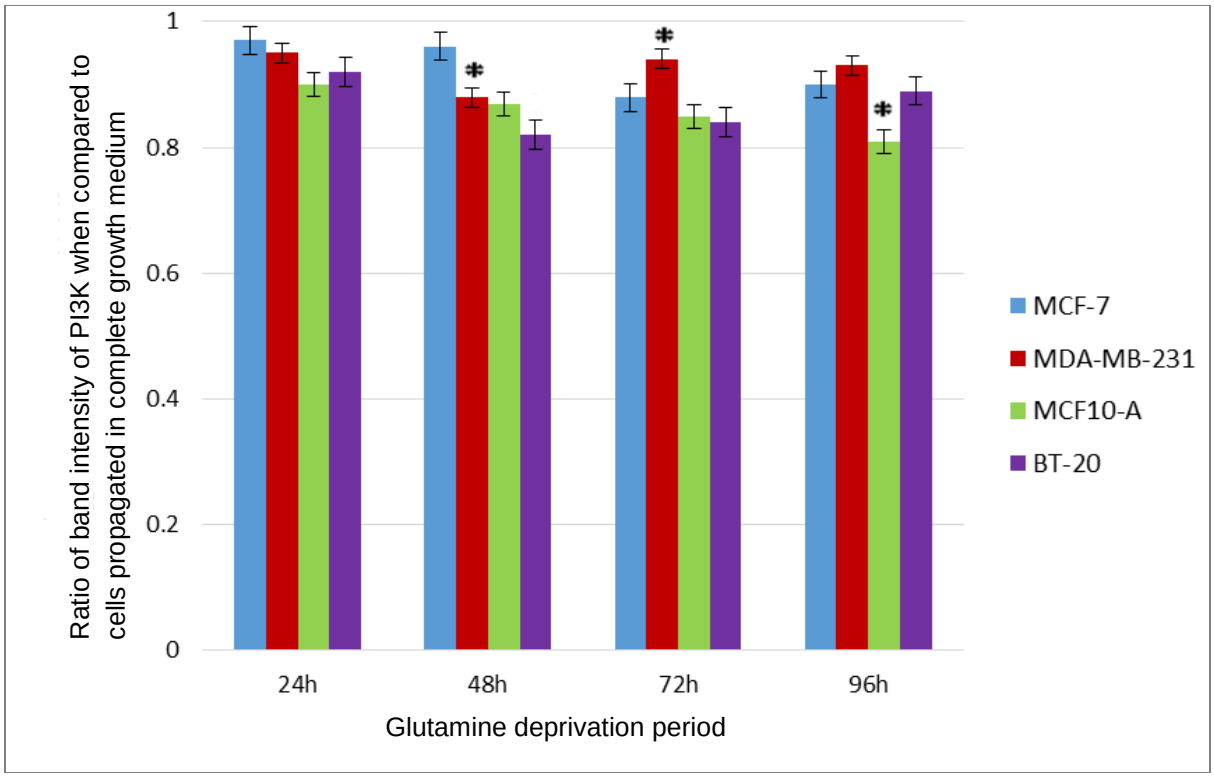

Figure 16: Graph illustrating the fold difference in the production of PI3K in glutamine deprived cells when compared to cells propagated in complete growth medium. The MCF-7-, MDA-MB-231-, MCF-10A- and BT-20 cell lines indicated a constant production of PI3K in comparison to cells propagated in growth medium. An asterisk (*) indicates significance with *p*-value < 0.05 when calculated by means of the student's t-test when compared to cells propagated in complete growth medium.

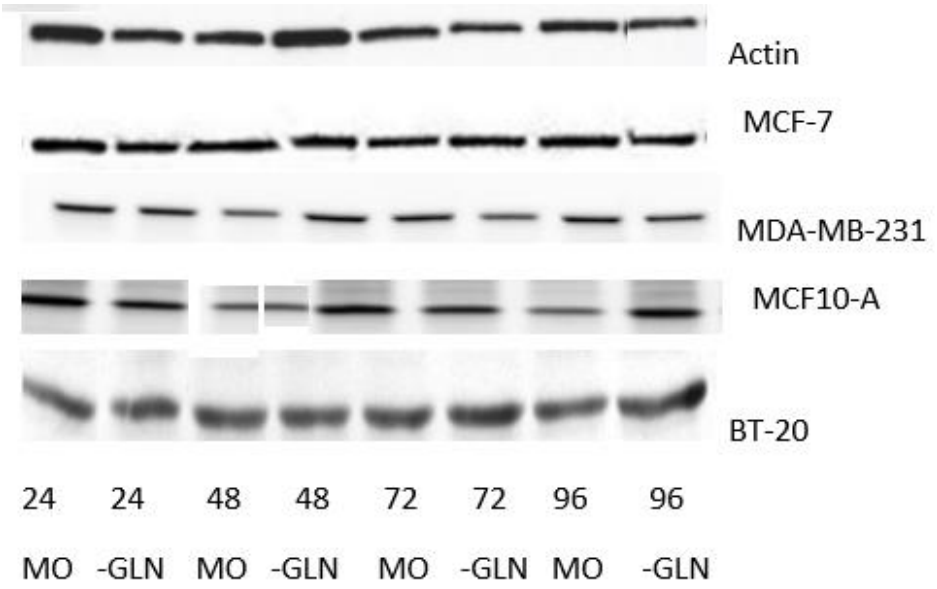

Figure 17: Diagram illustrating western blots of MCF-7-, MDA-MB-231-, MCF-10A- and BT-20 cell lines when deprived of glutamine compared to cells propagated in complete growth medium using actin as the control to indicate the production of PI3K in comparison to treated cells. MO refers to cells propagated in complete growth medium and -Gln (period) refers to cells deprived of glutamine for specified period. Actin was used as a loading buffer.

The influence of glutamine deprivation on extracellular-signal-regulated kinase (ERK) phosphorylation was investigated as an indicator of cell survival signaling. ERK is a pro-survival pathway which is also associated with proliferation, invasion and migration (135).

The MCF-7 cell line demonstrated non-significant fold decrease to 1.01-, 0.98-, 1.01- and 0.96 fold after 24 h-, 48 h-, 72 h- and 96 h of glutamine deprivation, respectively,

when compared to cells propagated in complete growth medium. The MDA-MB-231 cell line demonstrated significant fold decrease to 0.87 fold after 48 h of glutamine deprivation when compared to cells propagated in complete growth medium. The MCF-10A cell line demonstrated significant fold increase to 1.14 fold after 72 h of glutamine deprivation when compared to cells propagated in complete growth medium. The BT-20 cell line demonstrated a decrease to 0.93 fold after 24 h of glutamine deprivation when compared to cells propagated in complete growth medium (Figures 18-19).

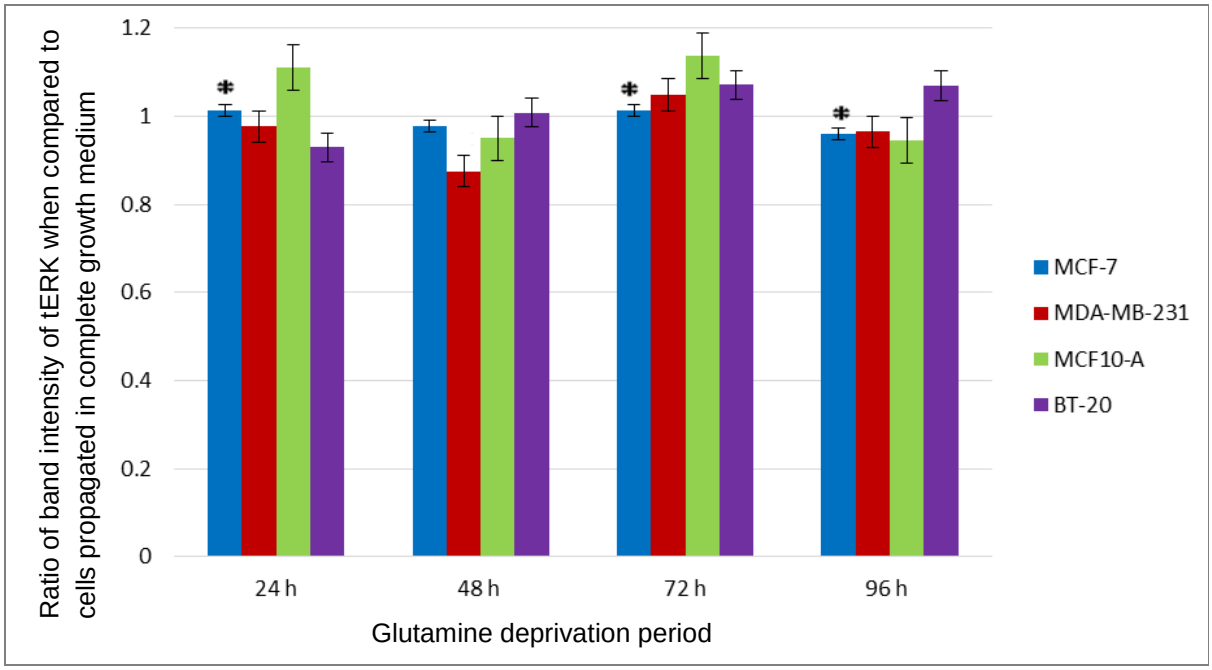

Figure 18: Graph illustrating the fold difference in the production of total ERK in glutamine deprived cells when compared to cells propagated in complete growth medium. The MCF-7-, MDA-MB-231-, MCF-10A- and BT-20 cell lines indicated a minimal change in the production of PI3K in comparison to treated cells. An asterisk (*) indicates significance with *p*-value < 0.05 when calculated by means of the student's t-test when compared to cells propagated in complete growth medium.

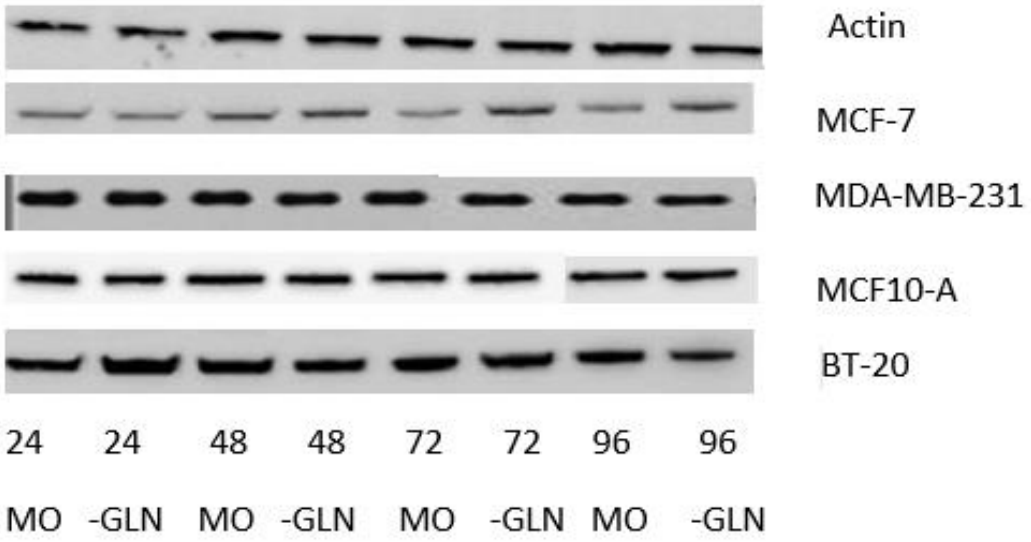

Figure 19: Diagram illustrating Western Blots of MCF-7-, MDA-MB-231-, MCF-10A- and BT-20 cell lines when deprived of glutamine compared to cells propagated in complete growth medium using actin as the control to indicate the production of tERK in comparison to treated cells. MO refers to cells propagated in complete growth medium and -Gln (period) refers to cells deprived of glutamine for specified period. Actin was used as the loading control.

4.7 Deoxyribonucleic acid (DNA) damage

The effects of glutamine deprivation on DNA damage were investigated by visualising 8-hydroxyguanosine formation which is derived from the nucleoside guanosine which is a component of DNA. 8-Hydroxyguanosine is a modified base that occurs in DNA due to damage by hydroxyl radicals formed during aerobic metabolism and is indicative oxidative stress. Anti-8 hydroxyguanosine is frequently used as a biomonitoring mechanism where the green is indicative DNA damage (114).

The MCF-7 cell line demonstrated increased fluorescent intensity of anti-8 hydroxyguanosine to 1.43 and 1.89 fold after 24 h and 48 h of glutamine deprivation, respectively, relative to cells propagated in complete growth medium (Figures 20-21). The MDA-MB-231 cell line indicated increased fluorescence after 48 h and 72 h of glutamine deprivation to 1.84 and 1.95 fold, respectively. After 48 h and 72 h of glutamine deprivation in the MDA-MB-231 cell line increased intensity of anti-8 hydroxyguanosine was observed in the cells. The MCF-10A cell line indicated

increased staining intensity after 24 h-, 72 h- and 96 h- of glutamine deprivation to 1.92, 1.95 and 1.97 fold respectively, when compared to cells propagated in complete growth medium. Increased intensity in the anti-8 hydroxyguanosine staining was observed in the MCF-10A cell line at the aforementioned time periods. The BT-20 cell line indicated minimal effects after glutamine deprivation after 24 h and 72 h of glutamine deprivation, where staining intensity was 1.24- and 1.07 fold respectively. There was an increase in the intensity of anti-8 hydroxyguanosine after 48 h and 96 h glutamine deprivation.

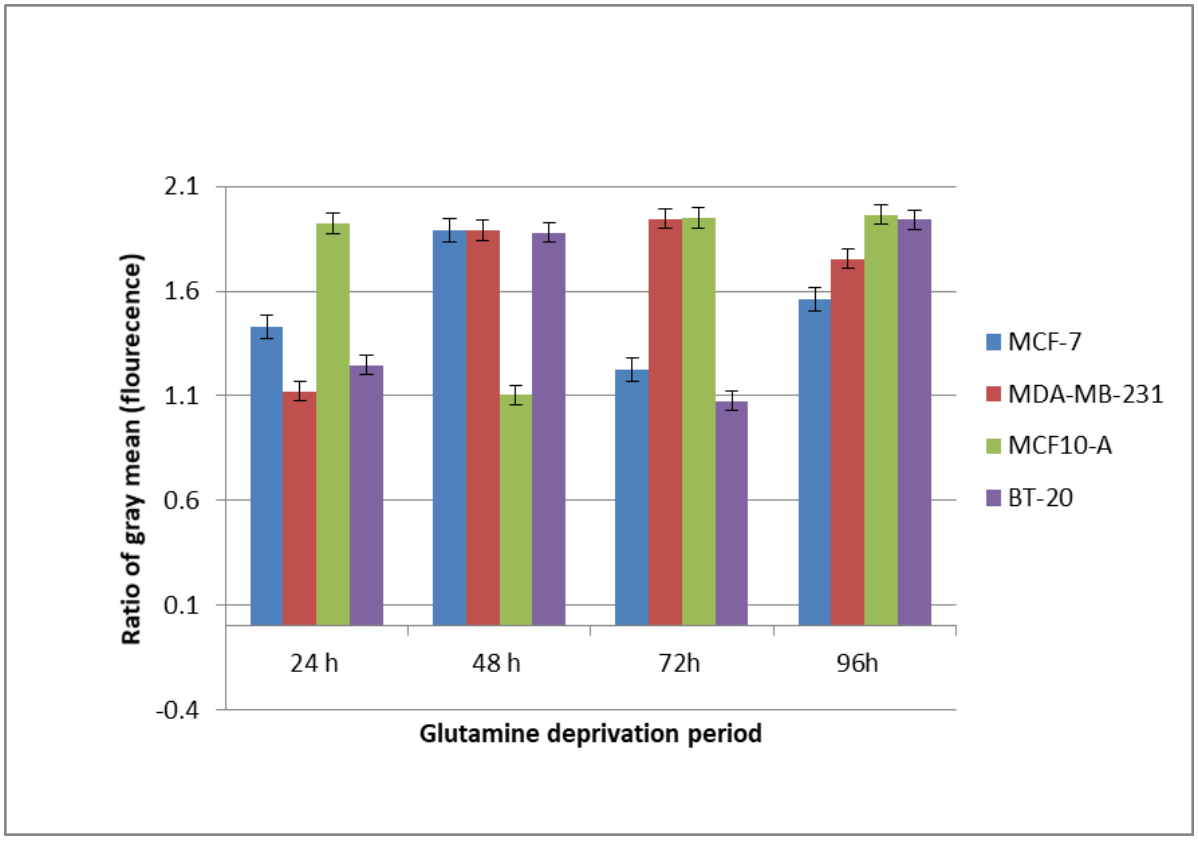

Figure 20: Graph illustrating the fluorescence intensity of anti-8 hydroxyguanosine fluorescence intensity when compared to cells propagated in complete growth medium. The MCF-7 cell line indicated the prominent increase in staining intensity after 48 h of glutamine deprivation where the ratio increased to 1.89 when compared to cells propagated in complete growth medium. The MDA-MB-231 cell line indicated a significant increase in staining intensity when compared to cells propagated in complete growth medium, after 48 h and 72 h of glutamine deprivation. An asterisk (*) indicates significance with *p*-value < 0.05 when calculated by means of the student's t-test when compared to cells propagated in complete growth medium.

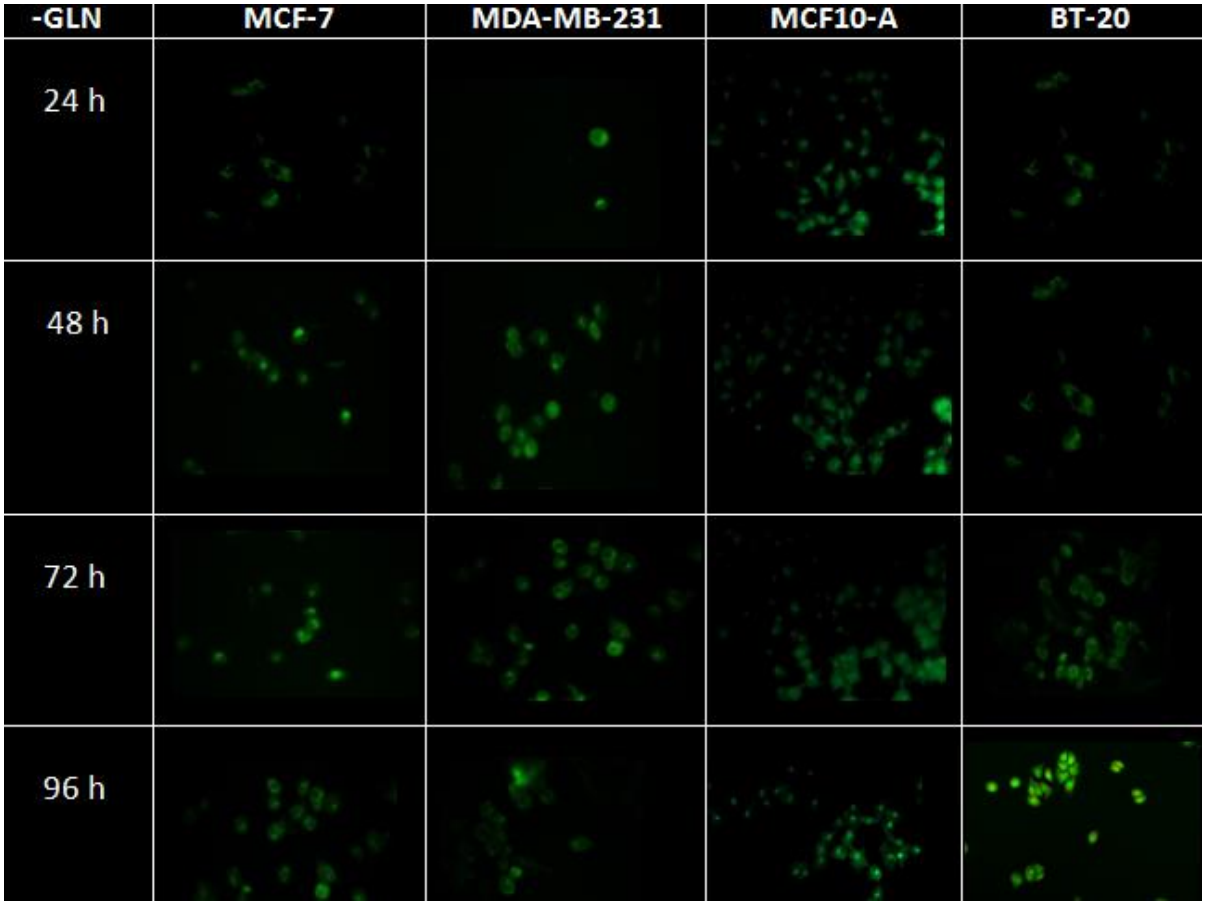

Figure 21: Graph illustrating fluorescent intensity of anti-8 hydroxyguanosine. The MCF-7 cell line indicated the most intense after 48 h and 72 h of glutamine deprivation. The MDA-MB-231 cell line indicated increased staining intensity after 48 h and 72 h of glutamine deprivation. The MCF-10A cell line showed increased intensity after 48 h and 72 h of glutamine deprivation whilst the BT-20 cell line was prominently affected after 96 h of glutamine deprivation as indicated by the increased intense green staining.

The effects of glutamine deprivation on DNA damage was assessed by visualising H2A phosphorylation where the green fluorescence is indicative of DNA damage experienced by the cells due to oxidative stress which caused double stranded breaks in the DNA (136). The MCF-7 cell line demonstrated severe DNA damage when compared to the MDA-MB-231-, MCF-10A- and BT-20 cell line after glutamine deprivation. The MDA-MB-231 cell line demonstrated prominent staining which is indicative of severe double stranded breaks after 72 h of glutamine deprivation (Figures 22-26).

MCF-7 cells propagated in complete medium for 24 h	MCF-7 cells deprived of glutamine for 24 h
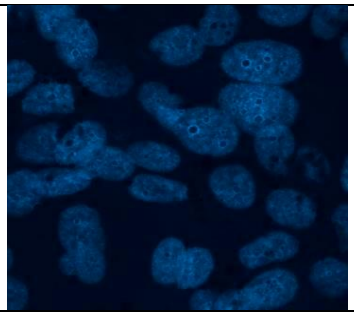	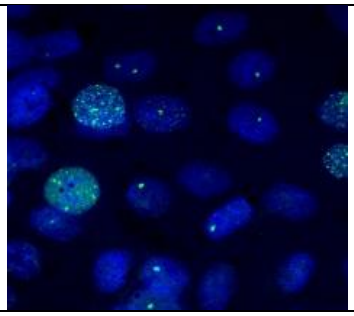
MCF-7 cells propagated in complete medium for 48 h	MCF-7 cells deprived of glutamine for 48 h
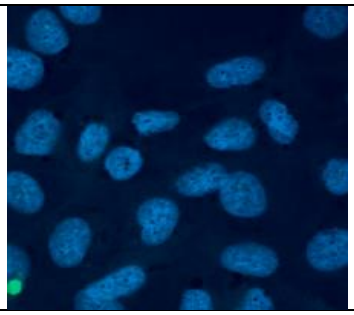	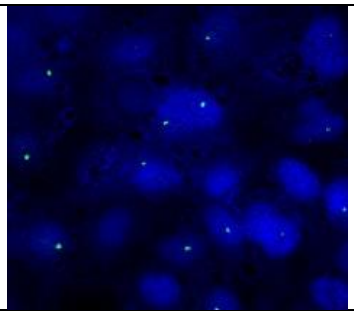
MCF-7 cells propagated in complete medium for 72 h	MCF-7 cells deprived of glutamine for 72 h
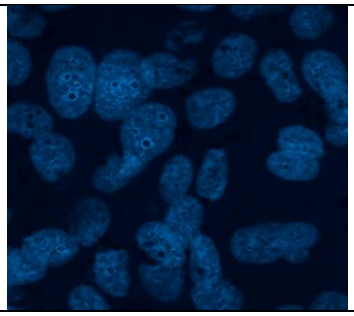	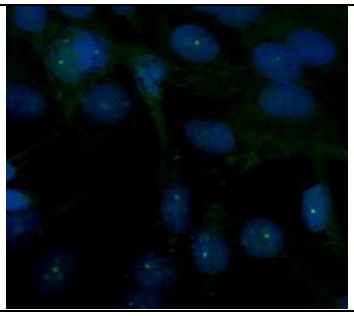
MCF-7 cells propagated in complete medium for 96 h	MCF-7 cells deprived of glutamine for 96 h
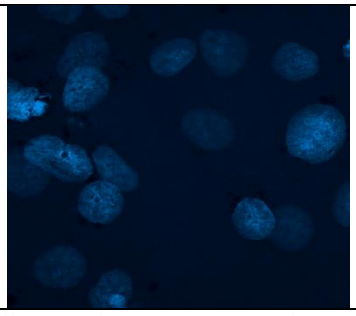	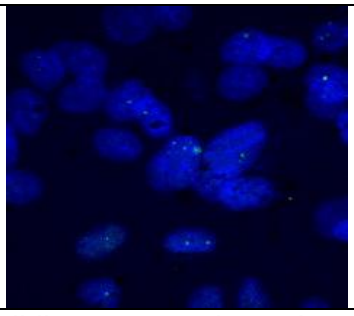

Figure 22: Illustration of H2AX damage in MCF-7 cell line after 24 h, 48 h, 72 h and 96 h of glutamine deprivation, indicating that 72 h is prominently affected.

MDA-MB-231 cells propagated in complete medium for 24 h	MDA-MB-231 cells deprived of glutamine for 24 h
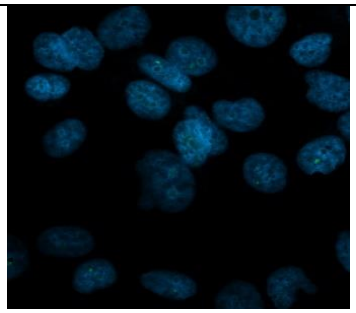	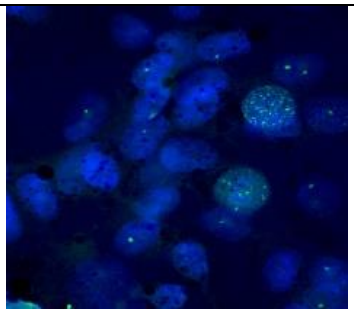
MDA-MB-231 cells propagated in complete medium for 48 h	MDA-MB-231 cells deprived of glutamine for 48 h
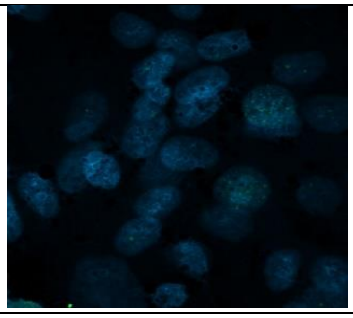	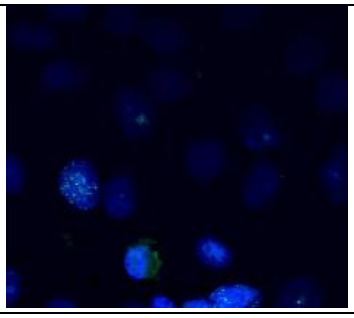
MDA-MB-231 cells propagated in complete medium for 72 h	MDA-MB-231 cells deprived of glutamine for 72 h
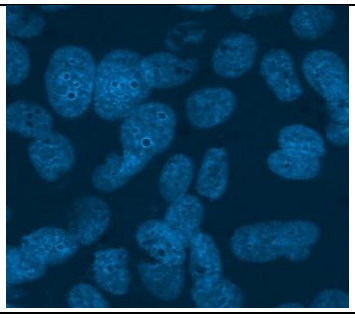	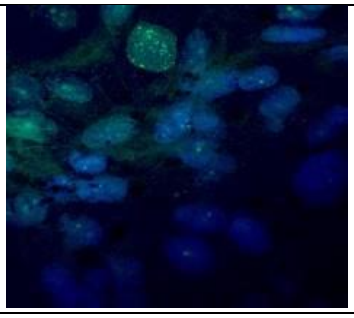
MDA-MB-231 cells propagated in complete medium for 96 h	MDA-MB-231 cells deprived of glutamine for 96 h
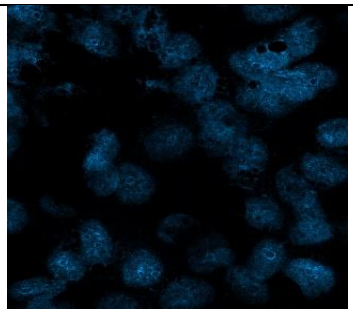	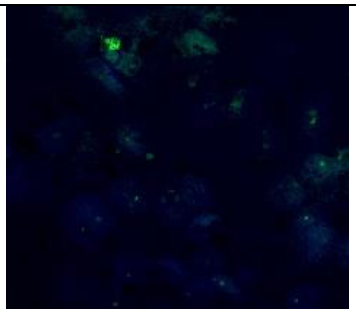

Figure 23: Illustration of H2AX damage in MDA-MB-231 cell line after 24 h, 48 h, 72 h and 96 h of glutamine deprivation, indicating that 72 h is prominently affected.

MCF-10A cells propagated in complete medium for 24 h	MCF-10A cells deprived of glutamine for 24 h
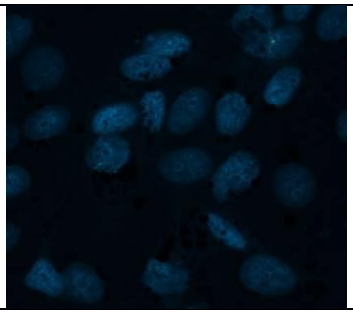	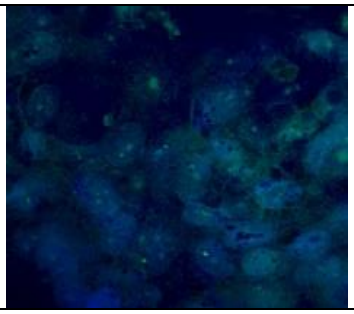
MCF-10A cells propagated in complete medium for 48 h	MCF-10A cells deprived of glutamine for 48 h
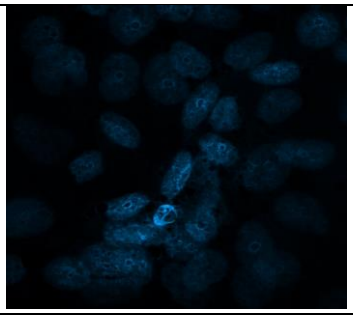	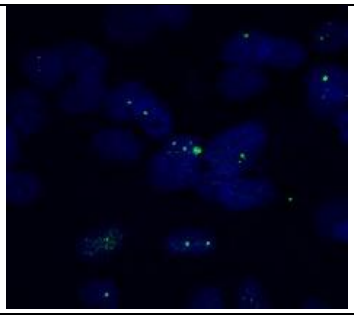
MCF-10A cells propagated in complete medium for 72 h	MCF-10A cells deprived of glutamine for 72 h
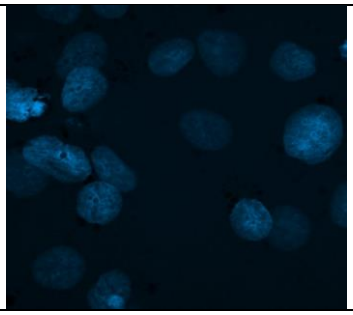	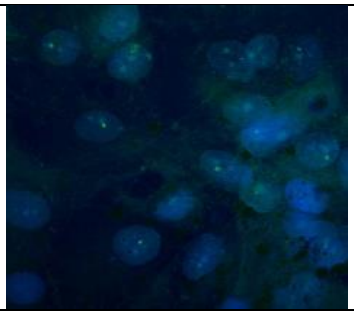
MCF-10A cells propagated in complete medium for 96 h	MCF-10A cells deprived of glutamine for 96 h
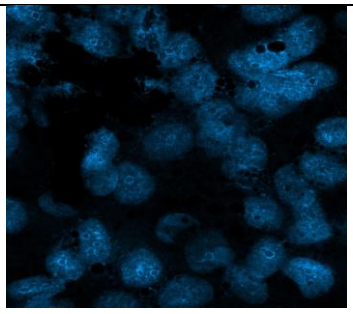	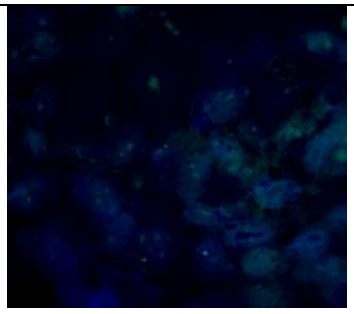

Figure 24: Illustration of H2AX damage in MCF-10A cell line after 24 h, 48 h, 72 h and 96 h of glutamine deprivation, indicating that 48 h is prominently affected.

BT-20 cells propagated in complete medium for 24 h	BT-20 cells deprived of glutamine for 24 h
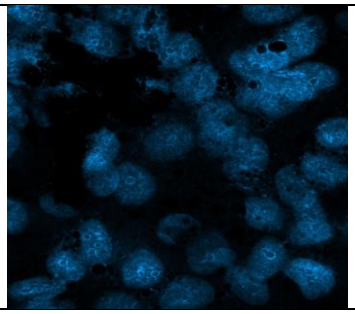	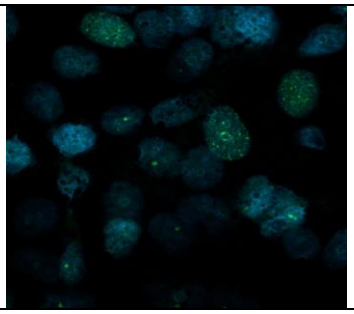
BT-20 cells propagated in complete medium for 48 h	BT-20 cells deprived of glutamine for 48 h
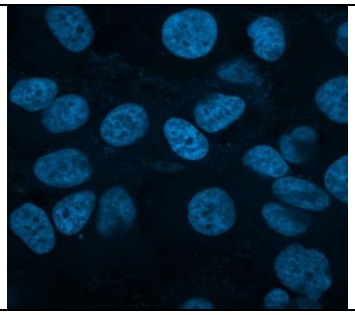	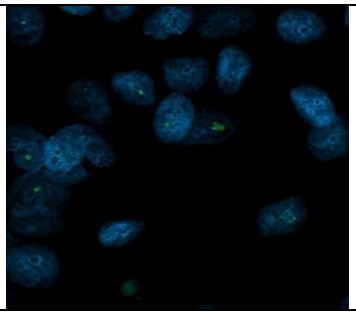
BT-20 cells propagated in complete medium for 72 h	BT-20 cells deprived of glutamine for 72 h
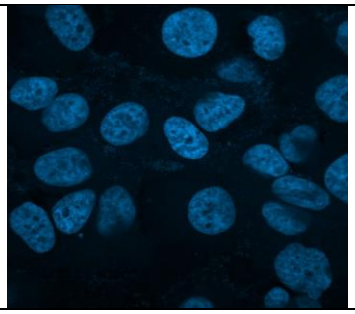	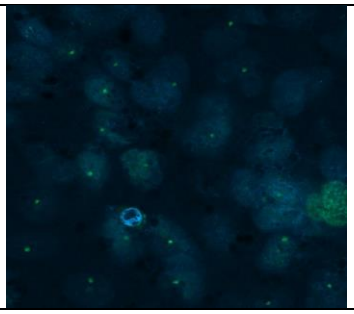
BT-20 cells propagated in complete medium for 96 h	BT-20 cells deprived of glutamine for 96 h
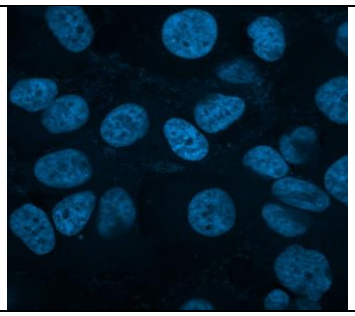	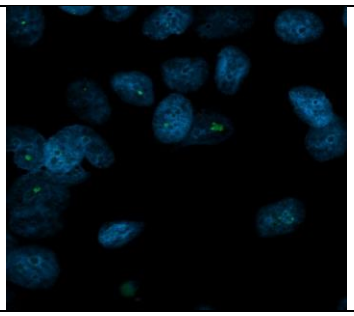

Figure 25: Illustration of H2AX damage in BT-20 cell line after 24 h, 48 h, 72 h and 96 h of glutamine deprivation, indicating that 24 h is prominently affected**.**

MCF-7 cells treated with bafiliomycin for 48 h	MDA-MB-231 cells treated with bafiliomycin for 48 h
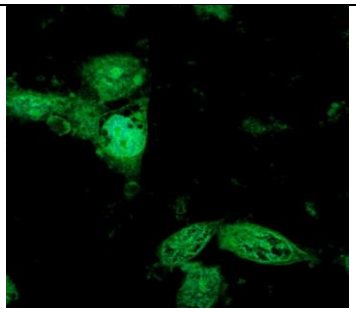	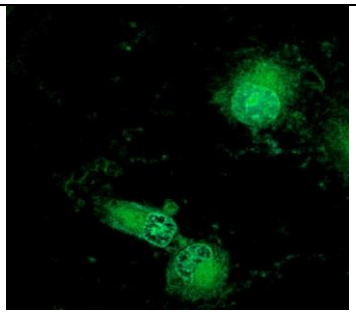
MCF-10A cells treated with bafiliomycin for 48 h	BT-20 cells treated with bafiliomycin for 48 h
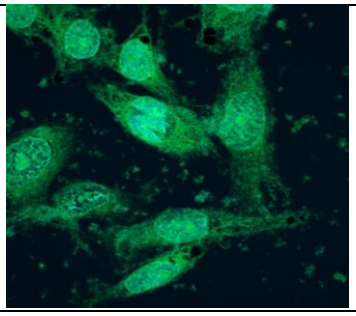	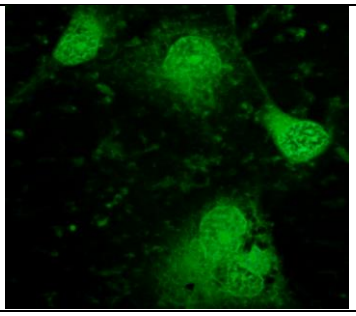

Figure 26: Graph illustrating H2AX damage in MCF-7-, MDA-MB-231-, MCF-10A- and BT-20 cell lines treated with bafiliomycin as a positive control.

4.8 Cell cycle progression

Propidium iodide stains the DNA and thus enables the quantification of DNA correlating with stages of the cell cycle during cell division (123). The effects of glutamine deprivation on the cell cycle was investigated by means of ethanol fixation, propidium iodide and flow cytometry.

Glutamine deprivation for 72 h in the MCF-7 cell line demonstrated a significant decrease in the number of cells occupying the G_1 phase (41%) accompanied by a significant increase in the number of cells occupying the S-phase (34%) when compared to cells propagated in complete growth medium (68%, 9% respectively) (Figure 27, Table 5-11). After 96 h of glutamine deprivation, the MCF-7 cell line demonstrated a significant decrease in the number of cells occupying the G_1 phase (47%) accompanied by a statistically significant increase in the number of cells occupying the G_2/M phase (34%) when compared to cells propagated in complete medium (68%, 22% respectively). The MDA-MB-231 cell line resulted in a statistically significant decrease in the number of cells present in the G_1 phase after 24 h (57%),

48 h (61%) and 96 h (56%) of glutamine deprivation when compared to cells propagated in complete growth medium (72%, 68% and 62%, respectively). In addition, the MDA-MB-231 cell line illustrated a statistically significant decrease in the amount of cells occupying the S-phase after 48 h (12%) of glutamine deprivation when compared to the cells propagated in complete growth medium (24%). Furthermore, glutamine deprivation of 24 h and 72 h displayed a statistically significant increase of cells occupying the G_2/M phase with 26% and 22% respectively when compared to cells propagated in complete growth medium. The MCF-10A cell line demonstrated statistically significant decrease in the cells present in the G_2/M phase (24%) after 48 h of glutamine deprivation when compared to the cells propagated in complete growth medium (12%). The BT-20 cell line demonstrated a significant increase of cells occupying the G_1 phase with 58% and 73% of cells present after 48 h and 72 h of glutamine deprivation when compared to cells propagated in complete growth medium (47% and 52% respectively). However, after 96 h of glutamine deprivation 51% of cells occupied the G_1 phase demonstrating a significant decrease when compared to cell propagated in complete growth medium (72%) (Figure 27).

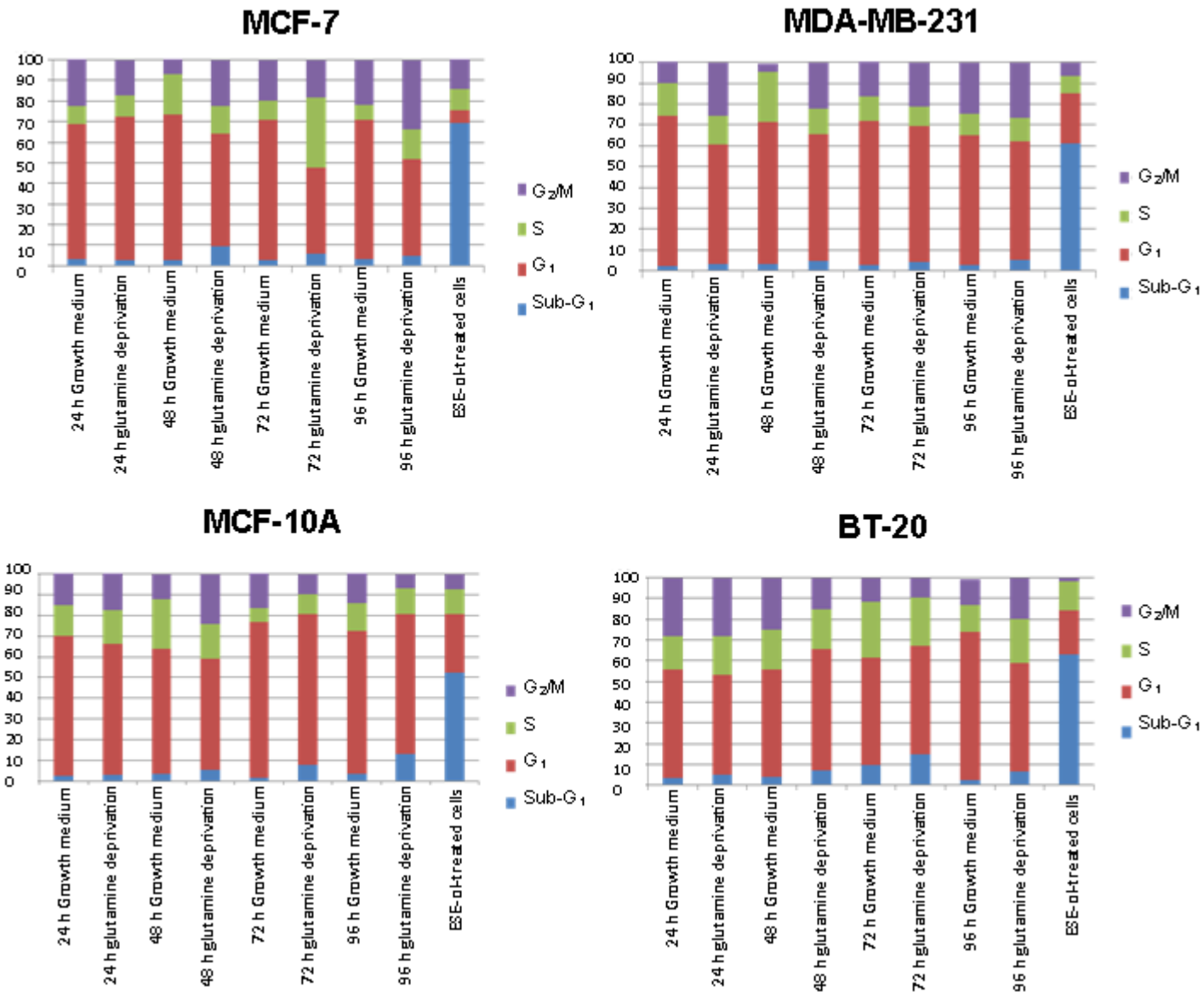

Figure 27: Graphs illustrating cell cycle progression after 24 h, 48 h, 72 h and 96 h of glutamine deprivation in MCF-7-, MDA-MB-231-, MCF-10A- and BT-20 cell lines. MCF-7 cell line (top left) illustrated increased amount of cells in the S-phase. MDA-MB-231 cell line (top right) illustrated increased amount of cells present in the G_2/M phase. MCF10-A cell line (bottom left) illustrated decreased amount of cells present in the G_1 phase and BT-20 cell line (bottom right) illustrated increased cells present in the G_1 phase.

Table 5: Percentage cells occupying each cell cycle phase of the MCF-7-, MDA-MB-231-, MCF-10A- and BT-20 cell lines, where an asterisk (*) indicates significance with *p*-value < 0.05 when calculated by means of the student's t-test when compared to cells propagated in complete growth medium and the average percentage present in each phase ± standard deviations.

Condition	**MCF-7**	**MDA-MB-231**	**MCF-10A**	**BT-20**
24 h Medium only	**Average ± SD (%)**	**Average ± SD (%)**	**Average ± SD (%)**	**Average ± SD (%)**
Sub G_1	3.37 ± 1.54	2.32 ± 1.94	2.4 ± 1.79	3.40 ± 4.42
G_1	65.36 ± 1.97	72.13 ± 4.25	67.89 ± 4.76	52.29 ±3.69
S	8.97 ± 3.98	15.39 ± 1.52	14.52 ± 1.987	16.19 ± 4.83
G_2/M	22.48 ± 4.98	10.35 ± 2.39	16.1 ± 3.85	29.08 ± 2.39
24 h without Glutamine	**Average ± SD (%)**	**Average ± SD (%)**	**Average ± SD (%)**	**Average ± SD (%)**
Sub G_1	2.36 ± 2.96	3.12 ± 0.394	2.95 ± 4.85	5.06 ± 0.21
G_1	69.69 ± 3.96	57.49 ± 3.99*	63.16 ± 4.07	48.33 ± 3.69
S	10.47 ± 0.79	13.86 ± 2.96	15.33 ± 3.26	18.34 ± 4.83
G_2/M	17.08 ± 2.28	25.51 ± 3.85*	18.56 ±1.36	29.25 ± 0.63

Table 6: Percentage cells occupying each cell cycle phase of the MCF-7-, MDA-MB-231-, MCF-10A- and BT-20 cell lines, where an asterisk (*) indicates significance with *p*-value < 0.05 when calculated by means of the student's t-test when compared to cells propagated in complete growth medium and the average percentage present in each phase ± standard deviations.

Condition	**MCF-7**	**MDA-MB-231**	**MCF-10A**	**BT-20**
48 h Medium only	**Average ± SD (%)**	**Average ± SD (%)**	**Average ± SD (%)**	**Average ± SD (%)**
Sub G_1	2.69 ± 4.69	3.23 ± 0.33	3.62 ± 4.25	3.89 ± 3.97
G_1	70.96 ± 2.39	68.39 ± 4.11	60.05 ± 4.6	47.05 ± 1.54
S	19.3 ± 1.44	23.6 ± 2.04	24.02 ± 5.01	15.087 ± 4.22
G_2/M	8.03 ± 0.18	4.086 ± 2.01	12.38 ± 3.59	20.85 ± 4.23
48 h without Glutamine	**Average ± SD (%)**	**Average ± SD (%)**	**Average ± SD (%)**	**Average ± SD (%)**
Sub G_1	9.38 ± 1.87	4.84 ± 1.23	5.21 ± 1.17	7.29 ± 3.57
G_1	54.58 ± 2.92*	60.72 ± 1.31*	54.07 ± 4.03	58.38 ± 4.57*
S	13.66 ± 1.99	12.00 ± 1.79*	16.75 ± 1.96	19.31 ± 1.61
G_2/M	22.36 ± 4.69*	22.41 ± 3.83	23.95 ± 2.28	15 ± 4.28
ESE-ol treated 48h	**Average ± SD (%)**	**Average ± SD (%)**	**Average ± SD (%)**	**Average ± SD (%)**
Sub G_1	69.3 ± 4.36 *	61.3 ± 2.42*	52.36 ± 3.32*	63.203 ±4.36*
G_1	6.3 ± 2.97	23.6 ± 3.95	28.3 ± 3.85	21.20± 3.24
S	10.39 ±1.92	8.64 ± 4.91	11.78 ± 1.36	13.78 ± 4.36
G_2/M	14.01 ± 2.39	6.46 ± 3.93	7.56 ± 4.23	2.04 ± 3.79

Table 7: Percentage cells occupying each cell cycle phase of the MCF-7-, MDA-MB-231-, MCF-10A- and BT-20 cell lines, where an asterisk (*) indicates significance with *p*-value < 0.05 when compared to cells propagated in complete growth medium and the average percentage present in each phase ± standard deviations.

Condition	**MCF-7**	**MDA-MB-231**	**MCF-10A**	**BT-20**
72 h Medium only	**Average ± SD (%)**	**Average ± SD (%)**	**Average ± SD (%)**	**Average ± SD (%)**
Sub G_1	2.73 ± 0.90	2.69 ± 3.24	1.77 ± 1.19	3.56 ± 1.28
G_1	68.26 ± 2.78	69.05 ± 1.19	75.25 ± 4.03	51.82 ± 2.97
S	9.22 ± 1.96	12.10 ± 2.27	6.76 ± 1.58	20.95 ± 2.4
G_2/M	19.78 ± 3.82	14.51 ± 3.16	17.22 ± 1.87	12.54 ± 3.97
72 h without Glutamine	**Average ± SD (%)**	**Average ± SD (%)**	**Average ± SD (%)**	**Average ± SD (%)**
Sub G_1	6.08 ± 3.95	4.40 ± 2.19	7.78 ± 1.57	1.46 ±0.33
G_1	41.33 ± 2.22*	65.01 ± 3.97	72.76 ± 4.26	73.4 ± 1.19*
S	34.38 ± 4.87*	9.53 ± 1.57	9.54 ± 0.53	14.42 ± 4.23
G_2/M	18.19 ± 2.36	21.05 ± 4.36*	9.91 ± 4.82*	11.54 ± 4.46
96 h Medium only	**Average ± SD (%)**	**Average ± SD (%)**	**Average ± SD (%)**	**Average ± SD (%)**
Sub G_1	3.18 ± 0.86	2.56 ± 1.23	3.42 ± 1.11	2.26 ±0.62
G_1	67.81 ± 1.82	62.48 ± 1.31	69.04 ± 2.61	71.56 ± 1.75
S	7.09 ± 1.21	10.46 ± 1.79	13.44 ±0.79	12.96 ± 0.91
G_2/M	21.9 ± 3.18	24.49 ± 3.83	14.37 ± 4.18	12.54 ±3.24
96 h without Glutamine	**Average ± SD (%)**	**Average ± SD (%)**	**Average ± SD (%)**	**Average ± SD (%)**
Sub G_1	4.89 ± 1.04	5.38 ± 0.85	12.93 ± 1.73	4.95 ± 0.86
G_1	46.89 ± 3.061*	56.47 ± 1.66*	67.79 ± 4.76	51.39 ± 1.62*
S	14.66 ±1.85	11.75 ± 2.03	12.64 ± 1.42	18.42 ± 0.54
G_2/M	33.54 ± 4.32*	26.39 ± 1.90	6.64 ± 3.39*	19.41 ± 2.05

Table 8: Histogram modellers of the MCF-7 cell line deprived of glutamine over a period of 96 h in comparison to cells propagated in complete growth medium.

MCF-7 cells 24 h propagated in complete growth medium	MCF-7 24 h deprived of Glutamine
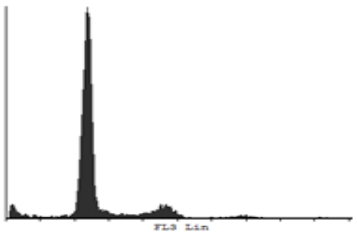	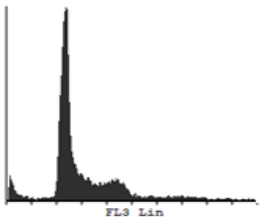
MCF-7 cells 48 h propagated in complete growth medium	MCF-7 48 h deprived of Glutamine
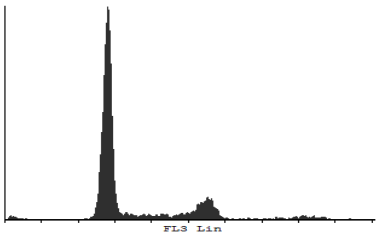	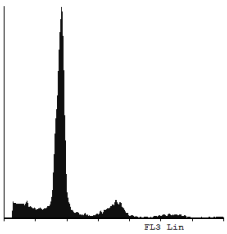
MCF-7 cells 72 h propagated in complete growth medium	MCF-7 72 h deprived of Glutamine
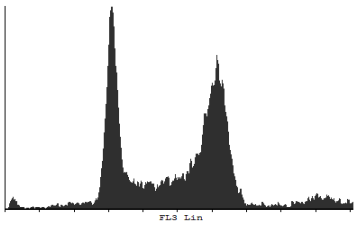	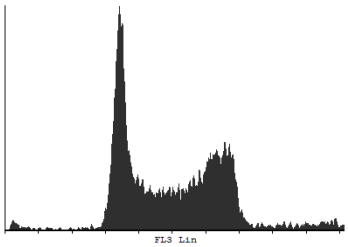
MCF-7 cells 96 h propagated in growth complete medium	MCF-7 96 h deprived of Glutamine
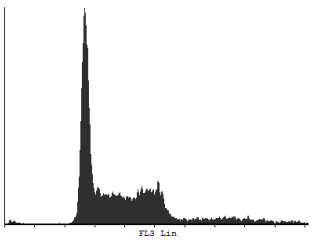	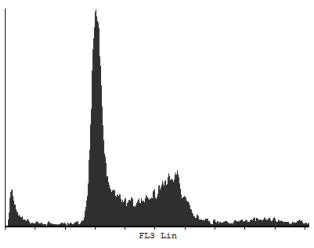

Table 9: Histogram modellers of the MDA-MB-231 cell line deprived of glutamine over a period of 96 h in comparison to cells propagated in complete growth medium.

MDA-MB-231 24 h cells propagated in complete growth medium	MDA-MB-231 24 h deprived of Glutamine
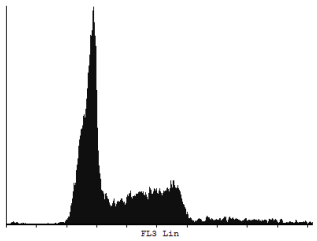	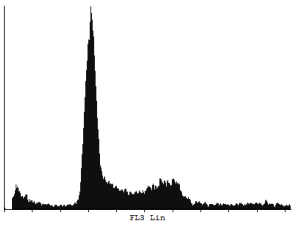
MDA-MB-231 48 h cells propagated in complete growth medium	MDA-MB-231 48 h deprived of Glutamine
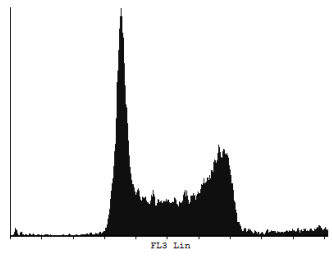	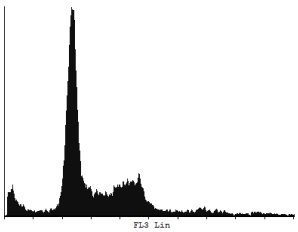
MDA-MB-231 72 h cells propagated in complete growth medium	MDA-MB-231 72 h deprived of Glutamine
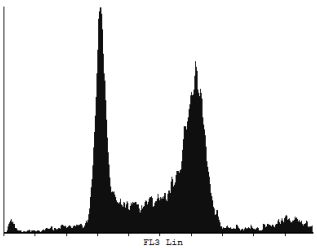	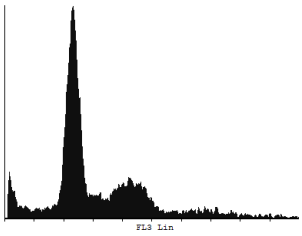
MDA-MB-231 96 h cells propagated in complete growth medium	MDA-MB-231 96 h deprived of Glutamine
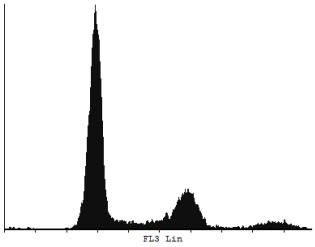	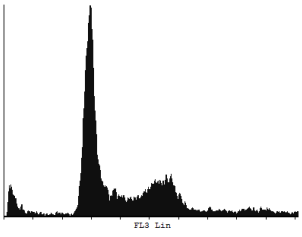

Table 10: Histogram modellers of the MCF-10A cell line deprived of glutamine over a period of 96 h in comparison to cells propagated in complete growth medium.

MCF-10A cells 24 h propagated in complete growth medium	MCF-10A 24 h deprived of Glutamine
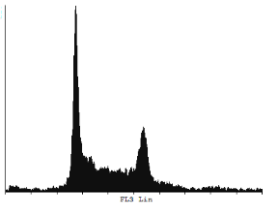	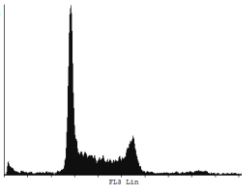
MCF-10A cells 48 h propagated in complete growth medium	MCF-10A 48 h deprived of Glutamine
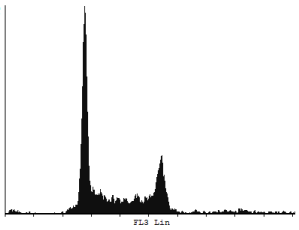	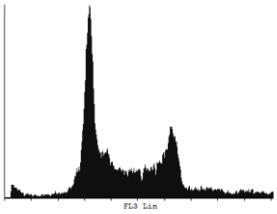
MCF-10A 72 h propagated in complete growth medium	MCF-10A 72 h deprived of Glutamine
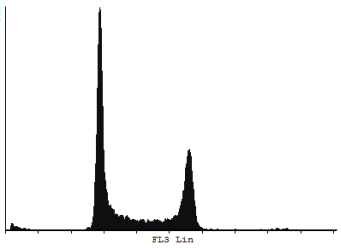	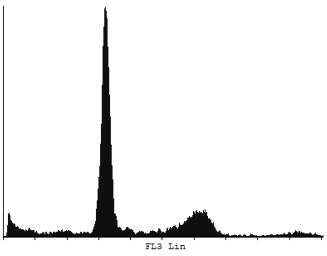
MCF-10A 96 h propagated in complete growth medium	MCF-10A 96 h deprived of Glutamine
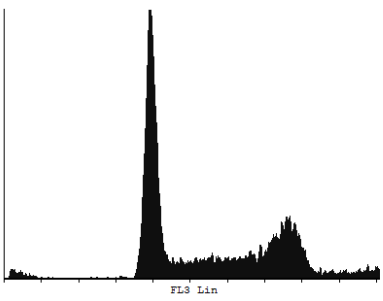	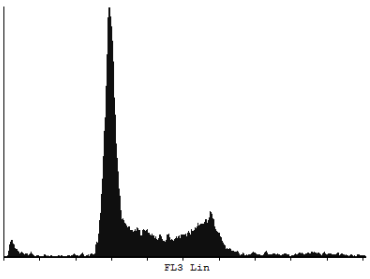

Table 11: Histogram modellers of the BT-20 cell line deprived of glutamine over a period of 96 h in comparison to cells propagated in complete growth medium.

BT-20 24 h propagated in complete growth medium	BT-20 24 h deprived of Glutamine
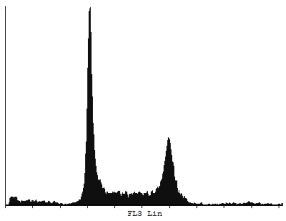	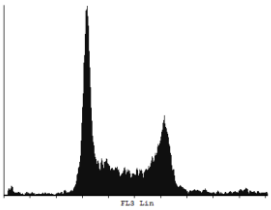
BT-20 48 h propagated in complete growth medium	BT-20 48 h deprived of Glutamine
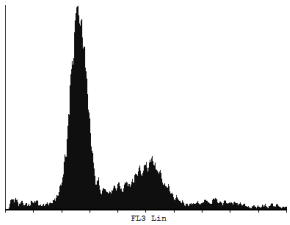	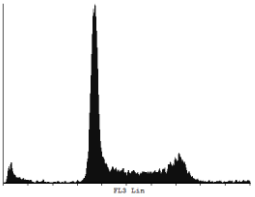
BT-20 72 h propagated in complete growth medium	BT-20 72 h deprived of Glutamine
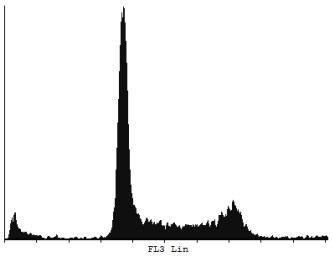	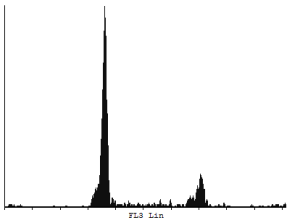
BT-20 96 h propagated in complete growth medium	BT-20 96 h deprived of Glutamine
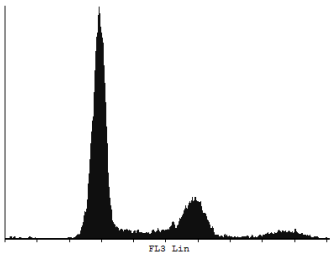	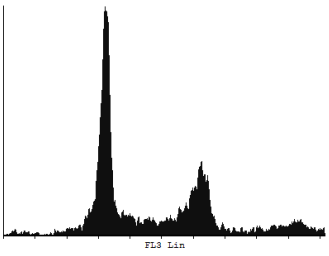

3.9 Mitochondrial membrane potential

Mitochondria are essential for energy metabolism, redox regulation, calcium homeostasis and other cellular functions. Upon high levels of physiological stress, various apoptosis-inducing factors are released from the mitochondria through mitochondrial transition pores into the cytoplasm resulting in induction of cell death (137). The permeability of the mitochondrial pore is dependent on the mitochondrial membrane potential, thus upon mitochondrial membrane depolarisation, apoptotic factors are released through the pores and initiate apoptosis, however, upon hyperpolarisation the membrane reduces its permeability and apoptosis-inducing factors cannot be released into the cytosol thus promoting cell survival (138).

The Mitocapture contains a cationic dye that accumulates in the mitochondria and fluoresces red in non-damaged cells. In cells possessing a depolarised mitochondria membrane potential, the dye cannot accumulate in the mitochondria due to compromised mitochondrial membrane potential and thus remains in the cytoplasm and fluoresces green (137). Furthermore, mitochondrial membrane potential can be hyperpolarised in the event of increased transmembrane potential. Thus, comparing cells propagated in completed medium with cells deprived of glutamine, a ratio above 1 is indicative of cells possessing a depolarised mitochondrial membrane potential and suggests apoptosis induction. A ratio of below 1 which is indicative of cells possessing a hyperpolarized mitochondrial membrane potential suggesting cellular survival (Gergely *et al* 2002) (120).

The MCF-7 cell line demonstrated significant mitochondrial membrane depolarisation after 24 h and 96 h deprivation from glutamine (1.5 and 1.37 fold, respectively) when compared to cells propagated in complete growth medium (Figure 28). The mitochondrial membrane potential of the MDA-MB-231 cell line remained unchanged up until 96 h of glutamine deprivation. The mitochondrial membrane potential of the MCF-10A cell line was depolarised after 24 h of glutamine deprivation and hyperpolarised at 48 h and 72 h of glutamine deprivation. The mitochondrial membrane potential of the BT-20 cell line was depolarised 24 h, 48 h, 72 h and 96 h of glutamine deprivation reaching a ratio of 1.20 after 72 h of glutamine deprivation when compared to cells propagated in complete growth medium (Figure 28).

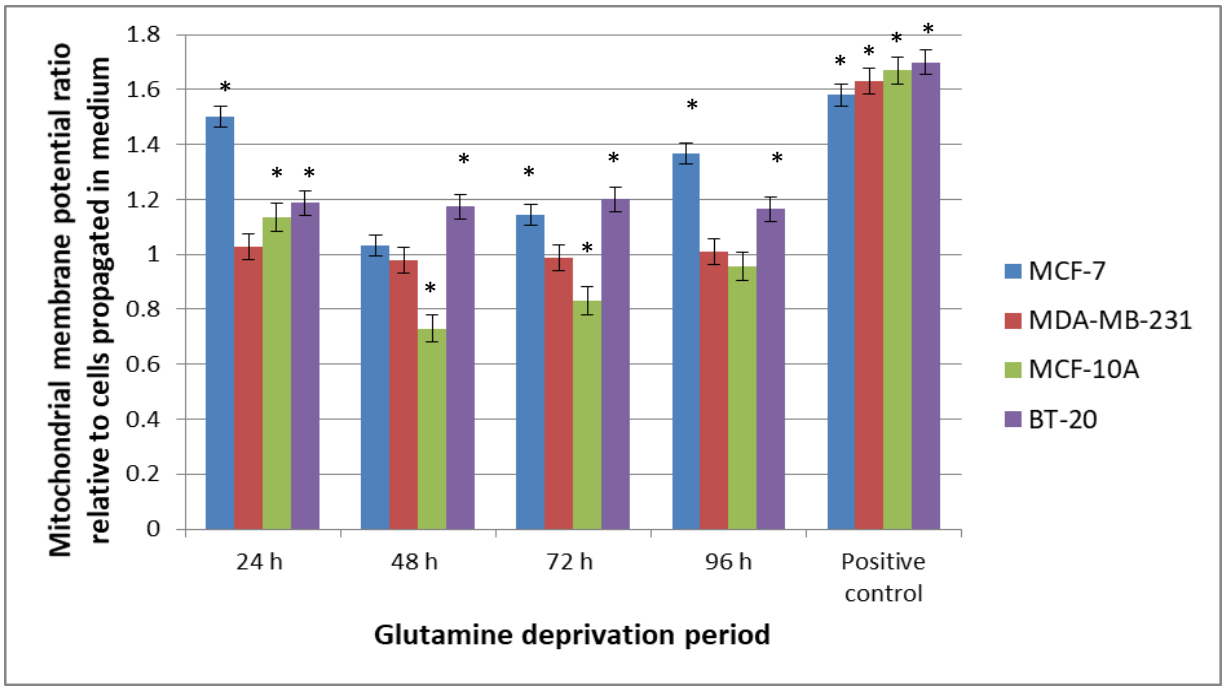

Figure 28: Graph illustrating mitochondrial membrane potential after 24 h, 48 h, 72 h and 96 h of glutamine deprivation in MCF-7-, MDA-MB-231-, MCF-10A- and BT-20 cell lines. MCF-7 and BT-20 cell line illustrated hyperpolarisation whilst the MDA-MB-231 and MCF-10A illustrated time-dependent, biphasic hyperpolarisation of the mitochondrial membrane potential. An asterisk (*) indicates significance with *p*-value < 0.05 when calculated by means of the student's t-test when compared to cells propagated in complete growth medium. Positive control refers to ESE-ol treated cells for 48 h.

4.9 Cell death

The influence of glutamine deprivation on apoptosis and necrosis were quantified using flow cytometry in combination with Annexin V-FITC and propidium iodide. This method allows for the identification of cells undergoing early apoptosis, late apoptosis and necrosis in addition to the viable cells which is differentiated into four quadrants visualised by the flow cytometry analysis software. Propidium iodide stains only the nucleus of compromised membranes since it is membrane impermeable (123). The surface expression of phosphatidylserine translocated from the inner membrane to the outer membrane is considered an early characteristic of apoptosis. The latter event was investigated by means of FITC-conjugated Annexin V.

MCF-7 cell line showed a significant decrease in the number of viable cells after 24 h and 48 h of glutamine deprivation to 88% and 79% respectively, when compared to cells propagated in complete growth medium (Table 12-19 and Figure 29). The MDA-MB-231 cell line demonstrated a significant decrease in cell viability after 96 h of glutamine deprivation to 75% when compared to cells propagated in complete growth medium (97%) of viable cells. The MCF-10A- and BT-20 cell lines illustrated cell viability of 94% and 91%, respectively after 96 h of glutamine deprivation observed (Figure 30).

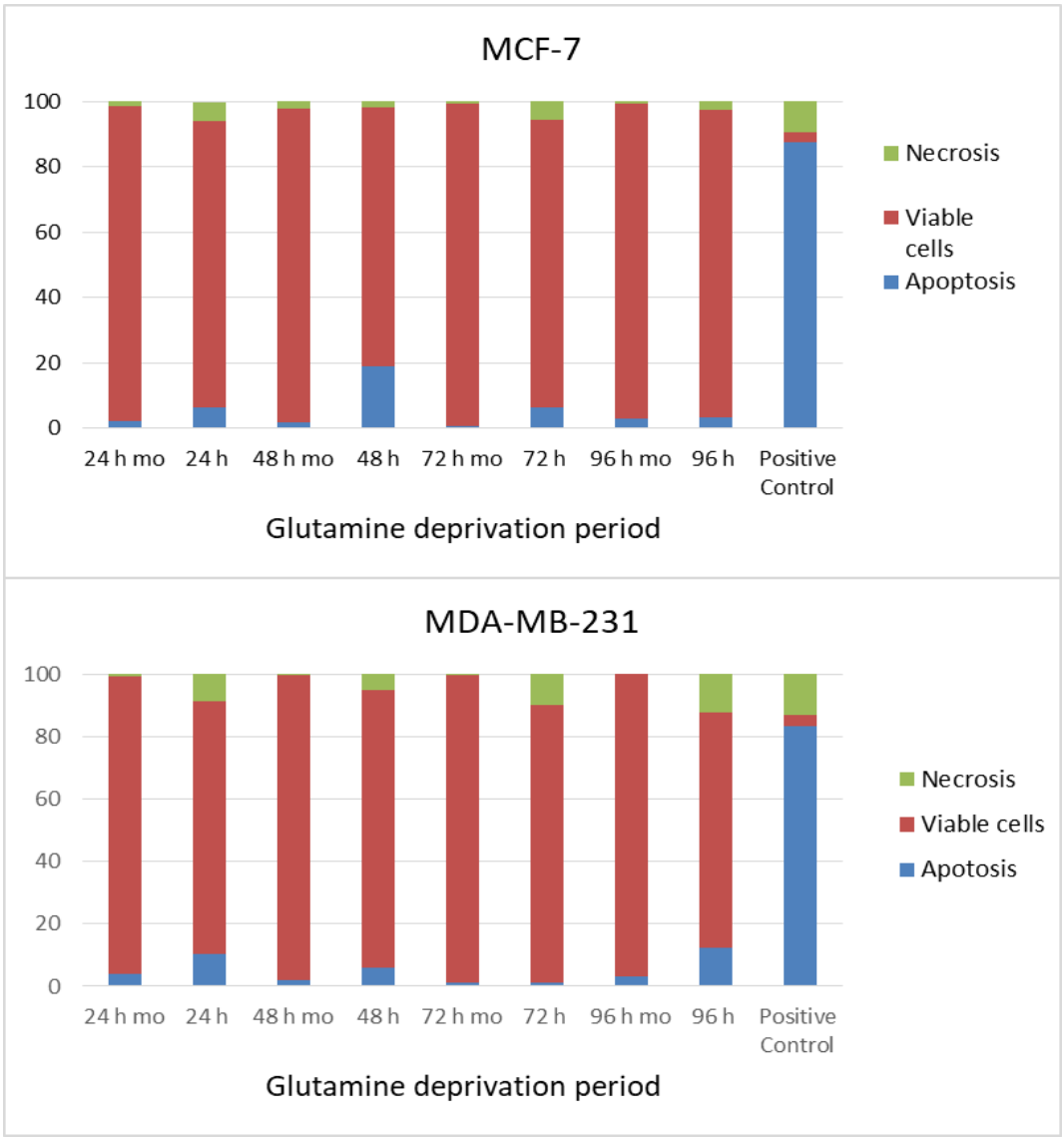

Figure 29: Graphs illustrating apoptosis induction after 24 h, 48 h, 72 h and 96 h of glutamine deprivation in MCF-7- (top) and MDA-MB-231- (bottom) cell lines, where mo (medium only) refers to cells propagated in complete medium and positive control refers to cells treated with ESE-ol-treated cells for 48 h. Decreased cell viability was the most prominently observed following glutamine deprivation in the MCF-7 cell line

(88% and 79%) after 24 h and 48 h. Viability in the MDA-MB-231 cell line decreased to 75% after 96 h of glutamine deprivation.

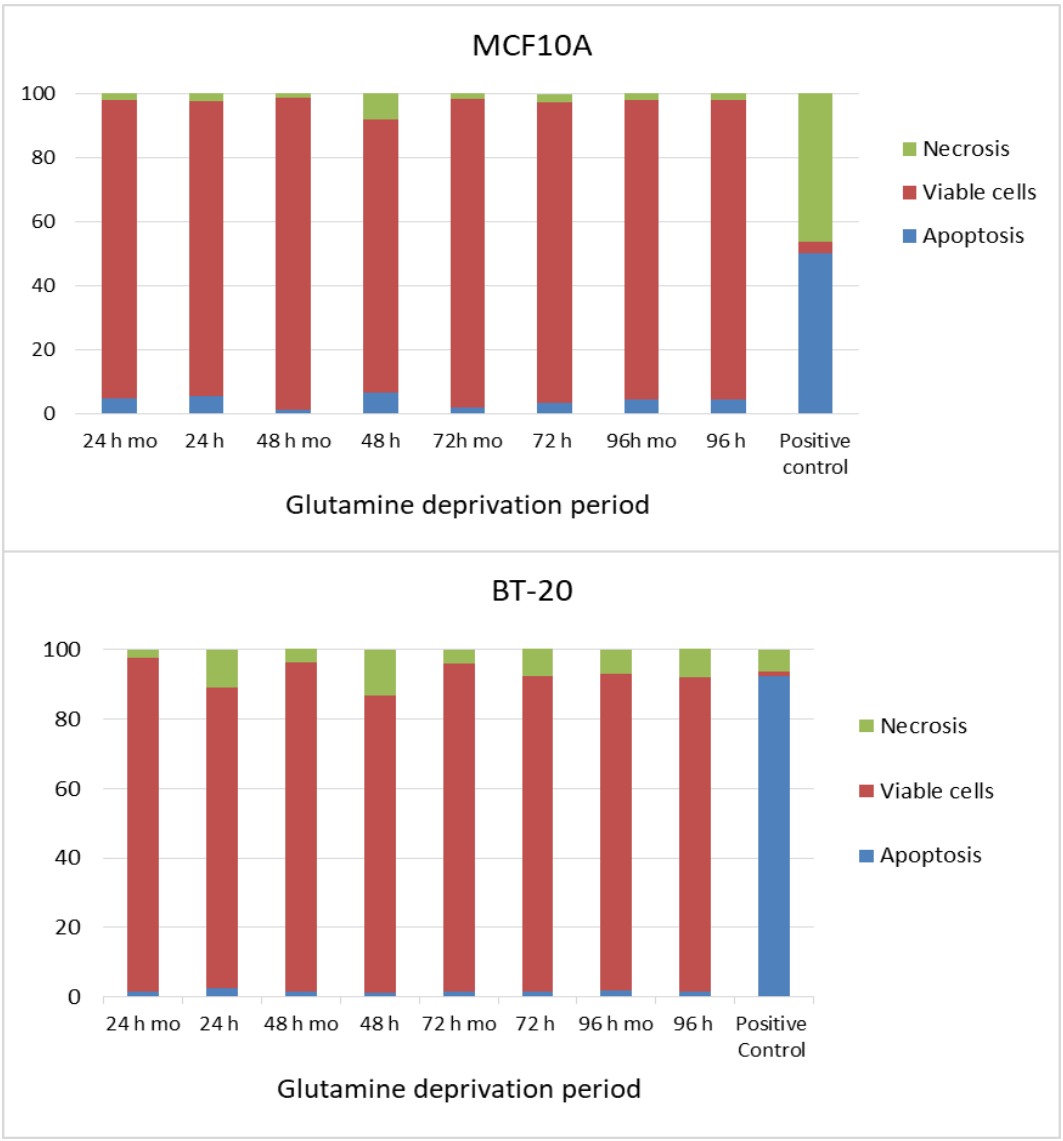

Figure 30: Graphs illustrating apoptosis induction after 24 h, 48 h, 72 h and 96 h of glutamine deprivation in the MCF-10A- (top) and BT-20 (bottom) cell lines, where mo (medium only) refers to cells propagated in complete medium and positive control refers to cells treated with ESE-ol-treated cells for 48 h. The MCF-10A and BT-20 illustrated decreased cell viability to 94% and 91% respectively after 96 h of glutamine deprivation.

Table 12: Illustration of different phases of apoptosis and viable cells with the percentage of cells found each of the particular phase ± standard deviations where an asterisk (*) indicates significance with *p*-value < 0.05 when calculated by means of the student's t-test when compared to cells propagated in complete growth medium in the MCF-7-, MDA-MB-231-, MCF-10A- and BT-20 after 24 h of glutamine deprivation.

Condition	**MCF-7**	**MDA-MB-231**	**MCF-10A**	**BT-20**
24 h Medium only	**Average ± SD (%)**	**Average ± SD (%)**	**Average ± SD (%)**	**Average ± SD (%)**
Early apoptosis	1.23 ± 1.4	1.96 ± 0.04	0.75 ± 0.63	0.99 ± 0.34
Late apoptosis	1.05 ± 2.63	2.18 ± 0.04	3.89 ± 0.96	0.39 ± 0.44
Viable cells	96.31 ± 2.7	95.42 ± 1.16	93.47 ± 1.03	96.29 ± 1.25
Necrosis	2.41 ± 1.09	0.73 ± 1.16	1.89 ± 0.97	2.33 ± 0.53
24 h without Glutamine	**Average ± SD (%)**	**Average ± SD (%)**	**Average ± SD (%)**	**Average ± SD (%)**
Early apoptosis	3.49 ± 1.78	3.72 ± 0.54	1.68 ± 0.3	1.81 ± 1.36
Late apoptosis	3.00 ± 1.7	3.49 ± 1.92	3.82 ± 1.5	0.53 ± 0.30
Viable cells	87.61 ± 4.87*	88.14 ± 1.92*	92.1 ± 1.1	86.86 ± 4.97*
Necrosis	5.69 ± 1.9	4.29 ± 2.27	2.9 ± 1.84	10.79 ± 2.75

Table 13: Illustration of different phases of apoptosis and viable cells with the percentage of cells found each of the particular phase ± standard deviations where an asterisk (*) indicates significance with *p*-value < 0.05 when compared to cells propagated in complete growth medium in the MCF-7-, MDA-MB-231-, MCF-10A- and BT-20 cell lines after 48 h of glutamine deprivation.

Condition	**MCF-7**	**MDA-MB-231**	**MCF-10A**	**BT-20**
48 h with Glutamine	**Average ± SD (%)**	**Average ± SD (%)**	**Average ± SD (%)**	**Average ± SD (%)**
Early apoptosis	0.21 ± 2.31	1.01 ± 1.49	0.93 ± 2.05	1.39 ± 0.43
Late apoptosis	1.74 ± 0.88	1.03 ± 1.99	0.41 ± 0.49	0.96 ± 0.34
Viable cells	95.75 ± 3.96	97.58 ± 2.17	97.29 ± 4.14	96.05 ± 0.98
Necrosis	2.3 ± 2.97	1.06 ± 0.89	1.37 ± 2.51	4.6 ± 0.60
48 h without Glutamine	**Average ± SD (%)**	**Average ± SD (%)**	**Average ± SD (%)**	**Average ± SD (%)**
Early apoptosis	9.87 ± 0.45*	3.06 ± 0.17	2.33 ± 0.9*	0.71 ± 0.21
Late apoptosis	9.25 ± 0.40*	2.71 ± 0.37	5.38 ± 2.24*	0.45 ± 0.19
Viable cells	78.91 ± 1.53*	89.33 ± 1.27*	88.24 ± 1.26*	85.6 ± 2.93*
Necrosis	2.97 ± 1.19	4.9 ± 1.17*	9.04 ± 2.56*	13.23 ± 4.28*
ESE-ol treated 48h	**Average ± SD (%)**	**Average ± SD (%)**	**Average ± SD (%)**	**Average ± SD (%)**
Early apoptosis	56.3 ± 0.16*	41.2 ± 0	39.47 ± 0.35	28.36 ± 0.37
Late apoptosis	31.2 ± 4.69*	42.32 ± 2.28	10.78 ± 0.62	63.89 ± 0.02
Viable cells	3.14 ± 2.82*	3.69 ± 4.00	3.45 ± 2.7	1.39 ± 1.37
Necrosis	9.36 ± 2.58	12.79 ± 2.7	46.3 ± 2.52	6.36 ± 1.41

Table 14: Illustration of different phases of apoptosis and viable cells with the percentage of cells found each of the particular phase ± standard deviations where an asterisk (*) indicates significance with *p*-value < 0.05 when calculated by means of the student's t-test when compared to cells propagated in complete growth medium in the MCF-7-, MDA-MB-231-, MCF-10A- and BT-20 cell lines after 72 h of glutamine deprivation.

Condition	**MCF-7**	**MDA-MB-231**	**MCF-10A**	**BT-20**
72 h Medium only	**Average ± SD (%)**	**Average ± SD (%)**	**Average ± SD (%)**	**Average ± SD (%)**
Early apoptosis	0.1 ± 1.19	0.3 ± 0.51	0.88 ± 0.41	1.69 ± 0.86
Late apoptosis	0.81 ± 1.96	0.69 ± 2.06	0.89 ± 1.84	1.76 ± 0.77
Viable cells	97.3 ± 3.09	98.65 ± 2.14	96.6 ± 2.37	96.57 ± 1.58
Necrosis	0.87 ± 1.52	0.99 ± 1.63	1.63 ± 0.56	3.98 ± 0.15
72 h without Glutamine	**Average ± SD (%)**	**Average ± SD (%)**	**Average ± SD (%)**	**Average ± SD (%)**
Early apoptosis	3.39 ± 0.5*	0.56 ± 0.43	0.75 ± 0.35	0.97 ± 0.31
Late apoptosis	3.06 ± 0.85*	0.49 ± 0.53	2.51 ± 1.05	0.58 ± 0.34
Viable cells	91.84 ± 1.74	89.21 ± 1.22	93.86 ± 4.23	90.95 ± 0.56
Necrosis	5.7 ± 0.52*	9.73 ± 0.39*	2.5 ± 2.19	7.74 ± 1.06

Table 15: Illustration of different phases of apoptosis and viable cells with the percentage of cells found each of the particular phase ± standard deviations where an asterisk (*) indicates significance with *p*-value < 0.05 when calculated by means of the student's t-test when compared to cells propagated in complete growth medium in the MCF-7-, MDA-MB-231-, MCF-10A- and BT-20 cell lines after 96 h of glutamine deprivation.

Condition	**MCF-7**	**MDA-MB-231**	**MCF-10A**	**BT-20**
96 h without Glutamine	**Average ± SD (%)**	**Average ± SD (%)**	**Average ± SD (%)**	**Average ± SD (%)**
Early apoptosis	1.55 ± 0.5	1.36 ± 1.42	1.36 ± 0.25	0.83 ± 0.45
Late apoptosis	1.36 ± 0.9	1.71 ± 2.23	2.91 ± 2.45	0.96 ± 0.52
Viable cells	96.3 ± 2.27	97.03 ± 3.48	93.77 ± 4.97	96.22 ± 1.1
Necrosis	0.79 ± 1.2	0.9 ± 1.13	1.96 ± 4.17	6.99 ± 0.44
96 h without Glutamine	**Average ± SD (%)**	**Average ± SD (%)**	**Average ± SD (%)**	**Average ± SD (%)**
Early apoptosis	1.68 ± 2.23	6.25 ± 3.27	1.26 ± 1.24	0.92 ± 1.23
Late apoptosis	1.75 ± 2.77	6.22 ± 1.92	3.06 ± 1.94	0.65 ± 0.28
Viable cells	93.81 ± 4.39	75.49 ± 1.64*	93.67 ± 4.67	90.61 ± 2.3
Necrosis	2.45 ± 1.05*	12.08 ± 1.56*	2.1 ± 1.76	8.07 ± 1.89

Table 16: Illustration of dot plots indicating different phases of apoptosis and viable cells where each of the four quadrants indicate a different phase of apoptosis and viable cells in the MCF-7 cell line when compared to cells propagated in complete growth medium over a period of 96 h. Top left- dead cells, top right- Late apoptotic cells, bottom left- Viable cells, bottom right- Early apoptosis.

MCF-7 24 h propagated in complete growth medium	MCF-7 24 h deprived of glutamine
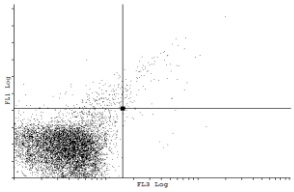	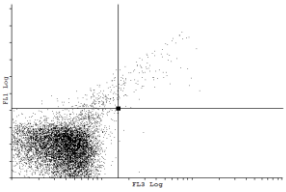
MCF-7 48 h propagated in complete growth medium	MCF-7 48 h deprived of glutamine
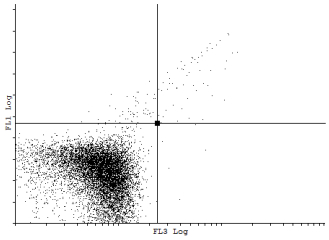	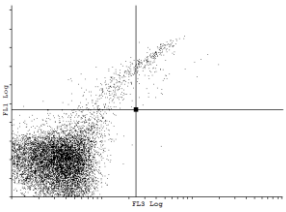
MCF-7 72 h propagated in complete growth medium	MCF-7 72 h deprived of glutamine
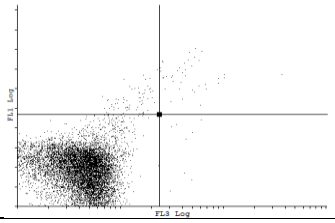	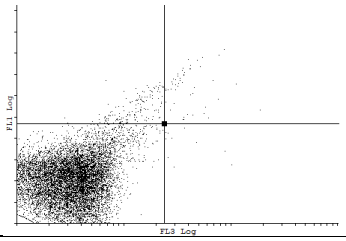
MCF-7 96 h propagated in complete growth medium	MCF-7 96 h deprived of glutamine
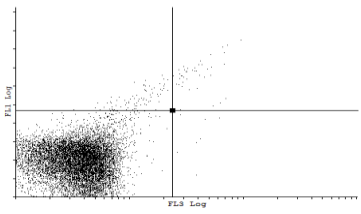	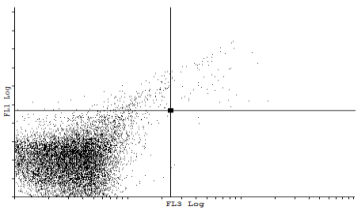

Table 17: Illustration of dot plots indicating different phases of apoptosis and viable cells where each of the four quadrants indicate a different phase of apoptosis and viable cells in the MDA-MB-231 cell line when compared to cells propagated in complete growth medium over a period of 96 h. Top left- dead cells, top right- Late apoptotic cells, bottom left- Viable cells, bottom right- Early apoptosis.

MDA-MB-231 24 h propagated in complete growth medium	MDA-MB-231 24 h deprived of glutamine
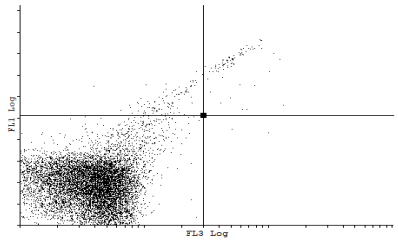	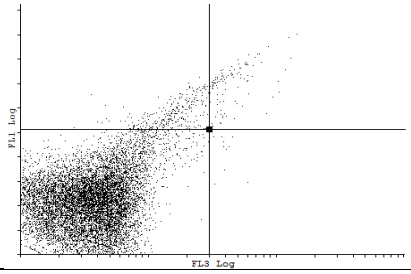
MDA-MB-231 48 h propagated in complete growth medium	MDA-MB-231 48 h deprived of glutamine
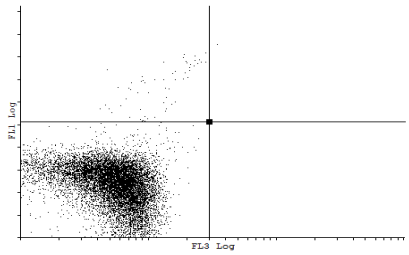	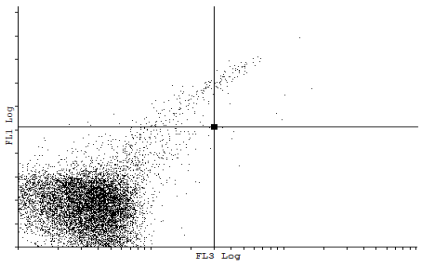
MDA-MB-231 72 h propagated in complete growth medium	MDA-MB-231 72 h deprived of glutamine
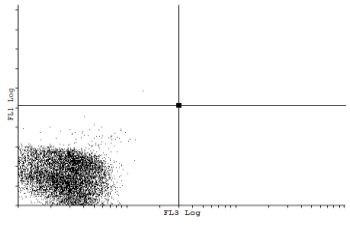	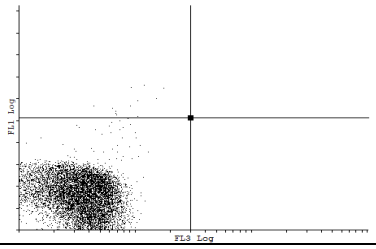
MDA-MB-231 96 h propagated in complete growth medium	MDA-MB-231 96 h deprived of glutamine
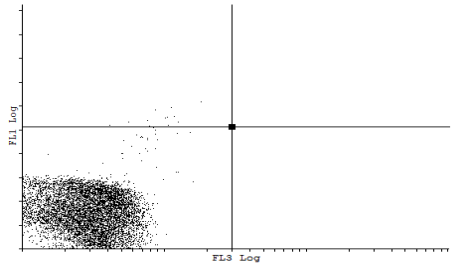	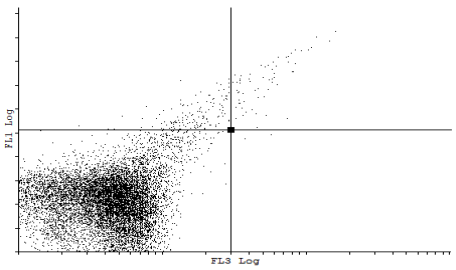

Table 18: Illustration of dot plots indicating different phases of apoptosis and viable cells where each of the four quadrants indicate a different phase of apoptosis and viable cells in the MCF10-A cell line when compared to cells propagated in complete growth medium over a period of 96 h. Top left- dead cells, top right- Late apoptotic cells, bottom left- Viable cells, bottom right- Early apoptosis.

MCF-10A 24 h propagated in complete growth medium	MCF-10A 24 h deprived of glutamine
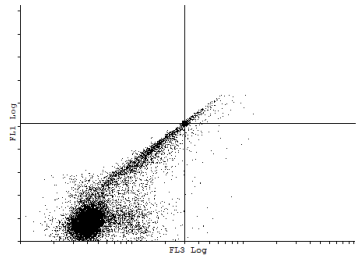	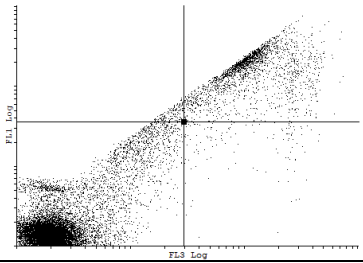
MCF-10A 48 h propagated in complete growth medium	MCF-10A 48 h deprived of glutamine
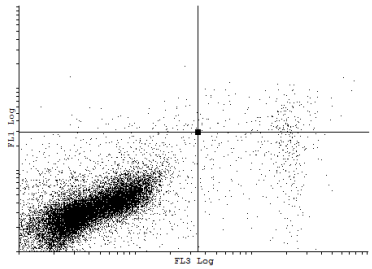	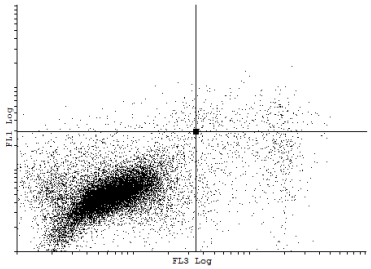
MCF-10A 72 h propagated in complete growth medium	MCF-10A 72 h deprived of glutamine
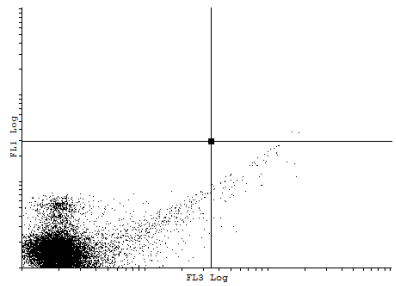	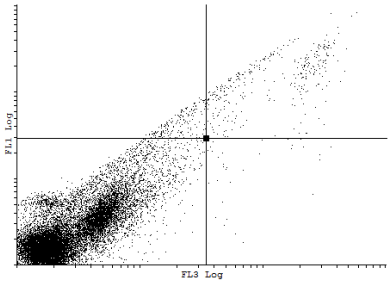
MCF-10A 96 h propagated in complete growth medium	MCF-10A 96 h deprived of glutamine
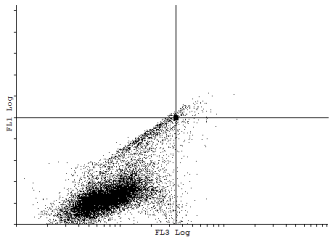	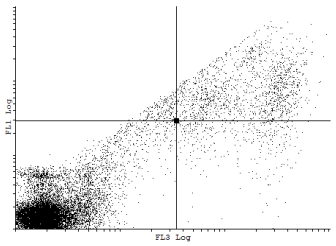

Table 19: Illustration of dot plots indicating different phases of apoptosis and viable cells where each of the four quadrants indicate a different phase of apoptosis and viable cells in the BT-20 cell line when compared to cells propagated in complete growth medium over a period of 96 h. Top left- dead cells, top right- Late apoptotic cells, bottom left- Viable cells, bottom right- Early apoptosis.

BT-20 24 h propagated in complete growth medium	BT-20 24 h deprived of glutamine
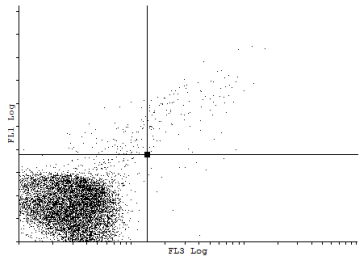	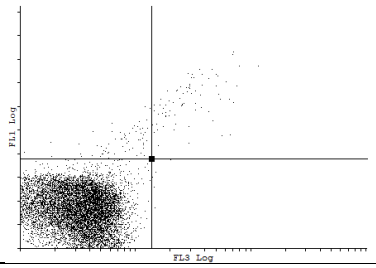
BT-20 48 h propagated in complete growth medium	BT-20 48 h deprived of glutamine
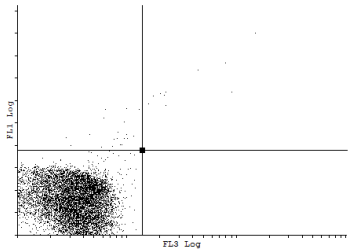	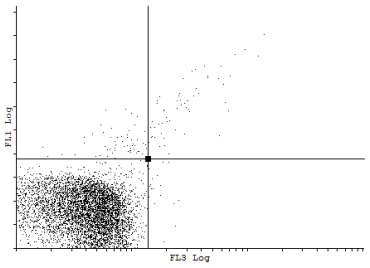
BT-20 72 h propagated in complete growth medium	BT-20 72 h deprived of glutamine
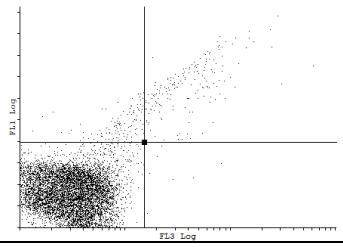	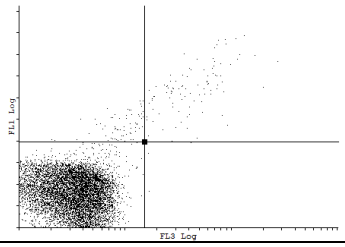
BT-20 96 h propagated in complete growth medium	BT-20 96 h deprived of glutamine
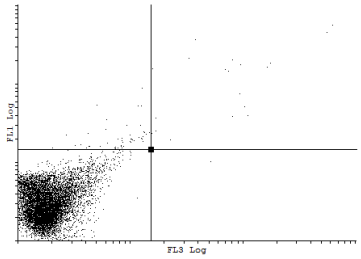	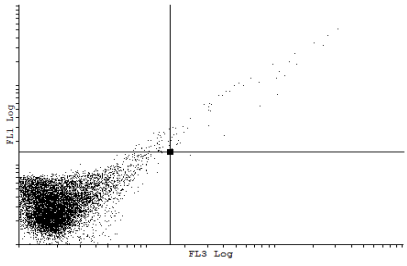

Autophagy is a compensatory mechanism that produces energy from cytoplasmic contents including damaged and/or redundant organelles and proteins which prevents accumulation of waste products thus maintaining homeostasis (139). Autophagy is induced by starvation and oxidative stress. The autophagy protein light chain 3 (LC3) is a mammalian protein is associated with the autophagosome membranes and used to identify autophagy induction. LC3-I is cytosolic whilst LC3-II is found in the membrane and is predominately located in the autophagic vacuole (140). The presence of LC3-II serves as an optimal marker for autophagy induction and is detectable via fluorescent microscopy and visualised as diffuse cytoplasmic pool or as punctate structures that primarily represent autophagosomes (141). The influence of glutamine deprivation on autophagy induction was demonstrated by means of LC3II visualisation.

The MCF-7 cell line showed no difference in staining intensity or in punctate structures after 24 h, 48 h, 72 h and 96 h of glutamine deprivation when compared to cells propagated in complete growth medium (Figures 31-34). The MDA-MB-231 cell line demonstrated minimal punctate structures after 24 h, 48 h, 72 h and 96 h of glutamine deprivation when compared to cells propagated in complete growth medium. The MCF-10A cell line showed no damage to the cells after 24 h, 48 h, 72 h and 96 h of glutamine deprivation when compared to cells propagated in complete growth medium. The BT-20 cell line demonstrated no effect caused by glutamine deprivation after 24 h, 48 h, 72 h and 96 h of glutamine deprivation when compared to cells propagated in complete growth medium. However, the cells appeared to be disseminated when compared to cells propagated in complete growth medium. Thus data suggest autophagy is not induced by glutamine deprivation (Figures 31-34).

MCF-7 cells propagated in complete medium for 24 h	MCF-7 cells deprived of glutamine for 24 h
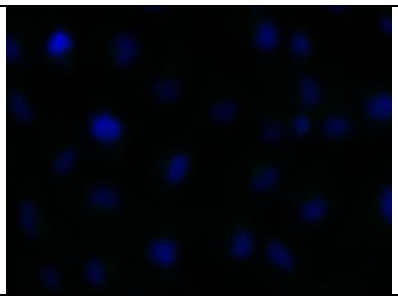	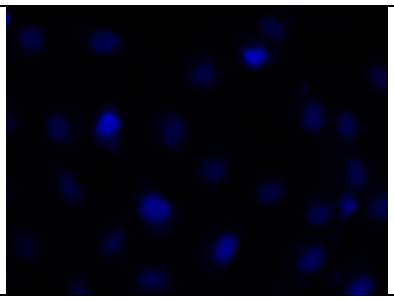
MCF-7 cells propagated in complete medium for 48 h	MCF-7 cells deprived of glutamine for 48 h
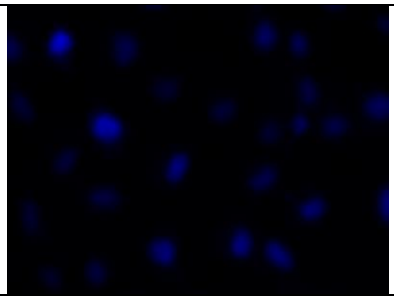	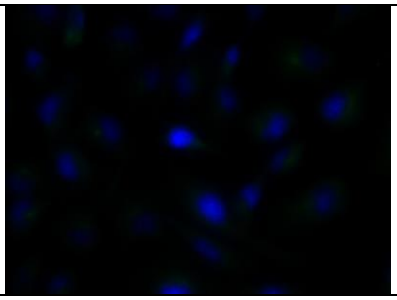
MCF-7 cells propagated in complete medium for 72 h	MCF-7 cells deprived of glutamine for 72 h
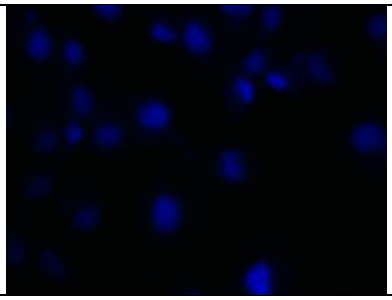	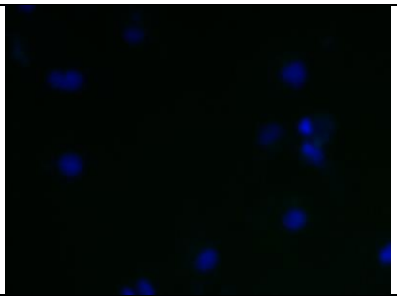
MCF-7 cells propagated in complete medium for 96 h	MCF-7 cells deprived of glutamine for 96 h
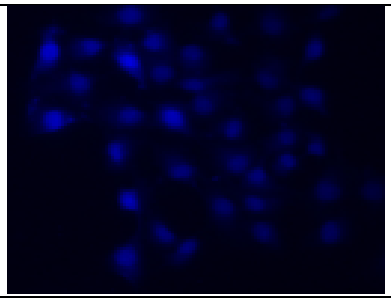	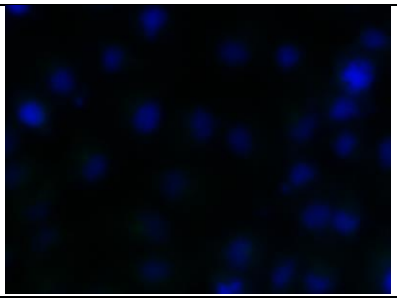

Figure 31: Illustration of LC3-IIB (green punctate structures around the nucleus) in MCF-7 cell line after 24 h, 48 h, 72 h and 96 h of glutamine deprivation, indicating a lack of autophagy induction.

MDA-MB-231 cells propagated in complete medium for 24 h	MDA-MB-231 cells deprived of glutamine for 24 h
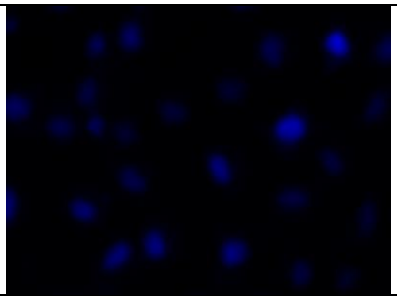	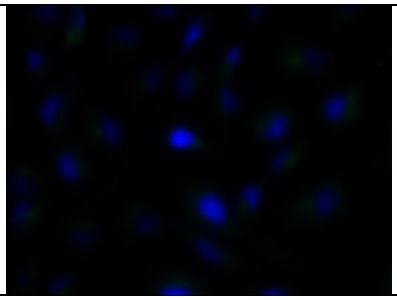
MDA-MB-231 cells propagated in complete medium for 48 h	MDA-MB-231 cells deprived of glutamine for 48 h
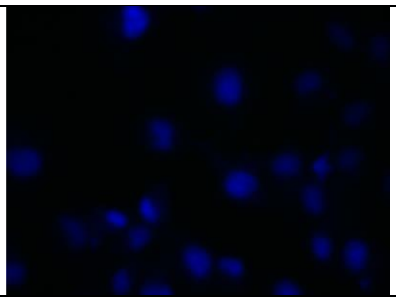	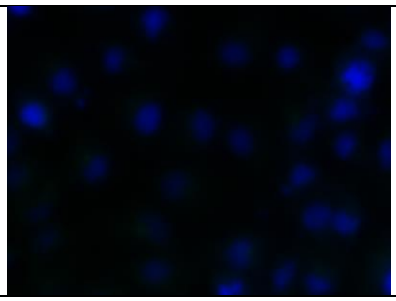
MDA-MB-231 cells propagated in complete medium for 72 h	MDA-MB-231 cells deprived of glutamine for 72 h
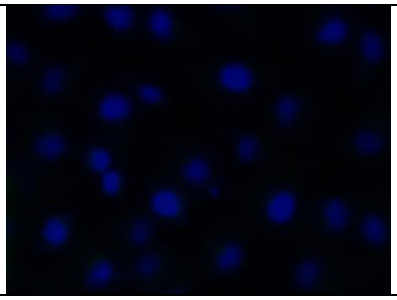	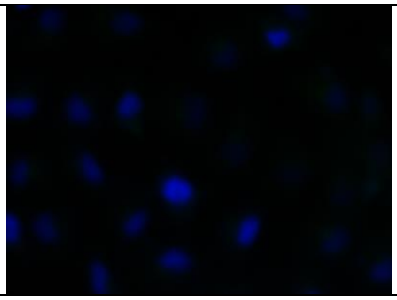
MDA-MB-231 cells propagated in complete medium for 96 h	MDA-MB-231 cells deprived of glutamine for 96 h
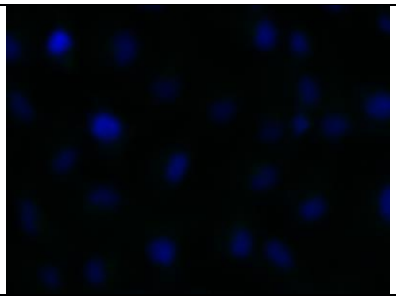	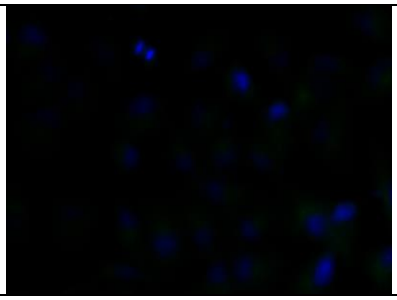

Figure 32: Illustration of LC3-IIB (green punctate structures around the nucleus) in MDA-MB-231 cell line after 24 h, 48 h, 72 h and 96 h of glutamine deprivation, indicating a lack of autophagy induction.

MCF-10A cells propagated in complete medium for 24 h	MCF-10A cells deprived of glutamine for 24 h
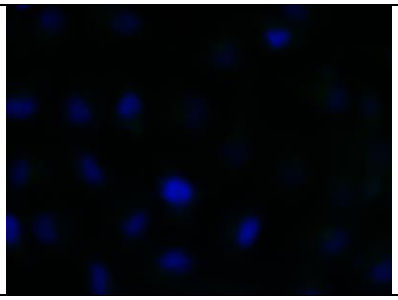	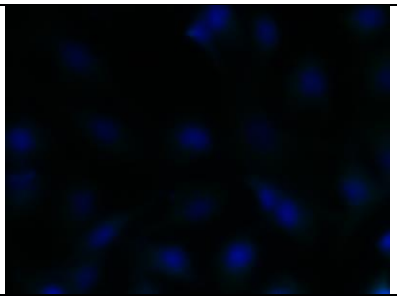
MCF-10A cells propagated in complete medium for 48 h	MCF-10A cells deprived of glutamine for 48 h
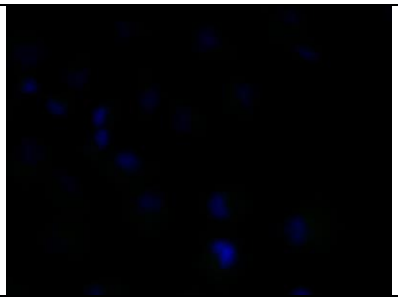	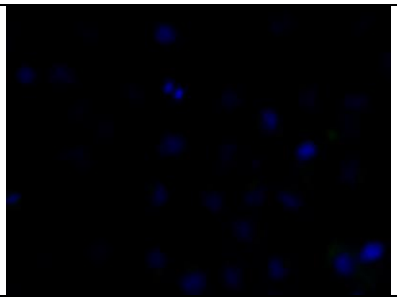
MCF-10A cells propagated in complete medium for 72 h	MCF-10A cells deprived of glutamine for 72 h
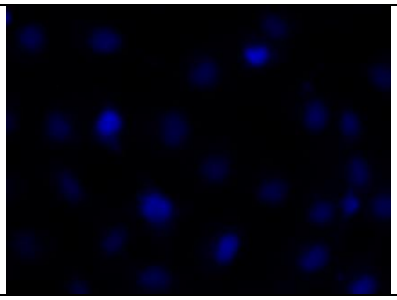	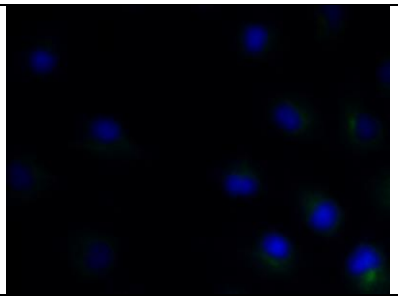
MCF-10A cells propagated in complete medium for 96 h	MCF-10A cells deprived of glutamine for 96 h
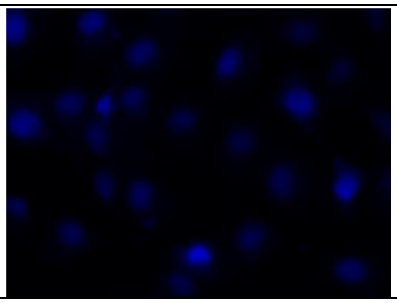	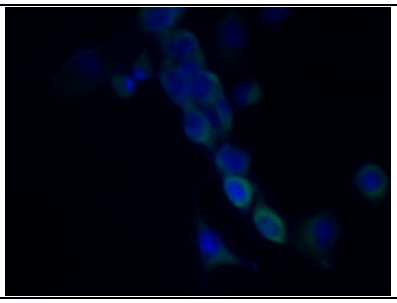

Figure 33: Illustration of LC3-IIB (green punctate structures around the nucleus) in MCF-10A cell line after 24 h, 48 h, 72 h and 96 h of glutamine deprivation, indicating a lack of autophagy induction.

BT-20 cells propagated in complete medium for 24 h	BT-20 cells deprived of glutamine for 24 h
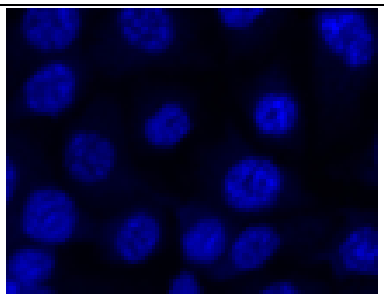	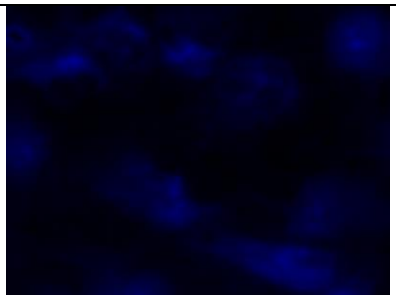
BT-20 cells propagated in complete medium for 48 h	BT-20 cells deprived of glutamine for 48 h
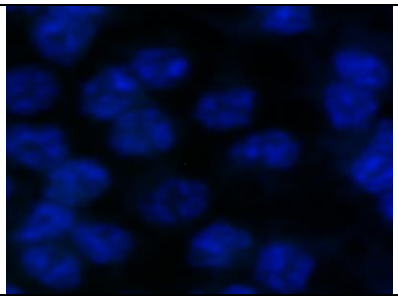	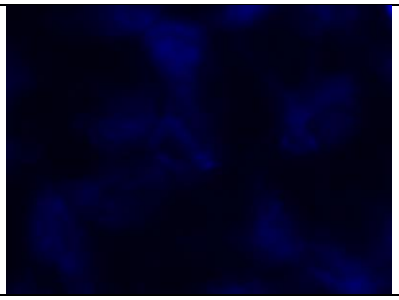
BT-20 cells propagated in complete medium for 72 h	BT-20 cells deprived of glutamine for 72 h
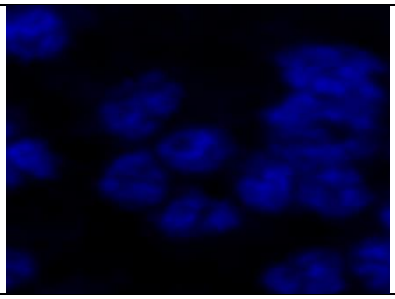	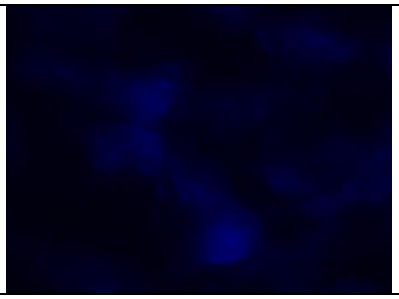
BT-20 cells propagated in complete medium for 96 h	BT-20 cells deprived of glutamine for 96 h
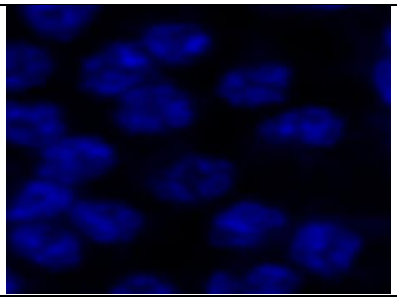	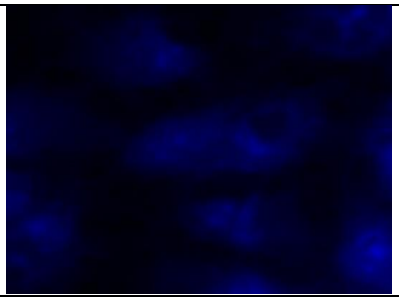

Figure 34: Illustration of LC3-IIB (green punctate structures around the nucleus) in BT-20 cell line after 24 h, 48 h, 72 h and 96 h of glutamine deprivation, indicating a lack of autophagy induction.

MCF-7 cells treated with bafiliomycin for 48 h	MDA-MB-231 cells treated with bafiliomycin for 48 h
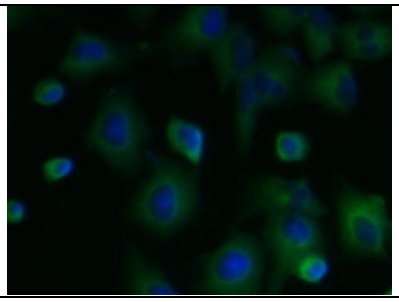	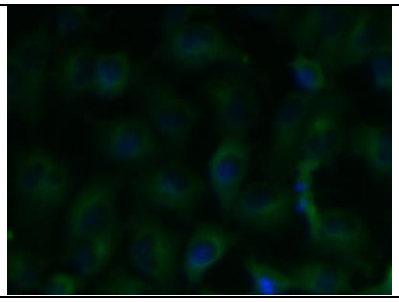
MCF-10A cells treated with bafiliomycin for 48 h	BT-20 cells treated with bafiliomycin for 48 h
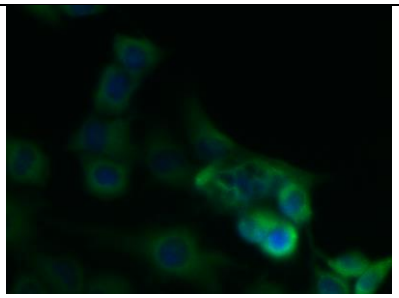	

Figure 35: Illustration of LC3-IIB (green punctate structures around the nucleus) in MCF-7-, MDA-MB-231-, MCF-10A and BT-20 cell line after treatment with bafiliomycin for 48 h used as positive control.

CHAPTER 5

5. DISCUSSION

Tumourigenic cells modify metabolic activities, including glycolysis and glutaminolysis, when compared to differentiated- and non-proliferating cells (142). These altered metabolic events exerted by tumourigenic cells are required for the hyperproliferative nature of transformed- and tumourigenic tissue in order to support the biosynthetic requirements for hyperproliferation, survival and prolonged energy maintenance which is characterised by glucose metabolism into lactate dehydrogenase independent of oxygen availability (Warburg effect) (143). Due to the upregulated metabolic activity, increased glycolysis and glutaminolysis, increased expression of glucose- and amino acid transporters is required which results in increased production of ATP (144). In order to fully take advantage of tumourigenic aberrant metabolism for potential future therapeutics, it is necessary to fully comprehend how glutamine deprivation influences tumourigenic proliferation, redox regulation, mitochondrial membrane potential, cell survival, DNA damage and cell death. In this study, the influence of glutamine deprivation on proliferation, morphology, ROS production, antioxidant defences, cell cycle progression, possible cell death via apoptosis- and autophagy induction, DNA damage and cell survival signaling were investigated in tumourigenic- and non-tumourigenic cell lines.

In this research project spectrophotometry data indicates that glutamine deprivation results in time-dependent antiproliferative effects in both metastatic tumourigenic MCF-7- and MDA-MB-231 cell lines. Furthermore, this study demonstrates that glutamine deprivation lead to more prominent antiprolifertaive activity in the luminal MCF-7 cell line when compared to the basal MDA-MB-231-, MCF-10A- and BT-20 cell lines. This suggests that the tumourigenic ER positive, luminal cell line is more dependent on glutamine as a source of energy for proliferation in comparison to basal, triple negative cell line MDA-MB-231 and BT-20 cell lines suggesting dependency of glutamine by metastatic and tumourigenic cells. These findings are supported by Kung, *et al* (2011) who reported that glutamine deprivation (48 h) resulted in compromised cell growth in the MDA-MB-231 cell line, breast tumourigenic basal oestrogen receptor negative (MDA-MB-157) cell line, MCF-7 cell

line and a breast tumourigenic luminal oestrogen receptor positive (BT-474) cell line (100). The resistance observed from MDA-MB-231-, MCF-10A- and BT-20 cell lines is due to the cell type's ability to synthesize *de novo* glutamine or opt for alternative routes for anaplerosis to provide energy generating pathways that utilize carbon and nitrogen to supplement the Krebs cycle which will subsequently support the cells with energy thus allowing the cell lines to survive without glutamine (145). Furthermore, this study demonstrated that glutamine deprivation refrained from affecting the non-tumourigenic MCF-10A cell line. This indicates that tumourigenic cell lines are more susceptible to glutamine deprivation when compared to non-tumourigenic cell lines thus confirming that glutamine is a crucial nutrient for optimal cell proliferation.

Reactive oxygen species play an important role in tumourigenesis. ROS are a group of molecules produced during metabolism and are signaling molecules at low and intermediary concentrations; however, in high concentration ROS is detrimental to the cells by damaging lipids, proteins, DNA and leads to oxidative stress (146). Flow cytometry data demonstrated that ROS production after glutamine deprivation is time-dependent. Superoxide is an anion radical and a precursor of a variety of other ROS (147). The production of superoxide in the MCF-7 cell line was increased after 96 h of glutamine deprivation and was most prominently affected when compared to the MDA-MB-231-, MCF-10A and BT-20 cell lines. These results are supported by other nutrient deprivation studies where glucose deprivation resulted in increased levels of superoxide in colon- and breast cancer cell lines (148). As superoxide is a precursor of a plethora of ROS, increased metabolism and ROS production will subsequently lead to increased levels of superoxide. Hydrogen peroxide is produced from an enzymatic reaction involving the detoxification of superoxide thus constitutes as ROS (149). Hydrogen peroxide production was significantly increased in the MDA-MB-231 cell line after 24 h of glutamine deprivation. Yuan *et al* (2013) confirmed that ROS was increased in the ovarian cancer cell lines HEY-, SKOV3- and IGOROV-1 after 24 h of glutamine deprivation (150). In addition, hydrogen peroxide with concentrations above 100 µM is known to be cytotoxic and induces DNA damage and thus inhibits proliferation. The decreased cell proliferation studies after 24 h of glutamine deprivation in the MCF-7 cell line correlate with increased hydrogen peroxide production and also confirm that significantly elevated ROS levels are detrimental to cell growth. Vilema-Eriquez *et al* (2016) observed that hydrogen

peroxide production (50-200 µM) inhibited proliferation in the MCF-7 cell line (151). However, hydrogen peroxide generation decreased thereafter in a time-dependent manner in MCF-7 and MDA-MB-231 cell lines following glutamine deprivation. The reduction in ROS quantities due to glutamine starvation indicates a possible decrease in cellular metabolism which correlates with the decrease in AMPK activity (prominently observed in the MCF-7 cell line) observed in this study which is responsible for the maintenance of energy status. Hydrogen peroxide generation in MCF-10A- and BT-20 cell lines increases in a time-dependent manner following glutamine deprivation. High ROS concentrations have physiological importance to tumourigenic cells as ROS participate in cellular signaling pathways and induction of mitogenic responses, thus correlating with the cell growth results where BT-20 cell line remains unchanged (152). Furthermore, an increase in hydrogen peroxide may suggest that the antioxidant mechanism in which superoxide is neutralized by superoxide dismutase to hydrogen peroxide is functional (153). The increased- and decreased quantities of ROS observed in this study following glutamine deprivation are time- and cell line-dependent and is possibly due to the shortage of carbon sources that supplies the Krebs cycle with intermediates to further support the survival of tumourigenic cells indicating a possible shift in cellular metabolism from glutaminolysis to alternative anaplerotic pathways that support pyruvate carboxylation (154).

Data demonstrated via flow cytometry that the mitochondrial membrane potential of the MDA-MB-231- and MCF-10A cell lines experienced time-dependent hyperpolarisation after glutamine deprivation. Eukaryotic cells maintain a hyperpolarised mitochondrial membrane potential to avoid the release of pro-apoptotic agents such as *cytochrome c* which will induce apoptosis (155). However, tumourigenic cells have elevated levels of hyperpolarisation as a pro-survival mechanism as described by Forrest M *et al* (2015) (156). Sastre-Serra *et al* (2010), suggests that an increase with mitochondrial membrane potential which is termed hyperpolarisation, enhances ROS production and thus promote tumourigenicity (157). The MDA-MB-231 cell line experienced hyperpolarisation as well as increased ROS production thus hyperpolarisation experienced correlates with increased ROS production in this study. Furthermore, the BT-20 cell line showed no antiproliferative effects further confirming adaptation following glutamine deprivation. Dmitry *et al*

(2014), reported that hyperpolarisation of the mitochondrial membrane potential coincided with the generation of excessive ROS (hydrogen peroxide) production, which further reiterates the increased hydrogen peroxide production of our study (158). The presence of transient hyperpolarisation is observed in the MDA-MB-231 cell line following glutamine deprivation and may possibly be explained by a temporal blockage in the electron transfer chain (159). Thus, mitochondria are able to withstand high levels of oxidative stress and develop adaptive mechanism to ensure optimal functioning thus supporting tumourigenicity (160).

Extensive antioxidant defence mechanisms counteract free radicals in cells in order to prevent oxidative stress which refers to a disturbance in the balance between the production of free radicals and antioxidant defences (161). Superoxide dismutase is an enzyme that converts superoxide anion to hydrogen peroxide which is further detoxified by catalase to water and oxygen. Spectrometry data obtained showed low levels of SOD inhibition rate suggesting that the SOD activity is high. Increased levels of SOD activity is associated with advanced tumours as described by Ennen *et al* (2011), hence on average, the SOD inhibition rate in this study, is decreased due to the advanced origin of the cell lines used (162). The MCF-7 cell line showed increased SOD activity after 24 h- and 48 h of glutamine deprivation. These results were confirmed by Hart *et al* (2015), where luminal breast cancer samples stratified by stage demonstrated SOD activity to be significantly elevated in progressing tumour stages (163). Furthermore, after 24 h of glutamine deprivation, the MCF-7 cell line demonstrated a significant increase in superoxide- and hydrogen peroxide production suggesting that SOD was functional as illustrated by decreased SOD inhibition suggesting the detoxification of superoxide to hydrogen peroxide aided by SOD. Although catalase is frequently downregulated in tumours the underlying mechanism remains unclear. Furthermore, spectrometry data demonstrated that MCF-7 cell line demonstrated significant increase in catalase concentration after 24 h of glutamine deprivation when compared to cells propagated in complete growth medium. Goh *et al* (2011) reported that the presence of catalase resulted in reduced intracellular ROS in tissue excised from transgenic mice that overexpresses PytMT referring to the expression of the T antigen from polyoma virus and subsequent enhanced tumor progression (164). In the current study, following the increase of catalase concentration after 24 h of glutamine deprivation, the MCF-7 cell line

experienced decreased hydrogen peroxide production thus correlating with findings reported by Goh *et al* (2011) (164).

Reactive oxygen species (ROS) produced either endogenously or exogenously damage lipids, protein and nucleic acid cells (165). In nuclear- and mitochondrial-DNA, 8-hydroxydeoxyguanosine, an oxidized nucleoside of DNA, is frequently detected and indicates oxidative stress-induced DNA damage (166). Fluorescent microscopy demonstrated that glutamine deprivation resulted in increased formation of 8-hydroxydeoxyguanosine which is indicative of an oxidative form of DNA damage. The MCF-7 luminal cell line demonstrated significant DNA damage caused by oxidative stress after 48 h of glutamine deprivation. In addition, previous studies indicated that significantly elevated levels of 8-hydroxydeoxyguanosine was observed in oestrogen receptor-positive tissue when compared with oestrogen-negative malignant tissues, and in breast cancer cell lines, suggests a positive relationship between 8-hydroxydeoxyguanosine formation and oestrogen responsiveness (167). Histone H2AX phosphorylation is a sensitive marker for DNA double-strand breaks which is a result of various factors including ROS production and oxidative stress (168). This study demonstrated that the luminal, MCF-7 cell line indicated more double stranded breaks when compared to the MDA-MB-231-, MCF-10A- and BT-20 cell lines. In addition, the MCF-7 cell line demonstrated increased ROS formation. Previous studies suggest that environmental factors including poor nutritional profile results in DNA damage which this study implements by depleting cells of nutrient (glutamine) (169). Given the complexity of breast cancer in which gene-environment interactions play a significant role in the development of cancer, oxidative stress may be an excellent model for exploring mechanisms mediating gene-environment interactions and investigations that may help to suggest future strategies for therapeutics.

Cell cycle progression analysis via flow cytometry demonstrated an increase in the number of cells present in the S-phase in the MCF-7 cell line after 72 h of glutamine deprivation accompanied by a significant decrease in the G_1 phase of the cell cycle. This suggests nucleotide depletion as glutamine serves a nitrogen donor to purine nucleobases namely guanine and adenine. Thus glutamine deprivation may induce slower cycling cells in the S-phase as elucidated by Gaglio *et al* (2009) due to

inadequate pairing of nucleotide bases (170). Cyclin D1 and CDK4 which promote the entry of cells into the S-phase are upregulated by glutamine in a concentration-dependent manner. The MDA-MB-231 cell line resulted in a significant increase in cells present in the G_2/M phase after 24 h of glutamine deprivation which was also found by Kansara *et al* (2004) who demonstrated that the fibrosarcoma cell line, KHT-C2-LP1, showed a significant number of cells present in the G_2/M phase of the cell cycle suggesting there is rapid protein synthesis due to the cells efforts to adapt to the lack of glutamine and thus adequate carbon sources needed for sufficient energy production (171). MCF-10A cells demonstrated a significant decrease in the G_1 phase after 96 h of glutamine deprivation. Glutamine deprivation in the BT-20 cell line resulted in a significant increase G_1 phase after 72 h of glutamine deprivation. These results suggest that glutamine deprivation differentially affects cell cycle progression phases in a time-dependent manner.

Programmed cell death is an evolutionarily conserved pathway resulting in a morphological cell death termed apoptosis or type I cell death. Hallmarks of apoptosis include membrane blebbing, cell shrinkage, chromatin condensation and endonucleolytic cleavage of DNA. During the initial stages of apoptosis, phosphatidylserine is translocated from the inner plasma membrane to the outer as a marker for phagocytosis (172). Annexin V paired with flow cytometry was utilized to detect the PS flip which demonstrated that the MCF-7 cell line is the only cell line to be significantly affected with regards to apoptosis induction after glutamine deprivation. These studies demonstrated that glutamine deprivation reduced cell viability in a time-dependent manner in the MCF-7 cell line to 75% after 96 h of glutamine deprivation, with a corresponding increase in cells observed in apoptosis and necrosis when compared to cells propagated in complete growth medium. This corresponds with earlier findings from the present study where glutamine deprivation resulted in decreased cell proliferation, oxidative stress and disruption in the mitochondrial membrane potential in the MCF-7 cell line indicating the induction of apoptosis including by means of the mitochondrial pathway.

The PI3K and ERK pathways are well known pathways that regulate of cell survival, cell proliferation, metabolism and differentiation (173). However, the production of PI3K and ERK in the luminal MCF-7 cell line was decreased after glutamine

deprivation, thus suggesting that glutamine has a direct effect on the cell survival signaling in luminal cell lines. ERK activation in the MCF-7 was decreased after 48 h of glutamine deprivation which further suggest that the survival mechanism in the luminal cell line is compromised correlating with the antiproliferative studies. The basal cell lines MCF-10A and BT-20 cell line demonstrated activation of ERK pathway after 72 h glutamine deprivation, which elaborates the maximal cell growth in the proliferation studies.

Autophagy is a catabolic process that functions in recycling and degrading cellular proteins, and is also induced as an adaptive response to the increased metabolic demand upon nutrient starvation (174). In this study glutamine deprivation did not induce autophagy in both luminal and basal subtypes cell lines. Studies suggest that glutamine is required for autophagy-induced mammalian target of rapamycin complex 1 (mTORC1) to be reactivated during amino acid starvation (175). Active mTORC1 also phosphorylates and activates p70S6K which in turn phosphorylates ribosomal protein S6 to enhance translation efficiency (176). Thus, mTORC1 increases protein translation when amino acids are available. Amino acids are considered the most critical regulator of mTORC1 because growth factors alone cannot activate the kinase efficiently during amino acid deprivation (177). Although autophagy releases free amino acids during amino acid deprivation, the level of replenishment is insufficient thus autophagy fails confirmed by Onodera *et al* (2005) (178).

CHAPTER 6

6. CONCLUSION

From this study it is evident that glutamine deprivation results in differential- and time dependent, antiproliferative activity and aberrant changes in the cell cycle progression; increased superoxide production, biphasic hydrogen peroxide production, negligible apoptosis- and autophagy induction, increased SOD- and differential catalase activity, decreased cell survival signaling and increased DNA damage. All of the mentioned effects more prominently observed in the luminal tumourigenic MCF-7 cell line when compared to the basal tumourigenic MDA-MB-231. The non-tumourigenic MCF-10A and non-metastatic BT-20 cell lines were least affected by glutamine deprivation. This study provides evidence that there are differential, time-dependent responses in different types of tumourigenic breast cell lines following glutamine deprivation in comparison to non-tumourigenic cell lines. Understanding how, when and which kind of cell types adapt to glutamine deprivation is essential in future treatments targeting tumourigenic metabolism since more drugs are being developed that target cancer cell metabolism. Furthermore, glutamine deficiency may influence non-tumourigenic tissue tolerance to antitumour treatment, and will potentially possess pre-sensitizing effects to chemotherapeutic treatments. In conclusion the hypothesis proved to be true where glutamine deprivation differentially affected proliferation, morphology, oxidative stress, cell survival, innate antioxidant systems, energy status, DNA damage, mitochondrial functioning, cell cycle progression, cell survival signaling and cell death induction in tumourigenic breast cell lines when compared to a non-tumourigenic breast cell line.

Limitations and future perspectives

Breast cancer varies greatly in patients when compared to the limited types of breast cancer cell lines utilized in cell culture. In addition, cell models may not translate in the whole body system, effects may prevail on cellular level however different effects in animal models and whole body system may be observed. Future investigations will elucidate the molecular pathway of glutamine addiction in tumourigenic cells which promotes proliferation, thus halting this process may have promising therapeutic strategies for anti-cancer agents.

CHAPTER 7

REFERENCES

1. Youlden DR, Cramb SM, Dunn NAM, Muller JM, et al. The descriptive epidemiology of female breast cancer : An international comparison of screening, incidence, survival and mortality. Cancer Epidemiol. 2012; 36(3):237-248.

2. Torre L a, Bray F, Siegel RL, Ferlay J, Lortet-tieulent J, Jemal A. Global cancer statistics, 2012: an update on the management of breast cancer in Africa; J Clin. 2015;65(2):87-108.

3. Dal Maso, C Buzzani, A Caldarella et al. Long-term survival, prevalence, and cure of cancer: a population-based estimation for 818 902 Italian patients and 26 cancer types. Ann Oncol. 2014;25(11):2251-2260.

4. Giacosa A, Barale R, Bavaresco L, Gatenby P, Gerbi V, Janssens J, et al. Cancer prevention in Europe. Eur J Cancer Pre. 2013;22(1):90-99.

5. Bhardwaj A, Tiwari A. Breast cancer diagnosis using genetically optimized neural network model.Sci. 2015;42(10):4611-4620.

6. Louie M.C, Sevigny M.B, Steroid hormone receptors as prognostic markers in breast cancer. Am J Cancer Res. 2017;7(8):1617-1636.

7. Negi P, Kingsley P.A, Jain K. Survival of triple negative versus triple positive breast cancers comparison and contrast. Asian Pacific Journal of Cancer Prev.2016; 17(8):3911-3916.

8. Larrionov A. Current therapies for human epidermal growth factor receptor 2-positive metastatic breast cancer patients. Front Oncol. 2018;89(8).

9. Jieun Koh, Min Jung Kim. Introduction of a new staging system of breast cancer for radiologists: an emphasis on the prognostic stage. Korean J.Radiol. 2018; 20(1):69-82.

10. Palma G, Fasci G, Chirico A, Siani, C et al. Triple negative breast cancer:

looking for the missing link between biology and treatments. Oncotarget. 2015 6(29): 26560-26574.

11. Sancho P, Barneda D, Heeschen C. Hallmarks of cancer stem cell metabolism Br J Cancer. 2016;114(12):1305-1312.

12. Cairns R a, Harris IS, Mak TW. Regulation of cancer cell metabolism. Nat Rev Can. 2011;10(3):85-95.

13. Shanware NP, Mullen AR, DeBarardinis RJ, Abraham R. Glutamine: pleiotropic roles in tumour growth and stress resistance. J Mol Med. 2011; 89(3):229-236.

14. Hensley CT, Wasti AT, Deberardinis RJ. Glutamine and cancer : cell biology , physiology , and clinical opportunities. J Clin Invest. 2013;123:3678-3684.

15. Zheng J. Energy metabolism of cancer: Glycolysis versus oxidative phosphorylation. Oncol Lett. 2012;4(6):1151-1157.

16. Suganuma K, Hiroshi M, Imai N. Energy metabolism of leukemia cells: glycolysis *versus* oxidative phosphorylation**.** Leukemia and Lymphoma. 2010; 51(11):2112-2119.

17. Chen JQ, Russo J. Dysregulation of glucose transport, glycolysis, TCA cycle and glutaminolysis by oncogenes and tumour suppressors in cancer cells. Biochim Biophys Acta. 2012; 1826(2):370-384.

18. Wellen KE, Lu C, Mancuso A, Lemons JMS, Ryczko M, Dennis JW, et al. The hexosamine biosynthetic pathway couples growth factor-induced glutamine uptake to glucose metabolism. Genes Dev. 2010;24(24):2784-2799.

19. Broer A, Broer S, Rahimi F. deletion of amino acid transporter ASCT2 (SLC1A5) reveals an essential role for transporters SNAT1 (SLC38A1) and SNAT2 (SLC38A2) to sustain glutaminolysis in cancer cells.JBC. 2016;291:1314-13205.

20. Zang J, Pavlova N, Thompson C. Cancer cell metabolism: the essential role of the nonessential amino acid, glutamine. EMBO J. 2017;36:1302-1315.

21. Jin L, Alesi GN, Kang S. Glutaminolysis as a target for cancer therapy. Oncogene. 2016;35(28):3619-3625.

22. Wang L, Li J,Alesi GN, Kang S. Molecular link between glucose and glutamine consumption in cancer cells mediated by CtBP and SIRT4.Oncogenesis. 2018;26.

23. Petronini P, Urbani S, Alfieri R. Cell susceptibility to apoptosis by glutamine deprivation and rescue: Survival and apoptotic death in cultured lymphoma-leukemia cell lines. J of Cellular Physio. 1996; 169(1):175-185.

24. Harnett CC, Guerin PJ, Furtak T, Gauthier ER. Control of late apoptotic events by the p38 stress kinase in l-glutamine-deprived mouse hybridoma cells. Cell Biochem Funct. 2013;31:417-426.

25. Poillet-Perez L, Despouy G, Delage-Mourroux R, Boyer-Guittaut M. Interplay between ROS and autophagy in cancer cells, from tumour initiation to cancer therapy. Redox Biol. 2014;4:181-192.

26. Turrens JF. Mitochondrial formation of reactive oxygen species. J Physiol. 2003;552:335-344.

27. West AP, Shadel GS, Ghosh S. Mitochondria in innate immune responses. Nat Rev Immunol.2011; 11(6):389-402.

28. Glasauer A, Chandel NS. ROS. Current Bio. 2013; 23(3):100-102.

29. Zhang D, Wang L, Yan L, Miao X, Gong C, Xiao M, et al. Vacuolar protein sorting 4B regulates apoptosis of intestinal epithelial cells via p38 MAPK in Crohn's disease. Exp Mol Pathol. 2015;98(1):55-64.

30. Pateras IS, Havaki S, Nikitopoulou X, Vougas K, Townsend PA, Panayiotidis MI, et al. The DNA damage response and immune signaling alliance: Is it good or bad? Nature decides when and where. Pharmacol Ther. 2015;154:36-56.

31. Ly JD, Grubb DR, Lawen A. The mitochondrial membrane potential ($\Delta\psi_m$) in apoptosis; an update. Apoptosis. 2003;8(2):15-128.

32. Forrest MD. Why cancer cells have a more hyperpolarised mitochondrial membrane potential and emergent prospects for therapy. Biorxiv. 2015:1-42.

33. Sastre-Serra S, Valle A, Garau I, Oliver J, Roca P. Estrogen down-regulates uncoupling proteins and increases oxidative stress in breast cancer. Free Radic Biol Med. 2010; 48: 506-512.

34. Hu P, Tirelli N. Scavenging ROS: Superoxide dismutase/catalase mimetics by the use of an oxidation-sensitive nanocarrier/enzyme conjugate. Bioconjug Chem. 2012;23:438-449.

35. Huutemann M, Pecina P, Rainbolt M, Sanderson TH. The multiple functions of cytochrome *c* and their regulation in life and death decisions of the mammalian cell: from respiration to apoptosis. Mitochondrion. 2011;11(3):369-381

36. Gloriux C, Calderon PB. Catalase, a remarkable enzyme: targeting the oldest antioxidant enzyme to find a new cancer treatment approach. Biol Chem. 2017;398(10)1095-1108.

37. Birben E, Sahiner UM, Sackesn C. Oxidative Stress and Antioxidant Defense. World allergy Organ J. 2012;5(1)9-19.

38. Yan Liu, Yue-Hong Long, Shu-Qing Wang, Yu-Feng Li and Jing-Hua Zhang, Phosphorylation of H2A.XTyr39 positively regulates DNA damage response and is linked to cancer progression.FEBS J. 2016; 4462-4473.

39. Kang J, Fergurson D, Song H Bassing C, Eckersdorff M, Alt FW, Xu Y. Functional Interaction of H2AX, NBS1, and p53 in ATM-dependent DNA damage responses and tumor suppression. Mol Cell Biol. 2005 Jan; 25(2):661-670.

40. Martins G, Tavares A, Fortunato E, Goreti M, Sales F. Paper-based sensing device for electrochemical detection of oxidative stress biomarker 8-hydroxy-2′-deoxyguanosine (8-OHdG) in Point-of-Care. Nature. 2017;7(14558).

41. Xu D, Huang C, Xie L, Shao B et. Mechanism of unprecedented hydroxyl radical production and site-specific oxidative DNA damage by photoactivation of the classic arylhydroxamic acid carcinogens. Carcinogenesis. 2019.

42. Luo J, Manning BD, Cantley LC. Targeting the PI3K-AKT pathway in human cancer: rationale and promise. cancer cell 2003;4(4):257-262.

43. Zhang W, Liu HT. MAPK signal pathways in the regulation of cell proliferation in mammalian cells. Cell Res. 2002;12(1):9-18.

44. Thompson N, Lyons J. Recent progress in targeting the Raf/MEK/ERK pathway with inhibitors in cancer drug discovery. Curr Opin Pharmacol. 2005;5(4):350-356.

45. McMahon S. Emerging concepts in the analysis of transcriptional targets of the myc oncoprotein. are the targets targetable. Genes Cancer.2010;1(6):560-567.

46. Gao P, Tchernyshyov I, Chang TC, Lee YS, Kita K, Ochi T, et al. c-Myc suppression of miR-23a/b enhances mitochondrial glutaminase expression and glutamine metabolism. Nature. 2009;458:762-765.

47. Dang CV. MYC, Metabolism, cell growth, and tumorigenesis.Cold Spring Harb Perspeect Med. 2013.3(8).

48. Davies C, Tournier C. Exploring the function of the JNK (c-Jun N-terminal kinase) signaling pathway in physiological and pathological processes to design novel therapeutic strategies.J Physiol. 2012;85-99.

49. Hemmings BA, Restuccia DF. PI3K-PKB/Akt Pathway. Cold Spring Harbour Perspect Biol. 2012;4(9).

50. Fayard E , Xue G, Parcellier A, Bozulic L, Hemmings BA. Protein kinase B (PKB/Akt), a key mediator of the PI3K signaling pathway. Curr Top Microbiol Immunol. 2010;346:31-56

51. Mendoza MC, Er EE, Blenis J. The Ras-ERK and PI3K-mTOR pathways : cross-talk and compensation. Trends Biochem Sci .2011; 36(6):320-328.

52. Huang J. Manning BD. The TSC1-TSC2 complex: a molecular switchboard controlling cell growth. Biochem J. 2008 Jun 1; 412(2): 179-190.

53. Parcellier A, Tintignac LA, Zhuravlea E, Hemmings BA. PKB and the mitochondria: AKTing on apoptosis. Cellular Sig. 2008;20(1): 21-30.

54. Van der Vos KE Eliasson P, Proikas-Cezanne T, Vervoort SJ, van Boxtel R, Putker M et al. Modulation of glutamine metabolism by the PI(3)K-PKB-FOXO network regulates autophagy. Nat Cell Biol. 2012;14(8):829-37.

55. Mihaylova MM, Shaw RJ. The AMP-activated protein kinase (AMPK) signaling pathway coordinates cell growth, autophagy, & metabolism. Mol Cell. 2012; 13(9):1016-1023.

56. Jeon S. Regulation and function of AMPK in physiology and diseases.Nat. 2016;48.

57. Woods A, Dickerson K, Heath H et al. Ca^{2+}/calmodulin-dependent protein kinase kinase-β acts upstream of AMP-activated protein kinase in mammalian cells.Cell Meta. 2005;2(1);21-23.

58. Daniel Garcia, Reuben J. Shaw. AMPK: mechanisms of cellular energy sensing and restoration of metabolic balance. Mol Cell. 2017;66(6):789-800.

59. Herzig S, Shaw J. AMPK: guardian of metabolism and mitochondrial homeostasis. Nat Rev Mol Cell Biol. 2018;19(2):121-135.

60. Hindupur S, Gonzalez A, Hall M. The Opposing Actions of Target of Rapamycin and AMP-Activated Protein Kinase in Cell Growth Control. Cold Spring Harb Perspect Biol. 2015;7(8):136-144.

61. Shaw R, Mihaylova. The AMP-activated protein kinase (AMPK) signaling pathway coordinates cell growth, autophagy, & metabolism. Nat Cell Biol. 2011; 13(9):1016-1023.

62. Faubert B, Vincent E, Poffenberger M, Jones R. The AMP-activated protein kinase (AMPK) and cancer: Many faces of a metabolic regulator. Cancer Letters. 2015;356(2):165-170.

63. Niba ETE, Nagaya H, Kanno T, Tsuchiya A, Gotoh A , Tabata C, Kuribayashi K, Nakano T, Nishizaki T. Crosstalk between PI3 Kinase/PDK1/AKT/Rac1 and Ras/Raf/MEK/ERK pathways downstream PDGF receptor**.** Cell Physiol Biochem**.** 2013; 31: 905-915.

64. Endo H, Owanda S, Inagak Y, Shida Y. Glucose starvation induces LKB1-

AMPK-mediated MMP-9 expression in cancer cells. Sci Rep. 2018;8:10122-10136.

65. Wu D. Innate and adaptive immune cell metabolism in tumor microenvironment. Imm Met Health and Tumor. 2017;10:211-223.

66. Bruce A. Edgar, Frank Sprenger, Robert J. Duronio, Pierre Leopold, Patrick H. O'Farrell. Distinct molecular mechanisms regulate cell cycle timing at successive stages of embryogenesis. Genes & Dev. 1994.8:440-452.

67. Cheng J, Imanishi H, Amuro Y. NS-398, a selective cyclooxygenase 2 inhibitor, inhibited cell growth and induced cell cycle arrest in human hepatocellular carcinoma cell lines. IJC. 2002;99(5):755-761.

68. Malumbers M, Barbacid. Cell cycle, CDKs and cancer: a changing paradigm. Nature Reviews Cancer. 2009;9:153-166.

69. Bertoli C, J Skothein, De Bruin R. Control of cell cycle transcription during G1 and S phases. Nat Rev Mol Cell Biol. 2013;14(8):518-528.

70. Bretones G, Delgado M, Leon J. Myc and cell cycle control. BBA Gene Reg Mech. 2015;1849(5):506-516.

71. Gubern A, Joaqiun M, Maseres P, Garcia-Garcia J et al. **T**he N-Terminal Phosphorylation of RB by p38 Bypasses Its Inactivation by CDKs and Prevents Proliferation in Cancer Cells. Mol Cell. 2016;64(1):25-36.

72. Woo RA, Poon RY. Cyclin-dependent kinases and S phase control in mammalian cell. Cell cycle. 2003;2(4):316-324.

73. Mikhail V, Blagosklonny A, Pardee B**.** The Restriction Point of the Cell Cycle. Landes BioSci. 2013;1:16-25.

74. Husteat N, Gasser S, Shimada K. Replication Checkpoint: Tuning and Coordination of Replication Forks in S Phase. Genes. 2013; 4(3):388-434.

75. Chaffey G, Lloyd B, David J. The Effect of the G_1 - S transition Checkpoint on an Age Structured Cell Cycle Model. Plos One. 2014.

76. Mercer WE. Checking on the cell cycle. J Cell Biochem Suppl. 1998;30-31:50-54.

77. Gaurisankar SA, Tanya D. Anti cancer effects of curcumin: cycle of life and death.Cell Div. 2008;36-59.

78. Kerr, Wyllie, Currie A. Apoptosis: a basic biological phenomenon with wide-ranging implications in tissue kinetics. J Cancer 1972; 26(4):239-57.

79. Brown NS, Bicknell R. Hypoxia and oxidative stress in breast cancer Oxidative stress - its effects on the growth, metastatic potential and response to therapy of breast cancer. 2001

80. Dickens L, Boyd RS, Jukes-Jones R, Hughes M et al. A death effector domain chain disc model reveals a crucial role for caspase-8 chain assembly in mediating apoptotic cell death. Mol Cell. 2012;47(2):291-305.

81. Yigong S. Mechanisms of caspase activation and inhibition during apoptosis. Mol Cell. 2002;9(3):459-470.

82. Ouyang L, Shi Z, Zhao S, Wang F, Zhou T, Liu B, et al. Programmed cell death pathways in cancer : a review of apoptosis , autophagy and programmed necrosis. Cancer Rev. 2012;15:487-498.

83. Stephan WG, Green DR. Mitochondria and cell death: outer membrane permeabilization and beyond. Nat Rev Mol Cell Biol. 2010;11:621-632.

84. Czabotar PE, Lessene G, Strasser A, Adams JM. Control of apoptosis by the BCL-2 protein family: implications for physiology and therapy. Nat Rev Mol Cell Biol. 2013;15(1):49-63.

85. Cheong H, Lu C, Lindsten T, Thompson CB. Therapeutic targets in cancer cell metabolism and autophagy. Nat Biotechnol. 2012; 30(7):671-688.

86. Levy JM, Towers CG. Thorburn A. Targeting autophagy in cancer. Nat Rev Cancer. 2017;17:528-542.

87. Nagelkerke A, Sweep FCGJ, Geurts-Moespot A, Bussink J, Span PN. Therapeutic targeting of autophagy in cancer. Part I: Molecular pathways controlling autophagy. Semin Cancer Biol. 2014; 13(3):1-21.

88. Kenific CM, Debnath J. Cellular and metabolic functions for autophagy in

cancer cells. Trends Cell Biol. 2015; 25(1):37-45

89. Runwal G, Stamatakao E, Siddiqi E, Puri C, Zhu Y, David C et al. LC3-positive structures are prominent in autophagy-deficient cells. Sci Rep. 2019; 9:15-32.

90. Mizushima N. Autophagy: process and function. Genes & Dev. 2007; 21:2861-2873.

91. R Kang, H J Zeh, M T Lotze,D Tang. The Beclin 1 network regulates autophagy and apoptosis. Cell Death Differ. 2011;18(4):571-580.

92. Hickerman JA, Geneste O, Kroemer G. Functional and physical interaction between Bcl-$X_L$and a BH3-like domain in Beclin-1. EMBO J. 2007;26:2527-2539.

93. Fingar DC, Salama S, Tsou C, Harlow E, Blenis J. Mammalian cell size is controlled by mTOR and its downstream targets S6K1 and 4EBP1/eIF4E. Genes Dev. 2002;16(12):1472-1487

94. Yuan H-X, Xiong Y, Guan K-L. Nutrient sensing, metabolism, and cell growth control. Mol Cell.2013;49(3):379-387

95. Qin JZ, Xin H, Nickoloff BJ. Targeting glutamine metabolism sensitizes melanoma cells to TRAIL-induced death. Biochem Biophys Res Commun. 2010;398(1):146-152.

96. Soule HD, Vazquez J, Long A, Albert S, Brennan M. A human cell line from a pleural effusion derived from a breast carcinoma. J Natl Cancer Inst. 1973;51:1409-1416.

97. Lui B, Zeyling F, Edgerton SM, Deng X, Alimova IN, Stuart E, Thor AD. Metformin induces unique biological and molecular responses in triple negative breast cancer cells. Cell Cycle. 2009;8:2031-2040.

98. Guo J, Liu C, Zhou X, Xu X, Deng L, Li X, Guan F. Conditioned medium from malignant breast cancer cells induces an emt-like phenotype and an altered N-Glycan profile in normal epithelial MCF-10A cells. Int J Mol Sci. 2017;18:1528-1542 .

99. Visagie MH, Joubert AM. 2-Methoxyestradiol-bis-sulfamate induces apoptosis

and autophagy in a tumorigenic breast epithelial cell line. Mol Cell Biochem 2011; 357: 343-352.

100. Kung HN, Marks JR, Chi JT. Glutamine synthetase is a genetic determinant of cell type-specific glutamine independence in breast epithelia. PLoS Genet. 2011;7:1-26

101. Visagie MH, Joubert AM. The in vitro effects of 2-methoxyestradiol-bis-sulphamate on cell numbers, membrane integrity and cell morphology, and the possible induction of apoptosis and autophagy in a non-tumorigenic breast epithelial cell line. Cell Mol Biol Lett. 2010;15:564-581.

102. Bindokas VP, Jordán J, Lee CC, Miller RJ. Superoxide production in rat hippocampal neurons: selective imaging with hydroethidine. J Neurosci 1996;16(4):1324-1336.

103. Visagie MH, Mqoco TV, Liebenberg L, Mathews EH, Mathews GE, Joubert AM. Influence of partial and complete glutamine-and glucose deprivation of breast-and cervical tumorigenic cell lines. Cell Biosci. 2015;5:56-70

104. Weydert CJ, Cullen JJ. Measurement of superoxide dismutase, catalase, and glutathione peroxidase in cultured cells and tissue. Nat Protocol. 2010;5(1):51-66.

105. Tachibana M, Watanabe K, Kim S, Suzuki H. Enzyme-linked immunosorbent assay for screening of canine brucellosis using recombinant Cu-Zn superoxide dismutase. J VetMedSci. 2008;70(12):1387-1387.

106. Glorieux C, Calderon P. Catalase, a remarkable enzyme: targeting the oldest antioxidant enzyme to find a new cancer treatment approach. BioChem. 2017; 398(10):436-461.

107. Lui C, Bramer L, Webb-Robertson et al.Temporal expression profiling of plasma proteins reveals oxidative stress in early stages of type 1 diabetes progression. J of Proteomics. 2018;100-110.

108. Hardie DG, Schaffr B, Brunet A. AMPK: An energy-sensing pathway with multiple inputs and outputs. Trends in Cell Biol. 2016;26(3):190-201..

109. Kim J, Yang G, Ha J. AMPK activators: mechanisms of action and physiological activities. AMPK activators: mechanisms of action and physiological activities. Exp Mol Med. 2016;48(4):133-145.

110. Kemp BE, Oakhill JS, Langendorf CG. AMPK drug binding sites through crystallization of full-length phosphorylated α2β1γ1 heterotrimer.Methods Mol Biol. 2018;1732:15-27.

111. Johnson GL, Lapadat R, Johnson GL, Lapadat R, Lapadat R. Mitogen-activated protein kinase pathways mediated by ERK, JNK, and p38 Protein Kinases. Sci. 2002; 298:1911-1925.

112. Visuttijai K, Pettersson J, Azar Y, van den Bout I, Orndal C et al. Lowered expression of tumor suppressor candidate *MYO1C* stimulates cell proliferation, suppresses cell adhesion and activates AKT.Plos One. 2016.

113. Jason S. L. Yu, Wei Cui. Proliferation, survival and metabolism: the role of PI3K/AKT/ mTOR signalling in pluripotency and cell fate determination. Dev of Biol. 2016;143:3050-3060.

114. Valavanidis A, Vlachogianni T, Fiotakis C. 8-hydroxy-2′-deoxyguanosine (8-OHdG): a critical biomarker of oxidative stress and carcinogenesis. J of Env Sci & Health. 2009;27(2):120-139.

115. Lee J, Kang J, Choi B, Keum Y. Sensitization of 5-fluorouracil-resistant snuc5 colon cancer cells to apoptosis by α-mangostin. Biomol Ther. 2016;24(6):604-609.

116. Podhorecka M, Sklandaowski A, Bozo P. H2AX Phosphorylation: Its role in dna damage response and cancer therapy. J Nucleic Acids. 2010;130-142.

117. Ruprecht N, Hungerbuhler M, Bohm I, Heverhagen J. Improved identification of DNA double strand breaks: γ-H2AX-epitope visualization by confocal microscopy and 3D reconstructed images. Radiation &Env Biophys. 2019;58(2):295-302.

118. Visagie MH, Van den Bout I, Joubert AM. A bis-sulphamoylated estradiol derivative induces ROS-dependent cell cycle abnormalities and subsequent apoptosis. PlosOne. 2017.

119. Bernardi P, Petronilli P, Di Lisa F, Forte M. A mitochondrial perspective on cell

death. Trends Biochem Sci. 2001;26:112-117.

120. Gergely P, Niland B, Gonchoroff N, Pullmann N, Phillips PE, Perl A. Persistent mitochondrial hyperpolarization, increased reactive oxygen intermediate production, and cytoplasmic alkalinization characterize altered IL-10 signaling in patients with systemic lupus erythematosus. J Immunol. 2002;169:1092-101.

121. Segawa K, Nagata S. An Apoptotic 'Eat me' signal: phosphatidylserine exposure. Trends in Cell Biol. 2015;25(11):639-650.

122. Hankins H, Baldridge R, Xu P, Graham T. Role of flippases, scramblases, and transfer proteins in phosphatidylserine subcellular distribution.Traffic.2015;16(1)35-47.

123. Chang L, Kuksin D, Laverty D, Saldi S, Qiu J. Morphological observation and analysis using automated image cytometry for the comparison of trypan blue and fluorescence-based viability detection method. Cytotech. 2015;67(3):461-473.

124. Tanida I, Ueno T, Komminami E. LC3 and Autophagy. Methods Mol Biol. 2008;44:77-88.

125. Tsukamoto S, Yamamoto A, Kito S, Minami N, Kubata T et al. Fluorescence-based visualization of autophagic activity predicts mouse embryo viability. Sci Rep. 2014;4535.

126. Marthur M, Sharma P, Yadav P, Joseph C. A Comparative docking analysis of non-carcinogenic dna staining dyes to propose the best alternative to ethidium bromide.IJARITT. 2017;3(2):215-220.

127. Visagie MH, Mqoco T, Joubert A. Sulphamoylated estradiol analogue induces antiproliferative activity and apoptosis in breast cell lines. Cell& Mol Biol Lett. 2012;17:549-558.

128. Zielonka J, Kalyanaraman B. Hydroethidine- and Mito-SOX-derived red fluorescence is not a reliable indicator of intracellular superoxide formation: Another inconvenient truth. 2010;48(8):983-1001.

129. Liguori I, Russo G, Curcio F, Bulli G et al. Oxidative stress, aging, and disease. Clin Interv Aging. 2018;13:757-772.

130. Glorieux C, Calderon P. Catalase, a remarkable enzyme: targeting the oldest antioxidant enzyme to find a new cancer treatment approach. Biochem.2017;2816-2825.

131. Shin M, Cheong J. Mitochondria-centric bioenergetic characteristics in cancer stem-like cells. Arch Pharm.2019;42(2):113-127.

132. Wang W, Yang X, Lopez I et al. AMPK activity is determined by change of AMP/ATP ratio. J Biochem. 2003;278(29):27016-27023.

133. Luo J, Manning B, Cantley L et al. Targeting the pi3k-akt pathway in human cancer: rationale and promise. Cancer Cell. 2003;4(4):257-262.

134. Fruman D, Chiu H, Hopkins B, Bagrodia S. The PI3K pathway in human disease. Cell. 2017;170(4):605-635.

135. McCain J. The MAPK (ERK) Pathway Investigational Combinations for the Treatment Of BRAF-Mutated Metastatic Melanoma. PT. 2013;38(2):96-108.

136. Ji J, Zhang Y, Redon C, Reinhold W et al. Phosphorylated fraction of H2AX as a measurement for DNA damage in cancer cells and potential applications of a novel assay. PLos One. 2017.

137. Perry SW, Norman JP, Barbieri J, Brown EB, Gelbard HA. Mitochondrial membrane potential probes and the proton gradient: a practical usage guide. Biotechniques. 2011;50(2):98-115.

138. Forrest MD. Why cancer cells have a more hyperpolarised mitochondrial membrane potential and emergent prospects for therapy. Biorxiv. 2015:1-42.

139. Karsli-Uzunbas G. et al. Autophagy is required for glucose homeostasis and lung tumor maintenance. Cancer Discov. 2014;4:914-927.

140. Lee Y, Lee J. Role of the mammalian ATG8/LC3 family in autophagy: differential and compensatory roles in the spatiotemporal regulation of autophagy.BMB Rep. 2016;49(8):424-430.

141. Mizushima N, Yoshimorim T, Levine B. Methods in Mammalian Autophagy Research.Cell. 2010; 140(3):313-326.

142. Herbel C, Patsoukis N, Bardhan K, Seth P, Weaver JD, Boussiotis VA. Clinical significance of T cell metabolic reprogramming in cancer. Clin Transl Med. 2016;5:29.

143. Zhu L, Ploessl K, Zhou R, Mankoff D, Kung HF. Metabolic imaging of glutamine in cancer. J Nucl Med. 2017;58:533-537.

144. Vo VT, Choi J-W, Phan ANH, Hua TNM, Kim M-K, Kang BH, et al. TRAP1 inhibition increases glutamine synthetase activity ion glutamine auxotrophic non-small cell lung cancer cells. Anticancer Res. 2018;38(38):2187-2193.

145. Qin JZ, Xin H, Nickoloff BJ. Targeting glutamine metabolism sensitizes melanoma cells to TRAIL-induced death. Biochem Biophys Res Commun. 2010;398(1):146-52.

146. Kongara S. Karantza V. The interplay between autophagy and ROS in tumorigenesis. Front Oncol. 2012;2:171.

147. Afans I. Mechanisms of superoxide signaling in epigenetic processes: relation to aging and cancer. Aging Dis. 2015;6:216-227.

148. Aykin-Burns N, Ahmad IM, Zhu Y, Oberley LW, Spitz D. Increased levels of superoxide and H2O2 mediate the differential susceptibility of cancer cells versus normal cells to glucose deprivation. Biochem J. 2009;418:29-37.

149. Afonso V, Champy R, Collin P, Lomri A. Reactive oxygen species and superoxide dismutases: role in joint diseases. Joint Bone Spinc. 2007; 74(4):324-329.

150. Yuan HX, Xiong Y, Guan KL. Nutrient sensing, metabolism, and cell growth control. Mol Cell. 2013;49:379-87.

151. Vilema-Enríquez G, Grijalva M, Ricardo I, Amador-Zafra Z, Camacho J. Molecular and cellular effects of hydrogen peroxide on human lung cancer cells: potential therapeutic implications. Oxi Med Cell Longev. 2016;2016:1908164.

152. Schieber M, Navdeep C. ROS function in redox signalling and oxidative stress. Curr Biol. 2014;24:453-462.

153. Wang Y, Bronicky R, Noe A, Hekimi S. Superoxide dismutases: Dual roles in controlling ROS damage and regulating ROS signaling.J Cell Biol. 2018; 217(6):1915-1928.

154. Yang L, Venneti S, Nagrath D. Glutaminolysis: a hallmark of cancer metabolism. Biomed Eng. 2017;19:163-194.

155. Ngugen C, Pandey S. Exploiting Mitochondrial Vulnerabilities to Trigger Apoptosis Selectively in Cancer Cells. Cancers. 2019; 11(7):916.

156. Forrest MD. Why cancer cells have a more hyperpolarised mitochondrial membrane potential and emergent prospects for therapy. bioRxiv. 2015. Sastre-

157. Sastre-Serra S, Valle A, Garau I, Oliver J, Roca P. Estrogen down-regulates uncoupling proteins and increases oxidative stress in breast cancer. Free Radic Biol Med. 2010; 48: 506-512.

158. Dmitry B, Juhaszova M, Sollot S. Mitochondrial ROS-induced ROS release: an update and review. Physiol Rev. 2014; 94: 909-950.

159. Schumacker P. Reactive oxygen species in cancer cells: Live by the sword, die by the sword. Cancer Cell. 2006; 10(3):175.

160. Kim S. Cancer energy metabolism: shutting power off cancer factory. Biomol Ther. 2018; 26(1):39-44.

161. Birben E, Sahina U, Sackesen C, Erzurum S, Kalayci O. Oxidative stress and antioxidant defense. World Allergy Organ J. 2012; 5(1):9-19.

162. Ennen M, Minig V, Grandemange S. Regulation of the high basal expression of the manganese superoxide dismutase gene in aggressive breast cancer cells. Free Radic Biol Med. 2011; 50(2):1771-1779.

163. Hart P, Mao M, Ekoue D, Ganin D et al. MnSOD upregulation sustains the Warburg effect via mitochondrial ROS and AMPK-dependent signaling in cancer. Nat Commun. 2015; 6:6053.

164. Goh J, Enns L, Fatemie S, Hopkins H et al. Mitochondrial targeted catalase suppresses invasive breast cancer in mice. BMC Cancer. 2011; 11:191.

165. Sabino C, Hamblin M. Celluar damage. 2017; Basics to Cliinc Prac.2017; 57-72.

166. Awooda H.Pathophysiology of Cerebral Ischemia: Role of Oxidative or Nitrosative Stress. J of BioSci Med. 2019; 7(3):90934.

167. Musarrat J, Arezina-wilson J, Wani A. Prognostic and aetiological relevance of 8-hydroxyguanosine in human breast carcinogenesis. J of Canc.1996;32(7):1209-1214.

168. Sharma A, Singh K, Almasaan A. Histone H2AX phosphorylation: a marker for DNA damage. Methods Mol Biol. 2012; 920: 613-626.

169. Ladeira C, Carolino E, Gomes M, Brito M. Role of macronutrients and micronutrients in dna damage: results from a food frequency questionnaire. 2017; 10:11786.

170. Gaglio D, Soldati C, Vanoni M, Alberghina L, Chiaradonna F. Glutamine deprivation induces abortive S-phase rescued by deoxyribonucleotides in K-ras transformed cells. PLoS ONE. 2009;4(3):e4715

171. Kansara M, Berridge MV. Oncogenes modulate cell sensitivity to apoptosis induced by glucose deprivation. Anticancer Res. 2004;24:2503-2510.

172. Feoktristova M, Wallberg F, Tenev T. Techniques to distinguish apoptosis from necroptosis. Cold Harb. Protoc. 2016; 4.

173. Sun Y, Liu W, Feng X, Yang N, Zhou H. Signaling pathway of MAPK/ERK in cell proliferation, differentiation, migration, senescence and apoptosis. J of Recept and Signal Transduc. 2015; 35(6): 600-604.

174. Kaur J, Debonath J. Autophagy at the crossroads of catabolism and anabolism. Nat Rev Mol Cell Biol. 2015; 16: 461-472.

175. Jewell J, Kim Y, Russel R, Yu F, Park H. Differential regulation of mTORC1 by leucine and glutamine. Sci. 2015; 347(6218):194-198.

176. Schmeizie T, Hall M. TOR, a central controller review of cell growth. Cell. 2000;103:253-262.

177. Tan H, Sim A, Long Y. Glutamine metabolism regulates autophagy-dependent mTORC1 reactivation during amino acid starvation. Nat Comm. 2017; 8:338.

178. Onodera J, Ohsumi Y. Autophagy is required for maintenance of amino acid levels and protein synthesis under nitrogen starvation. JBC. 2005; 31582-31586.